Power Sharing Control of Parallel Connected Inverter Systems

Li Lei

B.Eng., M.Sc.

A thesis submitted for the degree of

Doctor of Philosophy

January 2022

School of Engineering

Newcastle University

United Kingdom

Abstract

Microgrid is an emerging cutting-edge technology that can effectively improve the safety and reliability of the power system and promote the access and local consumption of renewable energy. It is also a key enabler for improving the utilization efficiency of renewable energy and the energy efficiency of the power distribution network. However, a standalone microgrid generally has shortcomings such as limited working capacity and weak anti-disturbance ability. These are normally coupled with the intermittent output power of renewable energy and the variability of the load. Some of these challenges can be overcome if the microgrid can be connected to the main grid.

With a high penetration rate of renewable energy, many technical problems in the coordinated control of power need to be solved in order to improve the power supply quality and reliability. Parallel operation of inverter-based distributed generation systems, in the two modes of islanded microgrid operation and grid-connected operation, brings many control challenges to the microgrid including load sharing, stability, amplitude and phase synchronization, and circulating current. Therefore, it is necessary to study the parallel control strategies for the inverters in microgrids and to develop novel solutions to the associated problems. This thesis conducts research into the islanded and grid-connected operation characteristics of microgrid inverters and also the switching between the two operation modes. The thesis covers the following:

(1) Islanded and grid-connected operation characteristics of microgrid converters. The different output droop characteristics of the microgrid converter are discussed considering different output impedances. The mathematical model of a microgrid with inverter-based generation is established and the full system is simulated in the islanded and grid-connected operation modes using MATLAB/Simulink platform. The simulation is used to verify the proposed control scheme which aims at improving the power-sharing ability between parallel-connected inverters, allowing the output power of each inverter to be based on its own capacity and improving immunity to power grid fluctuations.

(2) Power sharing control of parallel inverters with different line impedances. In an actual electricity distribution system, the distance between the power generation units in the

microgrid and the main grid access point may be different, which causes the power output of each distributed power source to be unable to reach equal distribution or to be distributed in proportion to the capacity. Some distributed power sources may likely operate at full power, while other sources may not be able to provide sufficient effective power output. In this thesis, a hierarchical control strategy for power distribution is proposed, and its effectiveness is verified by theoretical proof and MATLAB/Simulink simulation.

(3) Distributed and schedulable power droop control method. The traditional droop control cannot realize the tracking of a given active power reference signal, which makes it impossible for the distributed power supply operating in droop mode to perform accurate power dispatch control. Based on the hierarchical control architecture, this thesis proposes a schedulable distributed power droop control method, which retains the characteristics of traditional droop control, and realizes distributed power by modifying the power reference value in droop control, with accurate tracking of active reference signals. In addition, this method can keep the system frequency stable.

In summary, the improved droop control proposed in this thesis enables the inverter-based power generation system to operate smoothly under different system parameters and operating modes, thus solving the problem of not being able to distribute the output power according to the inverter capacity when multiple inverters are connected in parallel.

Key words: Microgrid, distributed generation, parallel-connected inverters, droop control, power sharing, pre-synchronization

Acknowledgements

I would like to express my deepest gratitude to my beloved parents for their encouragement and financial support in completing my research. I would also like to express my deepest gratitude to my partner, Zoe Yu, whose full support, and companionship gave me the strength to complete my PhD. As well as all my family, whose understanding and unconditional love are long to be forgotten.

I am extremely grateful to my supervisors, Dr. Mohammed Elgendy, Dr. Neal Wade and Dr. Salaheddine Ethni, for their invaluable guidance and consistent support. Without their excellent support, the successful completion of this research would not have been possible. Dr. Mohammed Elgendy, in particular, has been most helpful to me in completing my PhD research. I would like to thank him again for his patience and efforts.

I would like to express my sincere thanks to the School of Engineering, especially the staff of the Electrical Power Group, who provided me with significant assistance in my research work. I would also like to thank the students in the same group for their support and occasional active discussions during my program.

A courteous acknowledgement is made to other members of staff and technicians in School of Engineering in Newcastle University who provided me with assistance during the years of research.

Table of Contents

List of Figures

List of Tables

List of Abbreviations

AC	Alternating Current
BICs	Bidirectional Interfacing Converters
CAN	Controller Area Network
CSI	Current Source Inverters
DC	Direct Current
DG	Distributed Generation
DR	Demand Response
DSM	Demand Side Management
ESS	Energy Storage System
LF	Loop Filter
PCC	Point of Common Coupling
PD	Phase Detector
PFM	Pulse Frequency Modulation
PI	Proportional-Integral
PIR	Proportional-Integral-Resonant
PR	Proportional-Resonant
PSASP	Power System Analysis Software Package
PWM	Pulse Width Modulation
SPWM	Sinusoidal Pulse Width Modulation
SSRF-SPLL	Single Synchronous Reference Frame Software Phase Locked Loop
VCO	Voltage-Controlled Oscillator
VSI	Voltage Source Inverters

Chapter 1 Introduction

1.1 Background

The distributed power generation technology using renewable energy gradually penetrated into the power system and has become an important part of the power grid. The combination of large power grids and distributed power generation has been recognized by energy and power experts around the world as the main way to improve the reliability and replacement of power systems, and the main direction of the power industry in the 21st century [1].

Despite the economies of scale, security and reliability, the efficiency and sustainability of traditional centralised generation, transmission and distribution models are increasingly difficult to demonstrate. Decentralized power generation is usually produced close to the sites that consume this resource, and decentralized power generation involves a range of technologies that make use of various renewable energy sources, such as small hydro, wind, solar and biomass [2]. Compared to traditional centralized power generation structure, decentralized power generation has the following unique advantages:

(1) Improved the power supply reliability: Compared with traditional generators, distributed power supplies have a fast-dynamic response, are convenient and easy to operate, and can operate independently and complement each other, eliminating the failure risk of the full power generation system.

(2) Flexible installation location: The distributed power supply has a small standalone capacity, low investment, and is easy to design. It is more suitable for meeting the power needs of remote areas.

(3) Environment protection: Most distributed power generation is based on solar, wind and other renewable energy sources, which can greatly reduce greenhouse gas emissions.

(4) Transform with power electronics: Most distributed power sources are grid-connected using power electronic conversion systems. In such systems, power quality management functions can be achieved through proper control of the power electronic converters of the distributed power sources.

On the other hand, the large-scale utilization of renewable energy also poses huge challenges to the existing supply model. The traditional centralized power grid has been unable to cope with many dispersed, reduced capacity, intermittent and transitional renewable energy [3], and needs a more efficient grid organization and transformation form. To effectively manage the increasing number of distributed power sources, the 2002 American Electrical Insulation Technology Solutions Association formally put forward the concept of microgrid. Based on this concept, Professor Robert H. Lasseter of the University of Wisconsin-Madison proposed the definition of microgrid for the first time [4]. All kinds of distributed power sources, energy storage devices, and local loads are organically combined to form an independent power unit, giving full play to the advantages of different power sources, realizing the efficient use of nearby electric energy, or being integrated into a large power grid for grid operation. After more than ten years of development, various countries have made great progress in microgrid planning and design, economical optimization dispatch, stability analysis and operation strategies, power quality management, etc., and have established many demonstration projects, such as "Germany Mannheim Microgrid Demonstration Project", "Zhejiang Luxi Island Microgrid Demonstration Project". The microgrid has been generally regarded as an effective way for distributed power to access the distribution network [5, 6].

In this thesis, the microgrid is used as a research context to study the control theory of a multi-inverter parallel system in a microgrid, analysing different system parameters, including the inconsistent capacity of each inverter, the inconsistent output line impedance of each inverter, the mode of operation of the system and the smooth switching, and the variation of the components connected to the system.

1.2 Microgrid overview

Microgrid refers to a small power distribution system consisting of distributed power supplies, energy storage devices, energy conversion devices, loads, monitoring devices and protection devices. Microgrid is an autonomous system capable of self-control, protection, and management, which can be operated either connect with an external grid or in an isolated network. Microgrid has been proposed to achieve the flexible and efficient integration of distributed power sources, to accommodate the large number of diverse forms of distributed

power supply and to deal with distribution network problems [7]. Microgrid is a concept relatively to traditional large power grid, refers to many distributed power supplies and its related load in accordance with a certain topology of the network, and it is connected to the traditional power grid through a static switch. The development and promotion of microgrids can fully promote the large-scale access of distributed power sources and renewable energy sources and realize multiple forms of energy to supply power to loads with high reliability. It is also an effective way to realize active distribution networks, to make the traditional power grid transition to smart grid.

1.2.1 Microgrid structure

The microgrid structure refers to the design of the network topology, including the electrical wiring, the power supply system (DC/AC power supply and three-phase/single-phase power supply) within the microgrid, loads and node locations in the power grid…etc. Microgrid is normally a low voltage and medium voltage power grid. Medium voltage microgrid is suitable for power supply with medium capacity, higher power supply reliability requirements and more centralized user area [8]. On the other hand, low voltage microgrids are usually owned by power or energy users and are relatively small [9].

Depending on power supply type, microgrids can be divided into AC, DC and hybrid AC/DC type.

In DC microgrid, distributed power supply, energy storage devices, load etc. are connected to the DC bus. The DC network is then connected to the external AC power grid through a power electronic inverter. DC microgrids can provide power to different AC voltage and DC loads by means of power electronic conversion devices. The fluctuation of distributed power supply and load can be adjusted by the energy storage device on the DC side [10].

Similarly, in AC microgrid, distributed power supplies, energy storage devices, etc. are connected to the AC bus through power electronic devices. The AC microgrid is still the main form of microgrid. Through the control of the PCC switch, microgrid can switch between grid-connected mode and islanded mode [11].

AC-DC hybrid microgrid comprises both AC and DC buses and therefore can directly supply power to the AC and DC loads with no need to use converters for load supply [12].

Microgrids are still being researched as a new type of grid. In order to ensure safe and reliable operation of the microgrid, there are still many problems need to be resolved [13], such as micro-grid control methods, coordination between the microsources, energy management and scheduling, micro-grid communication, fault detection & protection and micro-grid power quality [14]. To solve these problems, many scholars have made unremitting efforts to put forward different control methods. R.Majumder et al. proposed a kind of inertial and non-inertial microsources composed of microgrid operation and control methods, and analyzed stable operation under different operating conditions [15]. A coordinated control strategy of microsources and energy storage devices in micro-grid system is proposed by M. Savaghebi *et al*., the experimental results show that this coordinated control strategy can adjust the voltage and frequency of the system and improve the reliability of the system [16]. An alternative voltage harmonic compensation method is proposed by N. Pogaku *et al*., which reduces the steady-state voltage harmonic and improves the voltage quality [17]. In F. Gao's literature, the microgrid based on the inverter is modeled by small signal, and the stability of the system is analyzed and verified by simulation and experiment [18]. The power loop of the inverter in the microgrid is analyzed and modeled by dynamic vector method, and the feasibility of the control method is explained by L. F. Ludwig [19]. In the literature [20], the micro-grid energy optimization management method is proposed for the micro-grid economic operation and management under the independent operation mode. Q. Song *et al.* proposed a microgrid protection strategy, this protection strategy in both the network operation mode or in the independent operation mode can effectively detect the failure, so as to achieve real-time protection [21].

1.2.2 Control methods in microgrid

The core target of microgrid control is to achieve the capacity distribution under the premise of maintaining the stability of the grid voltage and frequency. The reliability and robustness of microgrid system control are largely dependent on the accuracy of control of microsources in the microgrid. As most of the microsources are connected to the grid or load using voltage source inverters, the control of these microsources is normally achieved by controlling the inverters. Due to the system redundancy and the limitation of single microsource capacity, the parallel operation of the inverter in the microgrid becomes a technical challenge of microgrid control.

Compared with the traditional power grid, the microgrid system has great flexibility and uniqueness, but the operating conditions are complex, the control objectives of different modes are different, and there are stages in which different modes switch between each other. The microgrid performance should satisfy the following:

a. During grid-connected operation, the microgrid system needs to implement the coordinated operation of distributed power sources and loads within the system based on the characteristics of distributed power sources, energy complementation, and economics.

b. Under planned or unplanned island operating conditions, the microgrid system should quickly and steadily achieve smooth switching from grid-connected to islanded to provide stable power supply to the load within the system.

c. During islanding operation, the microgrid system needs to rely on energy storage or micro gas turbine power generation equipment in the system to maintain the stability of the system voltage and frequency, and to achieve a reasonable distribution of load power according to the characteristics of different distributed power sources.

d. In the process of island-to-grid switching, the microgrid system should coordinate the frequency and voltage amplitude of the distributed power regulation system to achieve smooth and stable grid connection.

The control of network operation with multiple inverters in the microgrid is developed from the parallel operation control methods of inverters. The parallel operation control of inverters mainly includes two kinds of method: interconnection control [21] and no interconnection control [22, 23], which are applied to the microgrid as known: master-slave control [24] and decentralized control [25, 26].

a. In Master-slave control, one or several micro-sources is/are responsible for providing voltage and frequency support for the entire microgrid. The other micro-sources in the microgrid simply provide the power required to load. Master-slave control is based on shared control signals between the master unit and different micro-sources. This technique requires a centralized micro-network controller to receive each inverter and the load terminal signal under different load conditions and assign it to different micro-source units [27]. Master-slave control methods have a lot of drawbacks. First, the dynamic sharing of signals requires

high-bandwidth transmission facilities, so that the cost is very expensive when the connection between the microsources is long distances, therefore unrealistic. Secondly, a failure of the main control unit (the master unit) will have a devastating impact on the entire system. Thirdly, the control signal reduces the reliability of the micro-grid system because the control signal takes an important role when system is running. Last but not the least, unlike with the traditional power generation unit, the load structure of the microgrid is unpredictable, which makes it difficult to design the distribution control algorithm.

b. In Decentralized control, also known as peer-to-peer control [28], each micro-source controls its own voltage and frequency and cooperate with the other micro-sources to supply active power and reactive power of the loads. The easiest way to achieve decentralized control is voltage and frequency droop control. This control method allows the power generation unit to assume the change of the load according to its droop characteristic. In this case, the system frequency and the voltage amplitude are considered as virtual control connection lines between power generation units.

1.3 Control of inverter in microgrid

There are various forms of energy sources that may be utilised in the microgrid system, including conventional easy-to-control power sources such as micro gas turbines, and renewable energy sources such as wind and photovoltaic generators that are difficult to control due to fluctuation in generated power. Also, the microgrid system is normally equipped with an energy storage system [29]. Due to differences in energy attributes, different distributed power sources play different roles in microgrid systems. For distributed power sources with power electronic devices as interfaces in microgrid systems, the output power control and output characteristics are different. Power output for each micro source based on the inverter capacity will be achieved through the control of power electronic devices. According to different control objectives and implementation forms, the microgrid converter control mode can be divided into three types: PQ control, constant voltage frequency ratio V/f control and droop control [30-32].

1.3.1 PQ control

This control mode is constant active and reactive power control, which controls the microgrid converter to output the corresponding active and reactive power according to the power command. The microgrid converters in this control mode of the microgrid system are mainly divided into two types [30]: one is the converter operates according to the given command of maximum power output, such as converter for wind turbines, photovoltaic systems and other power electronic grid-connected devices; another is the converter operates according to the higher-level scheduling instructions.

The microgrid converter using the PQ control needs to collect grid voltage frequency and angle information for synchronization, so it is mainly applicable to the grid-connected mode of the microgrid system. In the islanding state, other distributed power sources must provide voltage and frequency support for it.

1.3.2 Constant voltage frequency ratio V/f control

The constant voltage-frequency ratio control (referred to as the V/f control), which controls the microgrid converter output according to the voltage amplitude and frequency commands, and its output power is determined by the load. The distributed power sources in this control mode of the microgrid are mainly micro gas turbines and battery energy storage systems [31].

The microgrid converter in this control mode generates voltage amplitude and angle according to its own command, which is shown as the characteristics of the voltage source. With this control, it is prone to faults such as overcurrent when connected to the grid or in parallel with other microgrid converters employing other control modes. In the island mode, this control can provide the voltage and frequency support for the microgrid system.

1.3.3 Droop control

The droop control is to choose a frequency droop character curve similar to the traditional generator as the control method of the micro source, that is, to obtain stable frequency and voltage through P/f droop control and Q/V droop control, respectively. Sometimes P/V droop control and Q/f droop control are also used. The droop control method controls the active

power and reactive power of the micro-source output in the microgrid separately, without the need for communication coordination between the units, realizes the plug-and-play of the micro-sources, and ensures that the microgrid can easily and reliably achieve power balance and frequency unity in the island mode [32].

1.4 Power coordinated control in microgrid system

Microgrid power coordinated control technology is the key technology for reliable operation of multi-microgrid networking, especially when the system is operating in island mode. At present, the power supply reliability of each microgrid completely depends on whether the demand for distributed power and load power within the microgrid is constant. However, the output power of distributed power sources is intermittent and uncertain. In addition, during the operation of multiple microgrids, other power quality problems may also occur, such as secondary ripple current, three-phase power imbalance, and power sharing of interface converters [33]. Therefore, appropriate research must be conducted. Microgrid power coordinated control technology can coordinate the energy mutual aid between microgrids to ensure the safe and reliable operation. However, since the research on the key technologies of microgrid power coordination control is still in its development phase, there are still many key technologies to be considered.

1.4.1 Power coordinated control technology of DC microgrid

In DC microgrid, distributed generators usually use controllable power electronic interface converters connected to the DC bus. How to realize that DGs equally divide the power of the system load is a key task for the power coordinated control of DC microgrids. For this reason, the droop control strategy has been considered by many scholars. It is a very effective power sharing technology without any interconnection wires [34, 35]. Although the droop control strategy has many advantages, there are still some disadvantages that limit the applicability of the droop control strategy. The most obvious shortcoming is that it will lead to deviations in the bus voltage, and the current sharing accuracy varies with the line impedance. For this reason, a hierarchical control strategy is proposed in [36]. The top-level controller is used to restore the voltage, and the bottom-level controller is used to ensure accurate current sharing, effectively solving the problem of bus voltage deviation.

However, in the DC microgrid, due to the large-scale access of AC loads, the current flowing through the DC bus is not completely DC component, because the power absorbed by single-phase AC load or three-phase unbalanced AC load has double frequency Ripple, which will cause the inverter's input current to have a secondary ripple current [37]. However, the traditional droop control does not consider the control of the secondary ripple current. In this case, the distribution of the secondary ripple current depends on the line impedance, while the distributed energy storage system is generally distributed widely and connected to the bus. The different distances between the distributed energy storage systems will easily lead to different line impedances of the distributed energy storage systems, making some lines have relatively small impedances, distributing more ripple currents, or even exceeding their rated capacity, which will cause the DC bus voltage to vary.

1.4.2 Power coordinated control technology of AC hybrid microgrid

The currently widely used form of microgrids is still mainly AC microgrids as they have the same voltage and current characteristics as those of traditional large power grids. In recent years, many scholars have studied the topology, control theory and power quality of AC microgrids, especially in the power coordinated control technology of multiple inverters in parallel. At present, it mainly includes master-slave control mode, three-layer hierarchical control and decentralised control mode.

a. Master-slave control, that is, one or several microsources as the main unit, for the entire microgrid to provide voltage and frequency support, the other microsources attached to the main microsources, simply provide the power required to load. Master-slave control is based on shared control signals between different microsources. This technique requires a centralized micro-network controller to receive each inverter and the load terminal signal under different load conditions and assign it to different micro-source units. Master-slave control methods have a lot of drawbacks. First, the dynamic sharing of signals requires high-bandwidth transmission facilities, so that the cost is very expensive when the connection between the microsources is long distances, therefore unrealistic. Secondly, a unit as the main control unit, when the main control unit failure, will have a devastating impact on the entire system. Thirdly, the control signal reduces the reliability of the microgrid system because the control signal takes an important role when system running. Last but not the least, unlike with

the traditional power generation unit, the load structure of the microgrid is unpredictable, which makes it difficult to design the distribution control algorithm.

b. Microgrid three-layer hierarchical control refers to the use of a central controller to coordinate and manage the power output of each local distributed power source, so as to realize the safe, reliable and stable operation of the microgrid [38]. At present, the most used hierarchical control is the three-layer control structure. As shown in Figure 1.1, it is mainly divided into three layers: power distribution layer (tertiary level), microgrid layer (secondary level), and inverter layer (primary level). The distribution layer is mainly responsible for the top-level management and economic operation of the microgrid, so that the microgrid and the distribution network can coordinate with each other to meet the dispatching needs of the distribution network; the microgrid layer mainly works by obtaining other inverters status information and the relevant output information of the local inverter, combined with the data transmitted by the top-level controller to calculate the compensation required by the bottom-level inverter layer; the inverter layer mainly involves the control of the bottom-level inverter of the microgrid. To ensure that the output voltage and output current of the inverter meet the

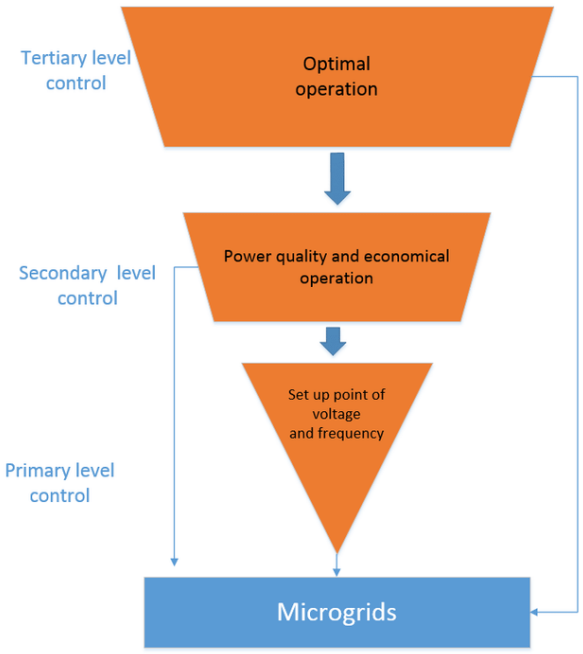

Figure 1.1 Three-layer hierarchical control structure of microgrid

basic requirements of relevant standards. For this project, secondary control loop will be added to the microgrid's inner control loop, to achieve the power sharing between parallel connected inverters with different parameters.

c. Decentralized control, also known as peer-to-peer control, each of the microsources are equal in microgrid, each micro-source alone to control their own voltage and frequency, also work together with other micro-sources to supply active power and reactive power of loads. The easiest way to achieve decentralized control is voltage and frequency droop control. This control method allows the power generation unit to assume the changes of the load according to its droop characteristic, in fact the system frequency and the voltage amplitude as the virtual control connection line between each power generation unit. The peer-to-peer control mode is very suitable for the microgrid system with multiple inverters operating in parallel. Compared with the master-slave control mode, the peer-to-peer control method can effectively realize the plug-and-play of distributed power sources, and it can also ensure the system seamless switching between different working mode [39].

However, it is worth noting that the above-mentioned control methods are all aimed at three-phase AC microgrid, and do not consider the power coordinated control technology of single-phase-three-phase AC hybrid microgrid [40]. With the addition of many single-phase micro-sources and single-phase loads in the micro-grid, the micro-grid has become a complex single-phase-three-phase hybrid power supply system. In addition, the output power of distributed power sources has obvious intermittent, time-varying and uncertainty have caused the voltage fluctuation and three-phase power imbalance of single-phase-three-phase hybrid microgrid to become more serious. To this issues, a centralized control method suitable for distributed single-phase inverters connected to a three-phase microgrid is proposed in [41], which can effectively control the power flow between the phases of the three-phase microgrid. However, the method adopted a centralized control strategy relies on the communication system, which reduces the reliability of the system. A hybrid single-three-phase microgrid structure with power management capabilities is proposed in [42], in which a power distribution unit composed of three groups of single-phase back-to-back converters is used to coordinate the three-phase single-phase microgrid power exchange. However, because there is no energy storage system, when all single-phase microgrids have insufficient power, the power distribution unit will be locked or stop working, resulting in a serious drop in the

frequency of the microgrid. At this time, the power distribution unit cannot provide frequency support and cannot solve the system's three-phase power imbalance.

Therefore, in order to solve power quality problems such as voltage fluctuations and three-phase power imbalances that occur during islanding operation of the traditional single-phase-three-phase AC hybrid microgrid, it is urgent to study the power coordination control applicable to the single-phase-three-phase AC hybrid microgrid. In this project, mainly focus on the three phase microgrid, for single-phase-three-phase AC hybrid microgrid, will be studied in the future.

1.4.3 Power coordinated control technology of AC/DC hybrid microgrid

As an effective solution for consumption of energy from new power sources, microgrid has received widespread attention from scholars [43-45]. Because the voltage and current characteristics of AC microgrid are the same as traditional large power grids, AC microgrid was first proposed [46]. But in fact, a large part of the output characteristics of DGs are DC characteristics, at the same time DC loads are increasing year by year. To improve the utilization efficiency of renewable energy, DC microgrids have emerged. Compared with AC microgrid, DC microgrid only needs to consider the balance of active power without considering the problem of reactive power balance, let alone the problems of phase synchronization, harmonics, and reactive power loss [47]. However, due to the long history of traditional AC power grid developed, the existing AC infrastructure will be used for a long time in the future and it is not practical to use DC microgrids alone. Therefore, it is necessary to find a more reasonable microgrid with a structure to accommodate various types of DGs. For this reason, an AC/DC hybrid microgrid architecture is proposed in [12], which uses Bidirectional Interfacing Converters (BICs) to connect the AC microgrid and the DC microgrid together, integrating the advantages of both in a more economical and efficient way.

Like the DC microgrid and AC microgrid, the AC/DC hybrid microgrid needs to coordinate the power distribution of the DGs in the system. In island operation, the hybrid microgrid does not have a large grid to maintain the power balance of the system. It can only rely on the coordinated control of the bidirectional interlinking converters and the energy storage system (ESS) to ensure the power balance of the hybrid microgrid system. *M.*

Hosseinzadeh et al. uses an advanced energy management system to coordinate and manage the power of the hybrid microgrid, which makes the hybrid microgrid more reliable and economical [48]. *R. A. Kaushik et al.* uses master-slave control technology to achieve energy sharing on both sides of the hybrid microgrid [49]. Smooth and reliable exchange, but the above methods are all centralized control, and rely heavily on the communication system. Once the communication fails, it is easy to cause the system to crash.

Traditional droop control is suitable for power sharing control in DC microgrid or AC microgrid, while the AC/DC hybrid microgrid also requires BICs to coordinate power on both sides. Therefore, the traditional droop control is not suitable for BICs power coordination control. A new type of hierarchical coordination method been proposed by *L. Che et al.* which can realize the power coordinated control of BICs, ensure the power balance of the hybrid microgrid, and also make the autonomous control of the hybrid microgrid possible [50, 51]. However, due to the hybrid microgrid structure, there is always energy exchange on both sides, which will inevitably increase the power loss of the system. In addition, the above method is only applicable to the power coordinated control of a single BIC and does not consider the power sharing problem of multiple BICs. *H. Xiao et al.* [52] proposed an improved control method for multi-BICs parallel system, which can accurately realize the power distribution of multi-BICs in AC/DC hybrid microgrid. A parallel control strategy is been proposed by *X. Wang et al.* for AC/DC hybrid microgrid under the condition of unbalanced grid voltage [53]. By introducing an adjustable reference current coefficient to ensure constant active power transmission, the fluctuation of DC side voltage is reduced, and realize the power distribution of multiple BICs. However, the above control methods only focus on the power sharing effect of BICs, and do not consider the power exchange control of the subnets on both sides of the AC/DC hybrid microgrid.

1.5 Contribution

The main contributions of this research project are summarized as follows:

- Through the research on the control method of grid-connected inverters, the improved droop control with secondary control loop is proposed, which can make the parallel connected inverters output power sharing according to the capacity of each inverter, when

the output line impedance of each inverter is different, which is the most practical and reality condition.

- Combined proposed droop control with Single Synchronous Reference Frame Software Phase Locked Loop (SSRF-SPLL) pre-synchronization control, which allow the microgrid not only work stably in islanding mode with multiple inverters are operated in parallel, but also can work in grid-connected mode and smoothly switch between these two modes. It provides technical proof for the wide application of microgrid.
- Due to the low-level communication between the parallel inverters been used in this project, compare to other scholar's work, which can make the microgrid operation more flexible and more feasible.
- The proposed control method in this project, allows the microgrid with different output line impedance of each parallel inverters, not only can working in small scale power system model, also can working in large scale power system model, such as normal grid block and IEEE 14-bus test system. Which had been verified through MATLAB/Simulink.

In conclusion, this project makes a positive contribution in the area of the power sharing control between parallel inverters with different output line impedance for each inverter, and specifically in the combined improved droop control with pre-synchronization control, which has an impact on microgrid been widely used in the real world.

The following papers have been published during this project:

[1]. L. Lei, M. A. Elgendy, N. Wade, S. Ethni and H. M. Hasanien, "Power sharing between parallel inverters in microgrid by improved droop control," 2018 53rd International Universities Power Engineering Conference (UPEC), 2018, pp. 1-6, doi: 10.1109/UPEC.2018.8541970.

[2]. L. Lei, M. A. Elgendy, N. Wade and S. Ethni, "Power sharing between parallel inverters by using droop control with a secondary control loop," 2019 IEEE 10th International Symposium on Power Electronics for Distributed Generation Systems (PEDG), 2019, pp. 653-658, doi: 10.1109/PEDG.2019.8807661.

[3]. L. Lei, M. A. Elgendy, N. Wade and S. Ethni, "Combined Pre-Synchronization and Power Sharing Control for Microgrid Applications," 2020 55th International Universities

Power Engineering Conference (UPEC), 2020, pp. 1-6, doi: 10.1109/UPEC49904.2020.9209836.

1.6 Thesis overview

This thesis investigates the power coordinated control of microgrid and its power quality problem, based on the complex environment and different mode of microgrid operation in real world. The main focus is to solve the problem of precise power sharing among multiple parallel inverters in microgrid, enables the microgrid to operate more stably in island operation and grid-connected operation, as well as switching between the two operation modes, and cooperate with the main grid to supply power to the load. Parallel control technology of multiple inverters in microgrid operation, microgrid grid-connected technology, and IEEE 14 buses test feeder model have been given investigated. The main chapters of the thesis are arranged as follows:

Chapter 1 briefly describes the background and significance of this thesis from the development basis of renewable energy, the challenges facing it and the importance of microgrid technology in solving the global energy crisis. Then it introduces the basic structure of microgrid and summarizes the research status of the key technology of power coordinated control of microgrids.

Chapter 2 introduces the inverter control method in the microgrid in detail, as well as the droop control, current and voltage double loop control, PWM control, and power adjustment between parallel inverters in different working modes.

Chapter 3 mainly studies the energy flow and circulating current between parallel inverters. Firstly, the energy flow and the energy flow analysis in the network model considered in this research are introduced. Secondly, the generation of circulating current is introduced and the circulating current between parallel inverters is analysed with the support of numerical simulation.

Chapter 4 mainly proposes the control methods developed in this project. It focuses on the improved inverter and the synchronization control module of the microgrid. Simulation

results are presented to verify the performance of the proposed improved droop control combined with pre-synchronization control methods.

In Chapter 5, the developed control method is employed by a microgrid system with parallel DG systems. Simulation results of this chapter show that the improved control method proposed can enable the microgrid to operate in islands, grid-connected operation, or switching between the two modes. The system runs stably and achieves the expected results. For second part of Chapter 5, to combine the model of the microgrid controlled by the improved droop control method with the IEEE 14 buses test feeder. The analysis of the test feeder parameters shows that the improved microgrid can be well applied to more realistic power distribution systems. System operation is verified with the simulation results.

Chapter 6, summarizes the main research content and innovations of this thesis, points out the focus and direction of further research work in the future.

Chapter 2 Inverter control techniques

In addition to meeting basic requirements such as volume, weight, and electromagnetic compatibility, the inverter in a power supply system also requires high electrical performance, such as high output voltage steady-state accuracy, low current waveform distortion, strong overload capacity, anti-load shock ability, and fast dynamic response [54]. To meet these requirements, the main circuit and control system should be designed carefully. The realization of most performance indicators of inverter power supply depends on the control system.

2.1 Inverter configurations

The inverter is divided into single-phase and three-phase according to the number of output phases. The three-phase inverter can be composed of a three-phase half-bridge structure or can be composed of three single-phase inverters with a phase difference of 120 degrees. Therefore, the technology of single-phase inverter can also be applied to three-phase inverter.

There are many types of inverters, which can be classified in different ways [55, 56].

According to the frequency of the inverter's output AC energy, they can be divided into industrial-frequency inverters, medium-frequency inverters, and high-frequency inverters. The frequency of an industrial frequency inverter is 50 or 60 Hz inverter; the frequency of a medium frequency inverter is generally 400 Hz to a dozen kHz; the frequency of a high frequency inverter is generally a dozen kHz to MHz.

According to the number of phases of the inverter output, they can be divided into single-phase inverters and three-phase inverters.

According to the form of the main circuit of the inverter, it can be divided into single-ended inverters, push-pull inverters, half-bridge inverters and full-bridge inverters.

According to the DC power supply, they can be divided into voltage source inverters (VSI) and current source inverters (CSI). For VSI, the DC voltage is nearly constant, and the output

voltage is an alternating square wave; for CSI, the DC current is nearly constant, and the transmission current is an alternating square wave.

According to the inverter control method, they can be divided into pulse frequency modulation (PFM) inverters and pulse width modulation (PWM) inverters.

According to the number of levels at the output, they can be divided into regular two-level inverter and multi-level inverter. The multi-level inverter is divided into four parts: flying capacitor inverter, diode-clamped inverter, hybrid inverter and cascade H-type inverter.

In this project, the standard VSI H-bridge topology inverter is the main object to study.

2.1.1 Single-phase inverters

The main circuit topology of single-phase H-bridge topology inverter is shown in Figure 2.1. There are mainly three types: half-bridge, full-bridge, and push-pull.

The amplitude of the voltage waveform at the output of the half-bridge circuit is only half of the DC bus voltage, so the voltage utilization rate is low [57]. However, in the half-bridge circuit, two large capacitors $C1$, $C2$ can be used to automatically compensate for the asymmetric waveform, which is a major advantage of the half-bridge circuit.

The voltage utilization rate of the full-bridge circuit and the push-pull circuit is the same, both are twice as large as the half-bridge circuit. However, full-bridge and push-pull circuits have the problem of transformer DC imbalance, measures need to be taken to solve it. Also push-pull is adopted for low power scales, which has not be considered in this thesis [58]. Medium-capacity and large-capacity inverters mostly adopt the full-bridge structure. Its control method is relatively flexible, mainly including bipolar and unipolar frequency doubling.

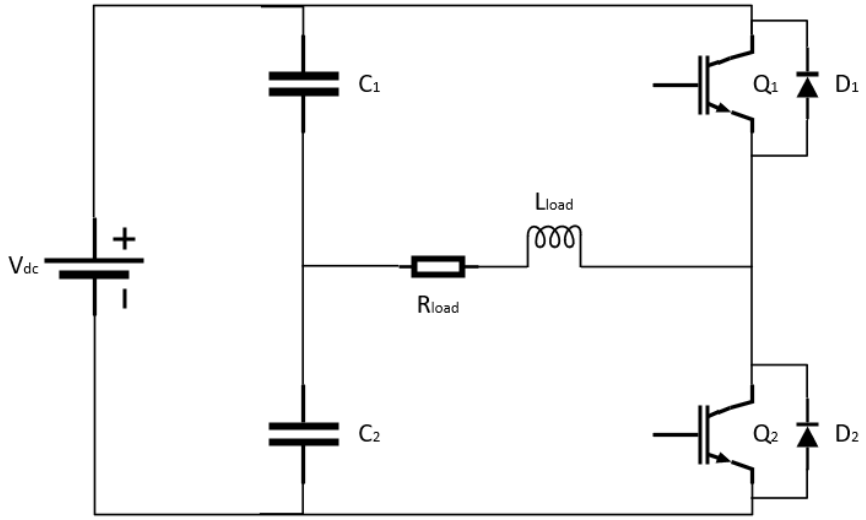

(a) Half-bridge

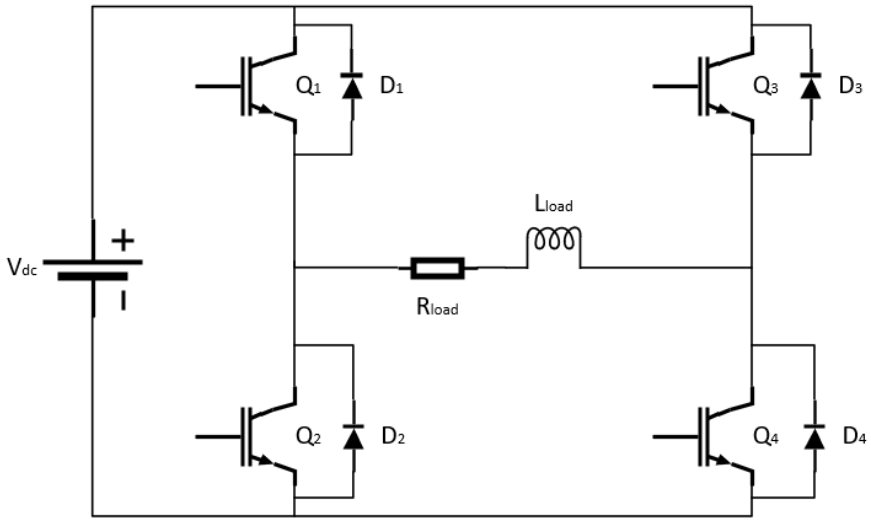

(b) Full bridge

Figure 2.1 Circuit topology of single-phase inverter

2.1.2 Three-phase inverters

The three-phase bridge and the three-phase based on single phase full bridge have formed a relatively fixed mathematical modelling method in long-term applications.

2.1.2.1 Three-phase H-bridge inverter configuration

The mathematical modelling of the traditional three-phase bridge inverters is established on two set voltage reference points, as shown in Figure 2.2. As shown, point O represents the midpoint of the three-phase voltage of the power grid, and point N is the midpoint assuming that the DC side capacitor voltage is divided into two.

Set the switching function S_i to characterize the turn-on and turn-off of the two switches of a single bridge arm i:

$$S_i = \begin{cases} 1 & Phase\ i\ up\ switch\ turn\ on, down\ switch\ turn\ off \\ 0 & Phase\ i\ down\ switch\ turn\ on, up\ switch\ turn\ off \end{cases} \qquad i = a, b, c$$

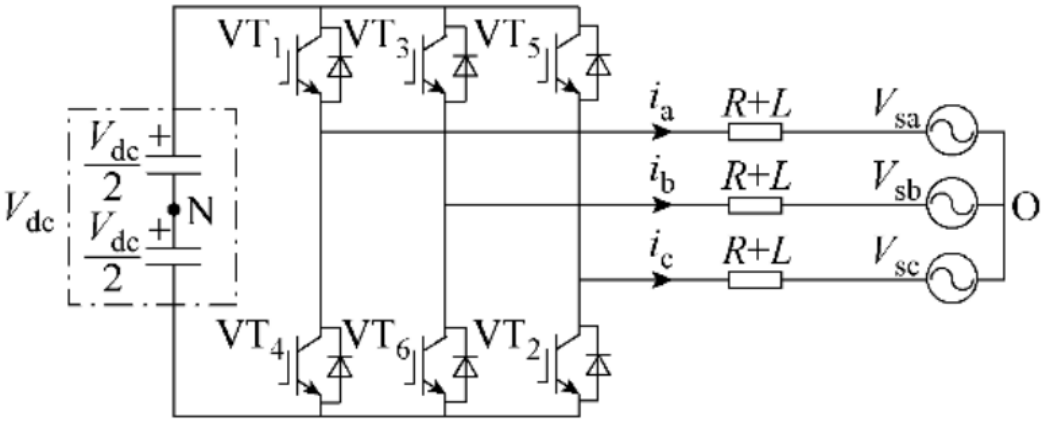

Figure 2.2 Three-phase bridge inverter configuration

Assuming that the three-phase output inductance and output resistance are all R+L, the mathematical model established based on figure 2.2 is shown in equation (2.1) below,

$$\begin{cases} L\frac{di_a}{d_t} + Ri_a = V_{sa} - S_a V_{dc} - u_{NO} \\ L\frac{di_b}{d_t} + Ri_b = V_{sb} - S_b V_{dc} - u_{NO} \\ L\frac{di_c}{d_t} + Ri_c = V_{sc} - S_c V_{dc} - u_{NO} \\ u_{NO} = \frac{1}{3} V_{dc}(S_a + S_b + S_c) \end{cases} \tag{2.1}$$

V_{sa}, V_{sb}, and V_{sc} represent the voltage of each phase of the power grid relative to the midpoint O at the point of common coupling (PCC) respectively. Usually the power grid is a

three-phase three-wire system, and the voltage at the midpoint is difficult to obtain, so V_{sa}, V_{sb}, and V_{sc} represent neither line nor phase voltages and have no real physical meaning [59].

2.1.2.2 Three-phase based on single phase full bridge inverter configuration

Single-phase full bridges are mostly used in single-phase systems, and three delta-connected single-phase full bridges can also be used as a three-phase inverter. This section discusses the mathematical model of this combined three-phase inverter, as shown in the Figure 2.3 [59].

Set the switching function S_j to characterize the turn-on and turn-off of a single-phase full-bridge switch

$$S_j = \begin{cases} 1 & (VT_1, VT_4\ turn\ on, VT_2,\ VT_3\ turn\ off) \\ 0 & (VT_1, VT_2\ turn\ on\ or\ turn\ off) \\ -1 & (VT_2, VT_3\ turn\ on, VT_1,\ VT_4\ turn\ off) \end{cases} \quad j = a, b, c$$

The DC side voltage can be directly used to describe the inverter single-phase output voltage V_{cAB}, V_{cBC}, V_{cCA} as S_j:

$$\begin{cases} V_{cAB} = S_a V_{dc} \\ V_{cBC} = S_b V_{dc} \\ V_{cCA} = S_c V_{dc} \end{cases}$$

From Figure 2.3, assuming the system line voltage of PCC are V_{sAB}, V_{sBC}, V_{sCA}, the mathematical modelling of three-phase based on single phase full bridge inverter is:

$$\begin{cases} V_{sAB} = S_a V_{dc} + i_a R + L\frac{di_a}{d_t} \\ V_{sBC} = S_a V_{dc} + i_b R + L\frac{di_b}{d_t} \\ V_{sCA} = S_a V_{dc} + i_c R + L\frac{di_c}{d_t} \end{cases} \tag{2.2}$$

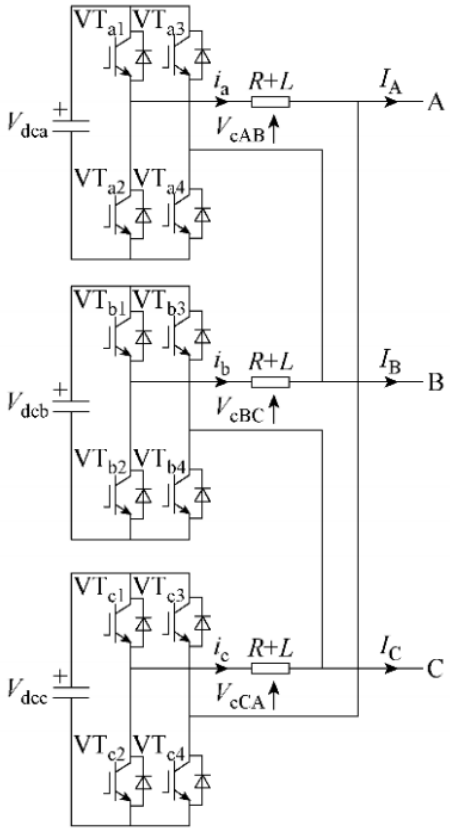

Figure 2.3 Three-phase based on single phase full bridge inverter configuration

2.2 Inverter operated in islanding mode and grid-connected mode

Distributed power sources with power electronic converters as interfaces in microgrid systems are mainly divided into two categories. One is grid-connected inverters for renewable energy, such as wind power, photovoltaic power generation and small hydropower, and the other is grid-connected inverters for non-renewable energy, such as micro gas turbines and energy storage systems [60-63]. For renewable energy power generation, such as wind and photovoltaic, the control goal is the maximum utilization of renewable energy, regardless of whether the system is operating in the island or grid-connected mode. In this case, the PQ control method is adopted. For micro gas turbines or energy storage systems, they are controlled according to the reference active and reactive power during grid-connected operation or droop control can be used. When the microgrid is running at islanding mode, droop control can provide voltage and frequency support for the system. When the system switches from grid-connected mode to the island mode, the support of voltage and frequency, power distribution during island operation and voltage synchronization control

during island-to-grid switching are all performed by grid-connected converters of micro gas turbines or energy storage systems. In the thesis, a detailed simulation analysis of islanding operation, grid-connected operation and switching between these two modes of the microgrid is presented.

2.2.1 Grid-connected mode

The main goal of the grid-connected inverter is to realize the output of active and reactive power according to the higher-level control order, as discussed in Chapter 1. The establishment of the mathematical model under the grid-connected state is a prerequisite for the analysis of the operation performance of the microgrid inverter. Decoupling control of active and reactive power, anti-interference of output power against grid voltage fluctuations, and output power quality are the main assessment criteria of grid-connected inverters' performance [64]. As discussed in Chapter 1, the grid-connected inverter in a microgrid can adopt the PQ control mode or the droop control mode. At present, the research on the grid-connected performance of the microgrid inverter in the PQ control mode has been sufficiently studied in the literature, while the grid connected inverter using the droop control mode needs to be further studied.

2.2.1.1 Grid connected inverter with PQ control

For the grid connected inverter with PQ control, whether it is based on the adjustment of the rotating coordinate system or the adjustment of the static coordinate system, the analysis of the mathematical model establishment, power de-coupling and noise immunity are fully discussed in the literature [65-68]. The mathematical model of the grid connected inverter with PQ control in the rotating coordinate system has been presented in [65, 66] with analysis of the control performance and parameter selection of the regulator. Likewise, the control performance of the grid connected inverter with PQ control in the static coordinate system is analysed in [67]. In [68], the de-coupling performance and anti-interference performance of the grid connected inverter with PQ control under static and rotating coordinate systems are analysed and a method is proposed to improve the dynamic performance of the grid connected inverter.

In terms of harmonic current suppression, research on grid-connected inverters for new energy power generation using PQ control modes has been carried out very early and is relatively mature. The application of various harmonic separation methods, synchronous rotating coordinate system with PI and Proportional-Integral-Resonant (PIR) control, stationary coordinate system with PR control have been fully studied and achieved good results [47, 69].

2.2.1.2 Grid connected inverter with droop control

For microgrid inverters using P-f and Q-V droop control modes, according to the idea of smaller resistance-inductance ratio, better decoupling performance [70]. Most of the current literature is aimed at the design of output impedance when modelling and analysing droop control [71-76], taking voltage and current closed-loop parameters and external hardware parameters, etc. as the main research objects. In [72], the output impedance is made to appear inductive by designing the voltage loop and current loop parameters of the microgrid inverter, which reduces the coupling of active and reactive power. In [74-76], the output impedance-to-inductance ratio of the microgrid converter is reduced by introducing virtual impedance, reducing the coupling of active and reactive power. In [71], the complementary method of virtual inductance and external inductance is adopted which puts forward the "proportioning principle" of virtual inductance and external inductance parameter selection by analysing the stability of the system. Some researchers use the above two methods of control parameters and virtual impedance to coordinate adjustment [73, 77]. In addition to considering the selection of control parameters for the design of output impedance, a small signal model for grid-connected inverters is derived and the influence of control parameters on system stability is discussed through root locus analysis in [78, 79]. In these papers, droop coefficients, power filter coefficients, etc. are the objects. At present, there is no effective overall modelling scheme for grid-connected inverters, which can be used to analyse the performance of microgrid inverters.

Similar to the new energy power generation grid-connected inverter, the output power quality of the grid-connected inverter using the droop control must meet certain standard requirements [80-82], especially under weak grid conditions (which means that the voltage at the connecting point will be very sensitive to any variation of the load) at the end of the distribution network, the power quality is poor. Achieving the power quality of the microgrid

inverter in the environment with background harmonic in the power grid is a problem that must be paid more attention, in most of the studies in the literature focus on the control of the harmonic voltage at the point of common coupling (PCC) of the grid-connected system [83] [98]. In [84], harmonic currents control loop is added to the droop control to suppress the harmonics in the output current of the microgrid inverter by modulating the harmonic current command. This method requires fast detection and separation of each subharmonic of the microgrid inverter output current. On the other hand, the suppression of harmonic current in [98] is carried out in the droop control voltage regulation. According to the idea of harmonic virtual impedance, the information of each harmonic voltage of the power grid is detected and introduced into the voltage loop command. To control the grid-connected harmonic current, the output harmonic current is compensated for and suppressed by changing the harmonic voltage command. This method requires rapid detection and separation of each harmonic voltage of the power grid. The harmonic current suppression methods in the above literatures all need to increase the detection and separation of harmonic components in the voltage or current, which requires high detection time and increases the burden on the controller. How can it be simple and effective suppression of output harmonic currents based on the droop control requires further discussion and research.

2.2.2 Grid synchronization

Grid synchronization refers to a very important step that needs to be taken before the generator is integrated into the main grid. Through this step, the four conditions required for the generator to be integrated into the grid can be met. Which are: the frequency of the generator is the same as the frequency of the main grid; the output voltage of the generator is the same as the voltage of the main grid, and the maximum error range should be within 5%; the phase sequence of the generator is the same as the phase sequence of the main grid; the phase angle of the generator voltage is the same as the phase angle of the main grid voltage. Therefore, the synchronization of the microgrid and the grid is an important prerequisite to ensure the stable operation of the microgrid [85].

2.2.2.1 Phase Locked Loop (PLL)

Phase locked loop (PLL) usually consists of three parts: a phase detector (PD), a loop filter (LF) and a voltage-controlled oscillator (VCO). The main block diagram of the phase locked loop is shown in the Figure 2.4 shows:

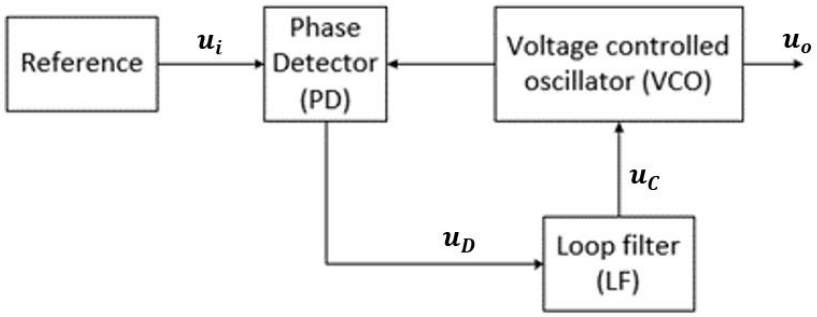

Figure 2.4 Principal block diagram of the phase locked loop

The phase detector in the PLL is also called a phase comparator. Its function is to detect the phase difference between the input signal and the output signal and convert the detected phase difference signal into a $u_D(t)$ voltage signal for output. The low-pass filter forms the control voltage $u_C(t)$ of the voltage-controlled oscillator, which controls the frequency of the oscillator output signal.

In the grid-connected system, accurate main grid voltage phase angle and frequency measurement are very important. It is related to the power factor correction and the control of active and reactive power output in the grid-connected operation mode of the microgrid. The phase angle estimation of SSRF-SPLL is adaptively updated by a closed loop to track the actual frequency and phase angle, which structure is very simple, and be widely used for grid connected systems [86].

2.2.2.2 Single Synchronous Reference Frame Software Phase Locked Loop (SSRF-SPLL)

The control block diagram of the single synchronous reference frame software phase-locked loop (SSRF-SPLL) used in this project is shown Figure 2.5. This PLL is generally suitable for the detection of phase, frequency, and amplitude when the grid voltage is balanced.

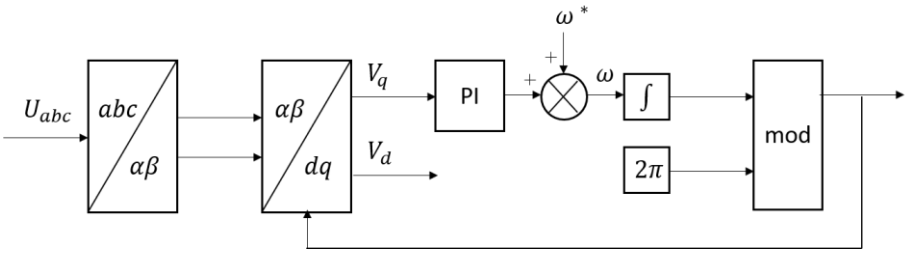

Figure 2.5 Three-phase PLL control block diagram

First, the sampled voltage is transformed from a three-phase stationary coordinate system to a two-phase stationary vertical coordinate system, referred to as abc/αβ transformation (also called Clarke transformation); then through a two-phase stationary coordinate system to a synchronous coordinate system, referred to as αβ/dq transformation (also called Park transform). The advantage of this transformation is that it can transform the sinusoidal signal in the three-phase stationary abc coordinate system into DC signal in the synchronous dq coordinate system. In the synchronous coordinate system, according to the basic performance requirements of the work of the phase-locked loop, that is, the vectors V_{pll} and V (V_{pll} is the vectors voltage of PLL controller; V is the actual vectors voltage) must be completely coincident to achieve phase lock, which requires that $V_q = 0$ to achieve phase lock. In fact, the output of the PI controller is

$$\Delta\omega = \omega^* - \omega$$

Where ω^* is the reference angular frequency and ω is the actual angular frequency. By proper setting, the K_p and K_i parameters of the PI controller, $\Delta\omega = 0$, and $V_q = 0$ can be achieved. Here, the limit of advanced mathematics is used. When $x \to 0$, $SinX = X$ holds and $V_q = Vsin\,(\omega^* - \omega)t$. And due to 100π is the rated frequency of the power grid, the target angular frequency can be fed to the integrator in Figure 2.5. In addition, there is another point to note, that is the limit value, because the engineering requires the fluctuation range of frequency f is 0.5 Hz [87], according to $\omega = 2\pi f$, calculate the range of $\Delta\,\omega$. This requires seeing the complete negative waveform when setting the PI regulator parameters, not the waveform that will be clipped. Then go through the integration link to get the phase. The role of Mod here is to set the phase output range, generally $0 \sim 2\pi$. From Figure 2.6, the closed-loop transfer function G_{pll} of the PLL can be obtained as:

$$G_{pll} = \frac{\theta\prime}{\theta} = \frac{U_s(k_p+\frac{k_i}{s})\frac{1}{s}}{1+U_s(k_p+\frac{k_i}{s})\frac{1}{s}} = \frac{U_s(sk_p+k_i)}{s^2+U_s(sk_p+k_i)} = \frac{U_s(sk_p+k_i)}{s^2+sk_pU_s+k_iU_s} \quad (2.3)$$

where U_s is peak phase voltage.

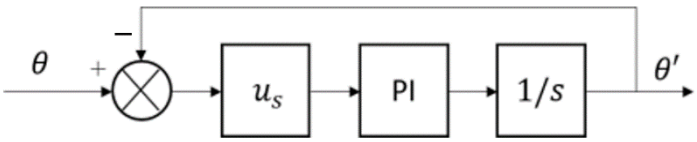

Figure 2.6 Equivalent control block diagram

2.3 Parallel connected inverter control method

2.3.1 Droop control

In Section 1.3.3 an introduction to droop control is given, as well as two different conventional droop control theories, P/f with Q/V droop control and P/V with Q/f droop control. In this thesis the main focus is on the former.

The conventional droop control strategy is based on the premise that the system impedance is inductive, but in the low-voltage transmission system, the line impedance is resistive, so that the system active power and reactive power cannot be decoupled well. Therefore, researchers have proposed that droop control can enable energy management for microgrids connected to the grid. However, certain adjustments have to be made, as there are large deviations in voltage and frequency during islanded operation. Therefore, the inclusion of a direct voltage and frequency regulation unit in the control loop enables energy management and also enables secondary regulation of voltage and frequency, so that the microgrid can maintain voltage and frequency at rated values or with small deviations in islanded operation mode.

There are two methods of droop control: one is based on measuring the frequency of the system and its output voltage amplitude to produce the reference frequency and reference voltage of inverter [32]. The other method is based on inverter output active power and reactive power to produce the reference output voltage amplitude and reference frequency of the inverter [88]. Since the main research objective of this thesis is the power distribution in parallel inverters with different line impedances, the latter control theory has been employed.

The relationship between inverter output active power, reactive power and frequency and output voltage can be expressed as:

$$f = f_0 - m(P_0 - P)\ ; V = V_0 - n(Q_0 - Q) \tag{2.4}$$

where V is the inverter voltage amplitude; f is the frequency of the output voltage of the inverter; V_0, f_0 are the output voltage amplitude and frequency when the inverter running at no load, respectively; m, n are droop coefficient of P/f and Q/V, respectively. f_0 and m are called the active power setting parameters of the inverter, while V_0 and n are called the reactive power setting parameters of the inverter. Dynamically adjusting f_0 and V_0 can achieve droop curve moving parallel, to realize the role of microgrid second frequency modulation (FM); dynamic regulation of m and n to change slope of the droop curve, to adjust the unbalanced power transients between the DGs, but also to achieve steady output power of the inverter. Figure 2.7 shows the droop characteristic of conventional droop control.

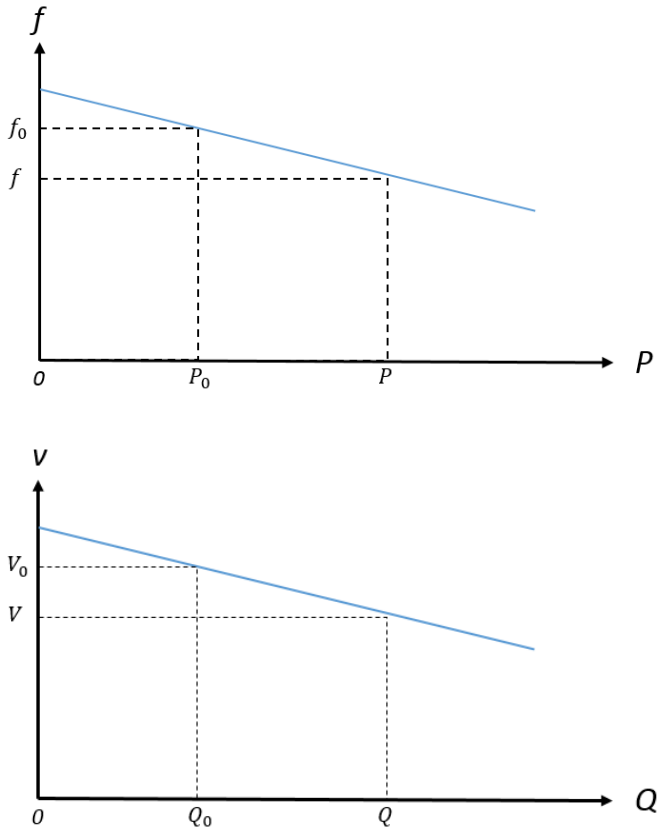

Figure 2.7 Droop characteristics of conventional P/f and Q/V droop control

2.3.1.1 Adaptive droop

In the low voltage microgrid, the impedance of the circuit is resistive, and the P-V droop control is often used in each inverter, the existence of the circuit impedance and the local load are the main reasons that affect the precision of load distribution. Some scholars have proposed methods to solve the low accuracy of load distribution.

In [89], a control strategy is proposed to share the load according to the capacity of the inverter, however, the local load is not simulated. In [78], the droop coefficient required for the load equalization of the isolated network is calculated by the line impedance and the local load estimated by the grid connection. This can improve the load sharing but cannot completely eliminate the distribution error. In [77], the traditional drooping control system with the line resistance and reactive power of the first term, better to complete the power division, but this approach needs line resistance value. In [90], the output voltage of each inverter is adjusted by the integral value of the difference between the reference value and the actual value of the reactive power. However, the power distribution is not accurate enough, and the output voltage is reduced.

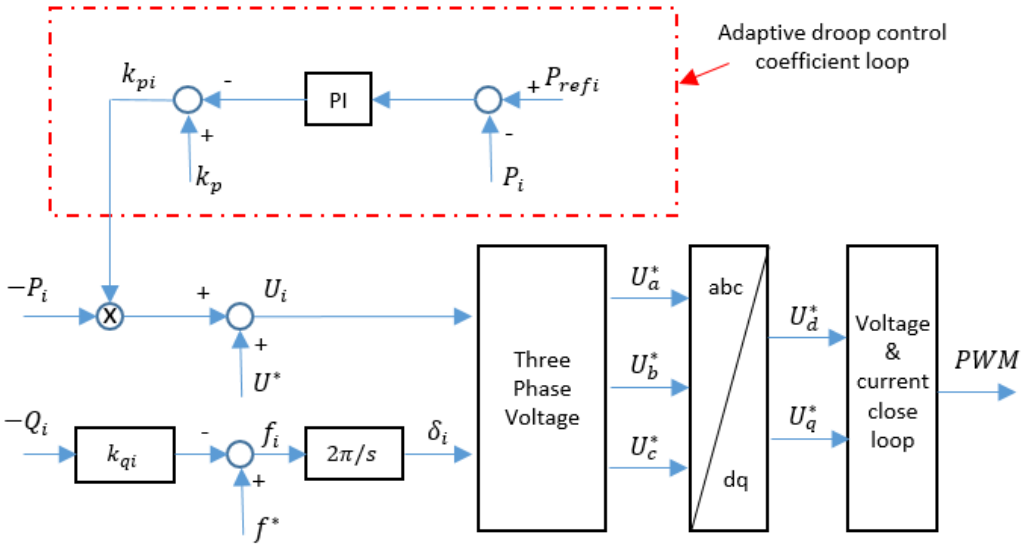

Figure 2.8 Block diagram of adaptive regulating droop coefficient control for DG

The block diagram of adaptive P-V droop control is shown in Figure 2.8. As shown, the outer loop is the power loop, responsible for the load distribution while the inner loop is responsible for stabilizing the output voltage and improve the dynamic response of the current. In this adaptive droop control method, the active droop coefficient is automatically adjusted according to the output power. The droop control equation is:

$$U_i = U_i^* - \left[k_p - \left(D_p + \frac{D_i}{s}\right)\left(P_{refi} - P_i\right)\right] P_i \tag{2.5}$$

$$f_i = f_i^* + k_{qi} Q_i \tag{2.6}$$

where k_p is the rated active droop coefficient; D_p and D_i are the proportional and integral coefficients of the PI regulator respectively; P_{refi} is rated active power of DG. To achieve active power be divided equally between n unit DG in island mode, need meet

$$P_{refi} = (P_1 + P_2 + \cdots + P_n)/n \tag{2.7}$$

To distribute the load proportionally, simply change P_{refi} which be sent from central controller to local controllers.

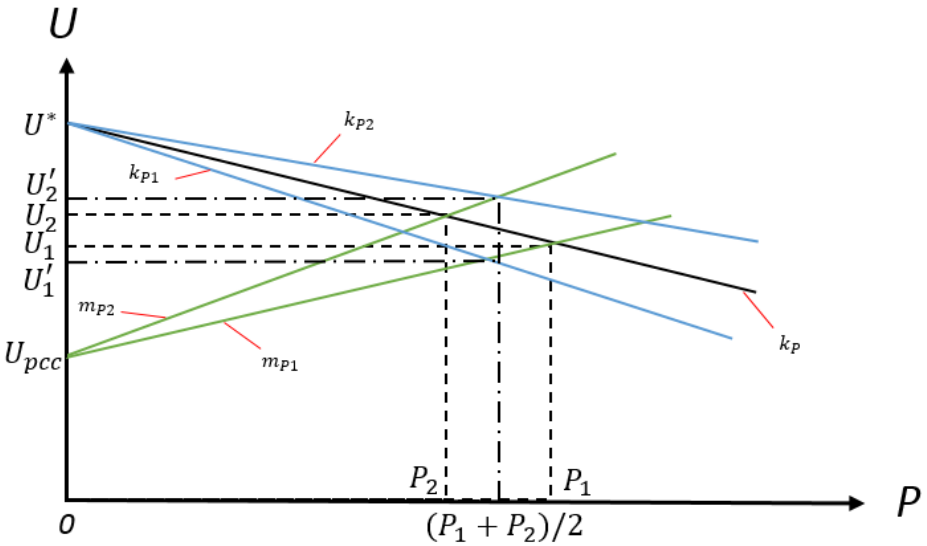

Figure 2.9 Adaptive regulating of P-V droop coefficient

Figure 2.9 shows how the droop curve adjust automatically. In this figure, it is assumed that two inverter-based generation systems (DG1 and DG2) are connected to the same PCC with different line impedances (Z1 and Z2) and they use the same drooping coefficient k_p at the start of the system operation. Since the line impedance does not coincide with ZL2>ZL1, the inverter outputs active power $P_2 < P_1$, and the output power of each inverter deviates from $P_{ref} = (P_1 + P_2)/2$, then P_{ref} is different from $P_1 and\, P_2$ to adjust the droop coefficient. For DG1, the inverter output power $P_1 > P_{ref}$, so after PI adjustment output is negative, because k_p is positive, DG1 droop coefficient gradually increased to k_{p1}, and finally when $P_1 = P_{ref}$, DG1 output active power is stable; for DG2, the droop coefficient decreases from k_p to k_{p2}, where $P_2 = P_{ref}$. To achieve accurate equalization of active power.

2.3.1.2 Partial hysteresis droop

In microgrids using a droop control strategy, the amplitude of frequency and voltage can change significantly at the expense of grid voltage and frequency, especially when there are significant changes in microgrid loads. This is not allowed for some electrical equipment that requires high voltage and frequency stability requirements. Therefore, frequency and voltage amplitudes need to be limited. Because of the limited range of frequency and voltage amplitude fluctuations, the droop factor is small and the micro source cannot change in time and responds slowly under heavy loads; if the droop factor is increased to improve dynamic performance, the output voltage will deviate from the rated range, so the droop factor must be chosen in a way that mitigates the inherent conflict between performance regulation and power output range when using the sag method, but it is difficult to regulate both.

With the traditional droop control, the voltage amplitude and frequency in the distributed generation system can significantly deviate when operating in the island mode [91, 92]. Droop control strategy of piecewise hysteresis has been proposed in [93] which ensures that the system output frequency and voltage fluctuate within a preset range. However, the output power range with this method is limited.

In order to overcome the limitation in power range, a partial hysteresis droop control strategy has been proposed [94]. In this strategy, a three droop curves with large slope are used to replace the one droop curve with a small droop coefficient normally used in

conventional droop control, as shown in Figure 2.10. As shown, P/f and Q/V control is used with three droop curves 1, 2 and 3 instead of curve 4 which is used with conventional droop control. As the output power increases or decreases, the operating point of the system moves between the three characteristic curves. Hysteresis control is used to ensure that the microgrid output power at the critical value, the output power and voltage will be kept within the hysteresis window.

The use of a larger droop coefficient can greatly improve the dynamic system response. For example, assuming that, at the initial condition, the system is operating at point P1 (Figure 2.10), the output power of the system is Pn1, the output frequency is fn, and the output frequency changes up and down along the curve 1 when the system output power changes. As the load increases through B1 to C1 and then the operating point goes from C1 to point B2, then the system frequency output changes along curve 2 as the power output changes, then the system output power may increase or the system operating point will jump to curve 3. When the system output power decreases, the system operating point will not jump directly from B2 to C1, the system output frequency will continue to increase and when curve 2 reaches point A2, the system operating point jumps from A2 to B1 and again to curve 1. Similarly, when the system operating point jumps between curves 2 and 3, the operating principle is the same. Thus, curve 1, curve 2, curve 3 and the two hysteresis lines B1-C1-B2-A2-B1 and C2-D2-B3-A3-C2 together form a partial hysteresis P-f droop control strategy. Similarly, Q-V droop control is used for segmental control with the same process.

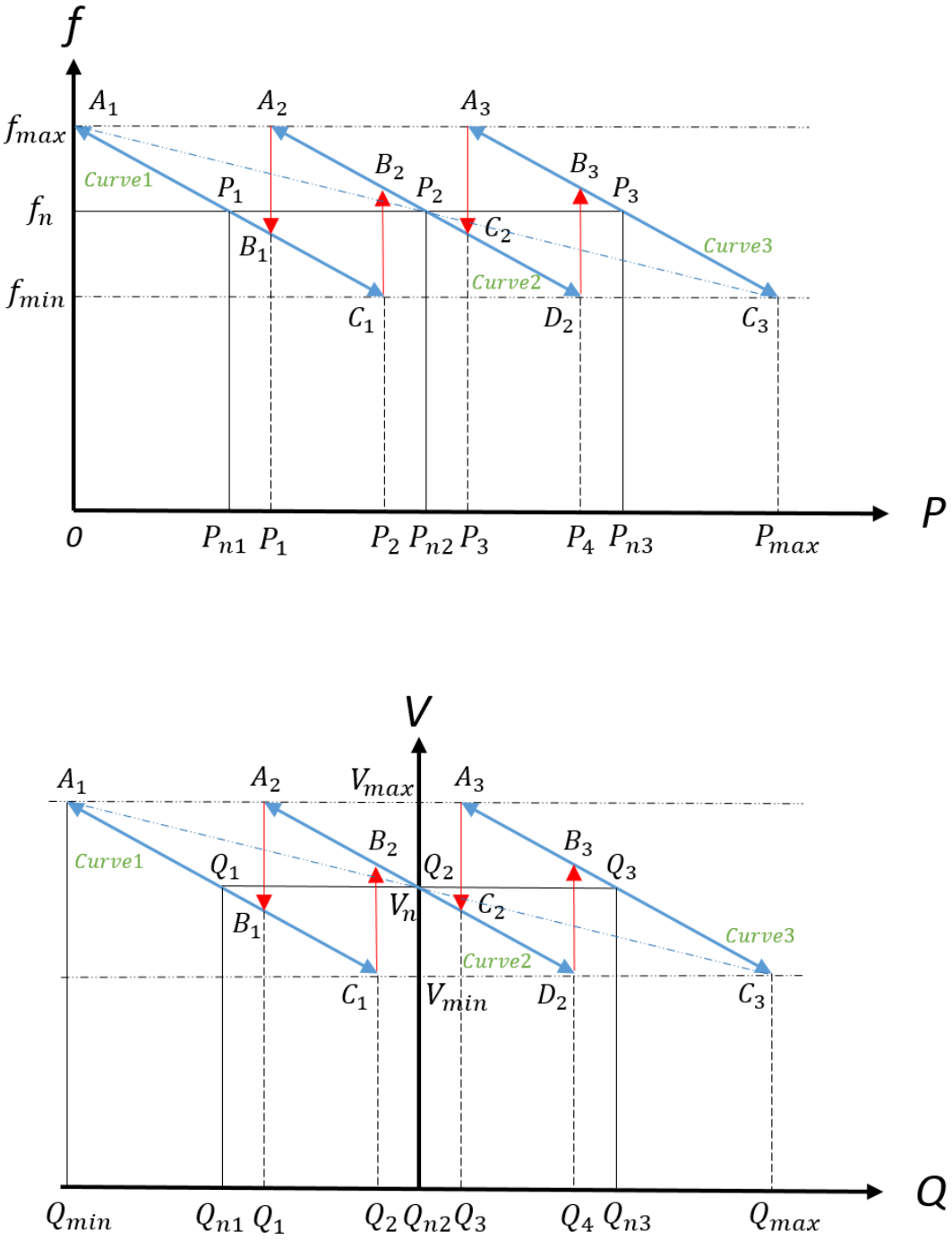

Figure 2.10 P/f and Q/V droop characteristics of partial hysteresis droop

2.3.1.3 Virtual impedance droop

The conventional droop control cannot provide a balanced reactive power sharing among parallel-connected inverters under line impedance mismatch. This imbalance in reactive power sharing is a serious problem in an AC microgrid. Also, with the traditional inverter droop control method, the line resistance should be much smaller than the line reactance as a prerequisite and the different conditions of different inverter circuit reactance are not considered. The method of adding the virtual impedance in the control can improve the inductive component of the inverter output impedance, but the excessive virtual resistance will reduce the output voltage and reduce the power quality [95].

In order to reduce power coupling, a virtual coordinate transformation method is proposed in [32], but the stability of the microgrid is reduced. Another way to solve the power coupling problem is to control the virtual impedance of the inverter [96]. This method converts the resistive line impedance into inductive to decouple the power supply. A familiar virtual impedance method to introduce a larger virtual inductance has been proposed [73]. Although this method limits the power coupling, the system harmonics increase, the presence of line resistance inevitably affects the decoupling effect. Another effective method of virtual negative impedance as a decoupling power is proposed in another general virtual impedance method [97]. However, reactive power sharing is not accurate with line voltage drop.

Figures 2.11 and 2.12 show the control block diagram of a parallel inverter system with conventional droop control and a parallel inverter system with virtual impedance droop control respectively.

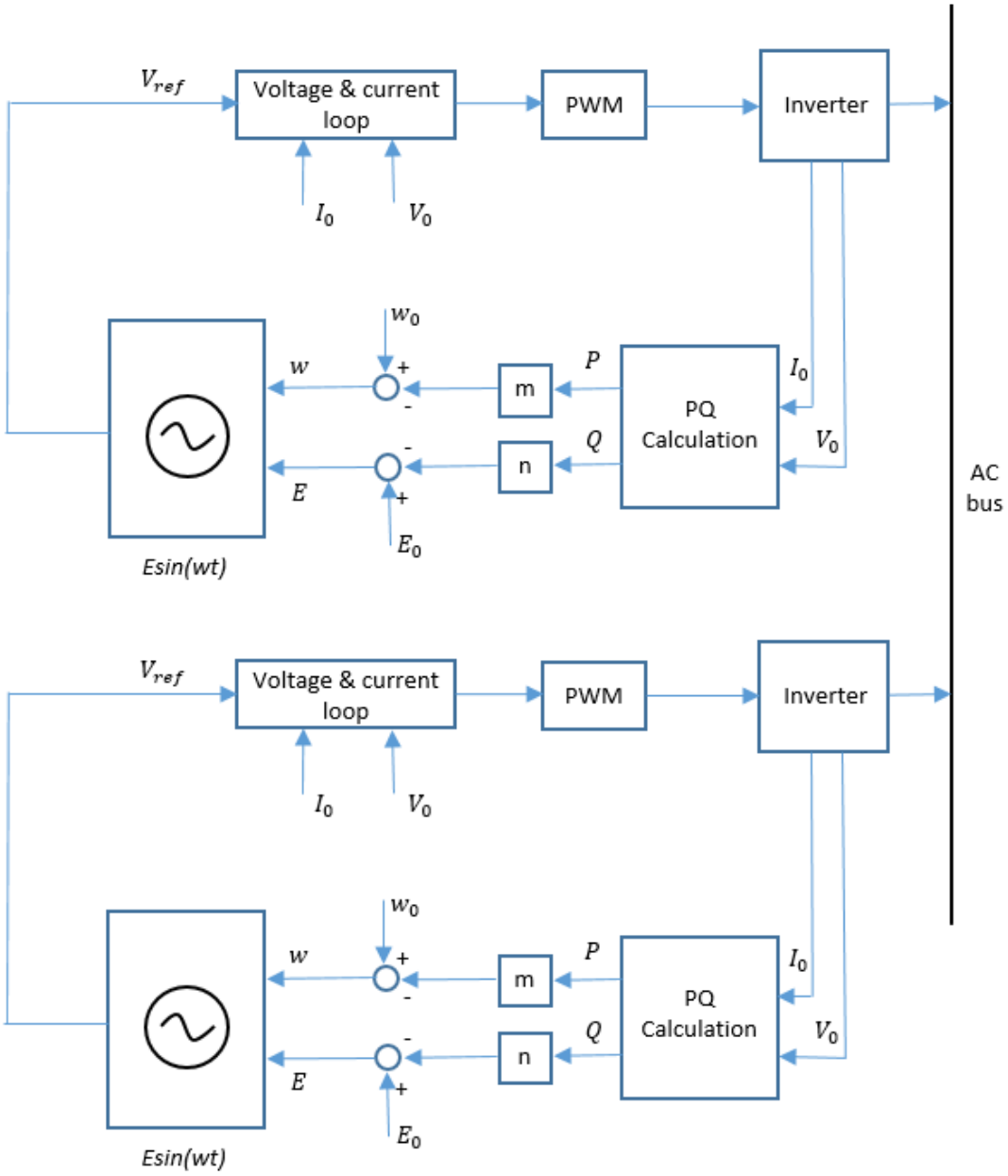

Figure 2.11 Block diagram of conventional droop control

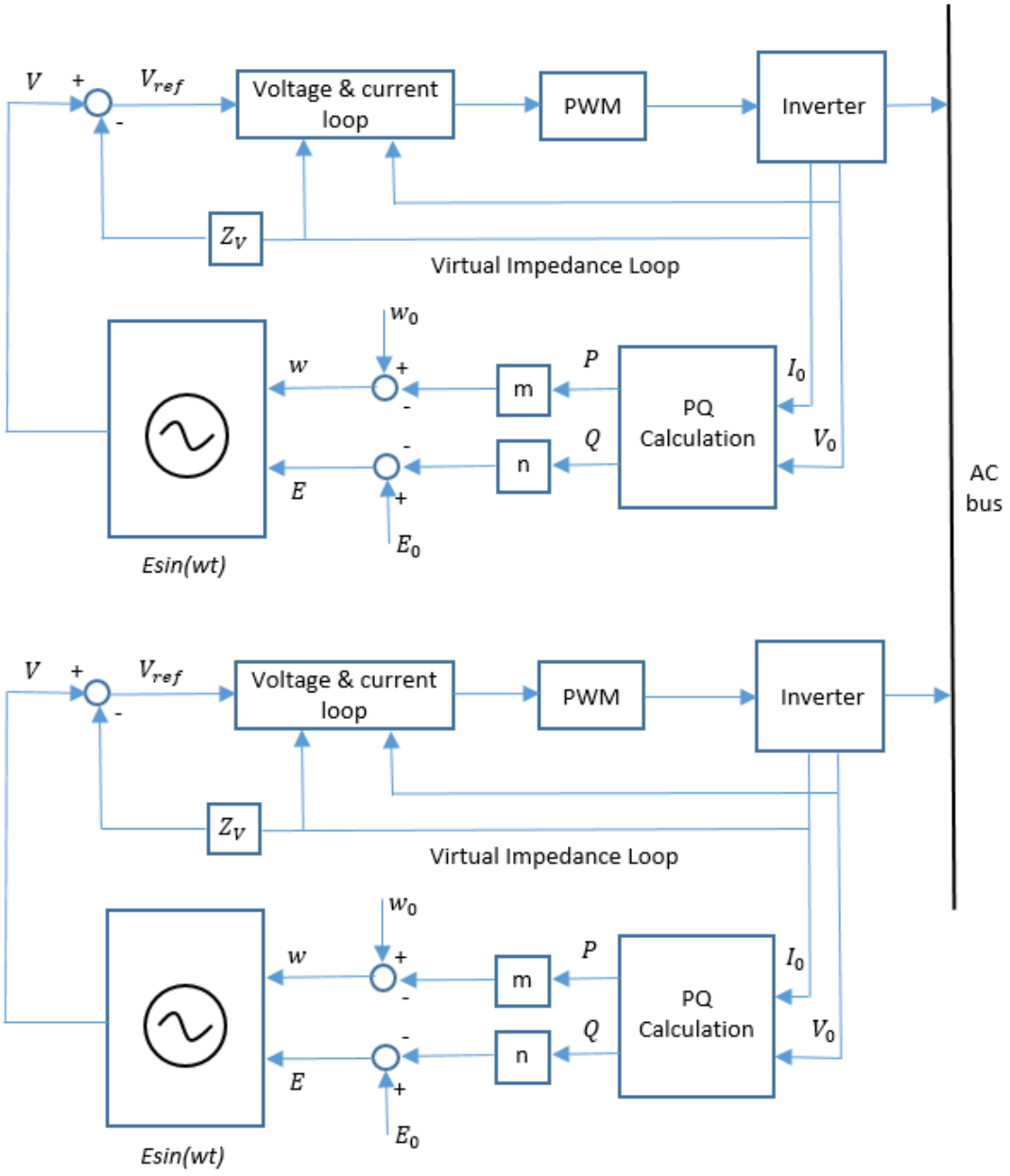

Figure 2.12 Virtual impedance loop-based droop control

For the parallel inverter system with virtual impedance droop control, the reference voltage from each inverter can be modified, as follow:

$$V_{ref} = V_0 - Z_V I_0 \tag{2.8}$$

Where: Z_V is the virtual output impedance.

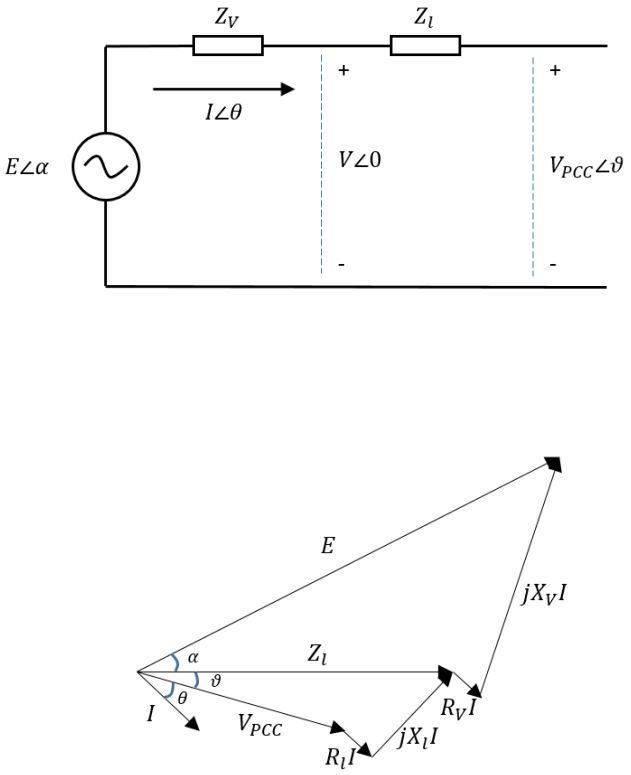

Figure 2.13 Equivalent model of a virtual impedance and phasor diagram

The equivalent model of virtual impedance and the phasor diagram of $Z_V > Z_l$ are showed in Figure 2.13. The virtual impedance is generally selected to control line impedance. So, the virtual output impedance can be chosen by the summation approach, in which balanced reactive power sharing is achieved if the voltage drops from every inverter to AC bus:

$$V_{drop1} = (Z_{l1}+Z_{v1})I_{l1} = V_{drop2} = (Z_{l2}+Z_{v2})I_{l2} \tag{2.9}$$

In this equation, Z_{v1} and Z_{v2} are the virtual output impedance of two parallel connected inverters, moreover, Z_{l1} and Z_{l2} are line impedance of two parallel connected inverter, respectively.

In the summation approach, one virtual output impedance is set at zero, and the other virtual output impedance is set to emulate the line impedance. Based on the equation and considering that one line impedance is larger than another, e.g., $Z_{l1} > Z_{l2}$, which permits the selection of $Z_{v1} = 0$ and the equation can be simplified as:

$$Z_{v2} = Z_{l1} - Z_{l2} \tag{2.10}$$

The value of the virtual impedance is decreased using the summation approach, which minimizes the degradation of voltage regulation. Reactive power sharing is improved if the change in output voltage is markedly higher than the voltage drops across the line than the reactive power. At the same time, for virtual impedance droop control, it has certain disadvantages. For example, when the system is sensitive to impedance measurements, this may lead to unstable operation or exceed the power output of the inverter. This thesis investigates parallel inverters with completely different output impedances, so virtual impedance droop control cannot be a suitable control method.

2.3.2 Voltage and current control loop design

The SPWM (Sinusoidal Pulse Width Modulation) based voltage and current dual-loop inverter control principal diagram is shown in Figure 2.14. The outer loop is an instantaneous voltage loop control, and the output voltage is compared with a reference voltage. The error signal is adjusted by the PI controller to provide the reference value to the inner current control loop which controls the inductor current. The inner loop provides the modulating signal which is compared with the triangular wave carrier to generate the SPWM control signal. Because the inductor current is controlled by the inner loop, this control method has the function of output current limiting. This increases the reliability of the system and has a better protective effect on inverter overload.

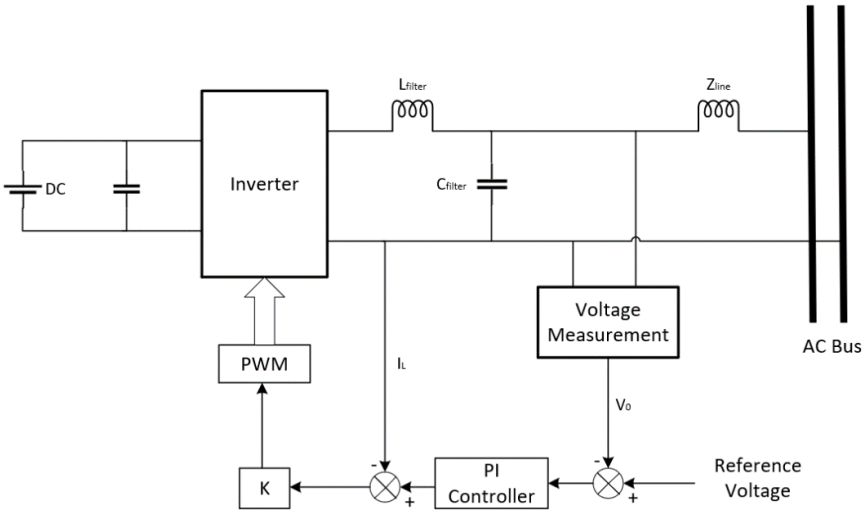

Figure 2.14 SPWM-based voltage and current dual-loop inverter control principal diagram

Ignoring the parasitic resistance of the inductor L and the capacitor C, the control block diagram of the voltage-current dual-loop inverter is shown in Figure 2.15. Where E is the DC bus voltage, R is the load impedance, L is the filter inductance value, C is the filter capacitor value, K_L is the inner loop current detection coefficient, K_U is the outer loop voltage detection coefficient, and K_{PWM} is the equivalent gain of the PWM link. The output voltage is compared with a given reference signal, and the error signal obtained is passed through the outer loop PI regulator $(K_{ps} + K_I)/s$, and its output is used as the inner loop given signal. The given signal of the inner loop is compared with the output current, the error signal obtained is calculated by the inner loop proportional regulator K times, and the control signal of the inner loop is obtained, and finally sent to the PWM modulator to control the generation of PWM pulses.

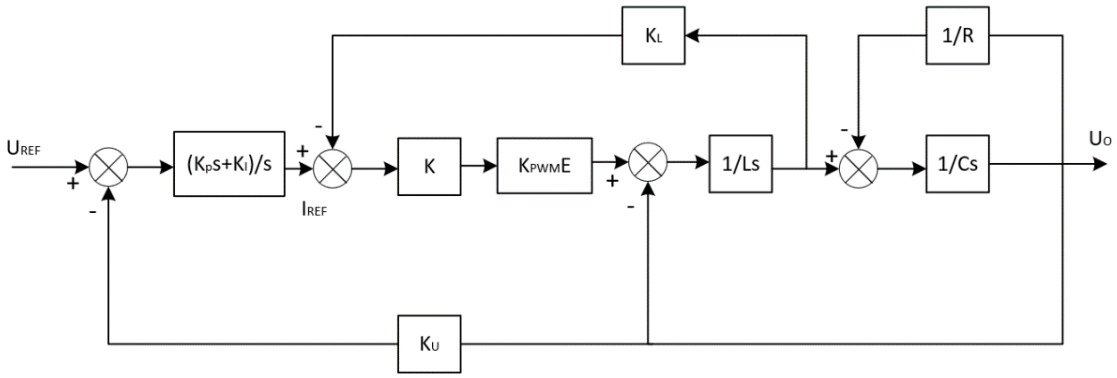

Figure 2.15 Control block diagram of the voltage-current dual-loop inverter

According to the control block diagram of the voltage-current dual-loop inverter in Figure 2.15, the current inner loop part is extracted as the object of analysis and research. Since there is a feedback component output voltage U_O in the current inner loop, to simplify the design process, we assume that the output voltage U_O is approximately constant within a switching cycle, and a simplified current inner loop block diagram is obtained, as shown in Figure 2.16.

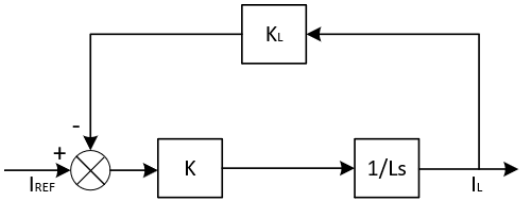

Figure 2.16 Simplified current inner loop block diagram

Assuming that there is no proportional coefficient K, the open-loop transfer function of the current inner loop G_{LO} is:

$$G_{LO} = \frac{K_L}{L_s} \tag{2.11}$$

At this time, the current path is a first-order system. When the feedback loop with a proportional coefficient of K is added, the open-loop transfer function of the system $G_{LO}{}'$ is:

$$G_{LO}{}' = \frac{KK_L}{L_s} \tag{2.12}$$

The closed-loop transfer function G_{LC} of the current inner loop is:

$$G_{LC} = \frac{\frac{KK_L}{L_s}}{1+\frac{KK_L}{L_s}} \tag{2.13}$$

When designing the voltage loop, it is considered that the output of the current loop can track the input. In the process of designing the voltage outer loop, the current loop is equivalent to a proportional link with a gain of 1. The block diagram of the voltage outer loop is shown in Figure 2.17.

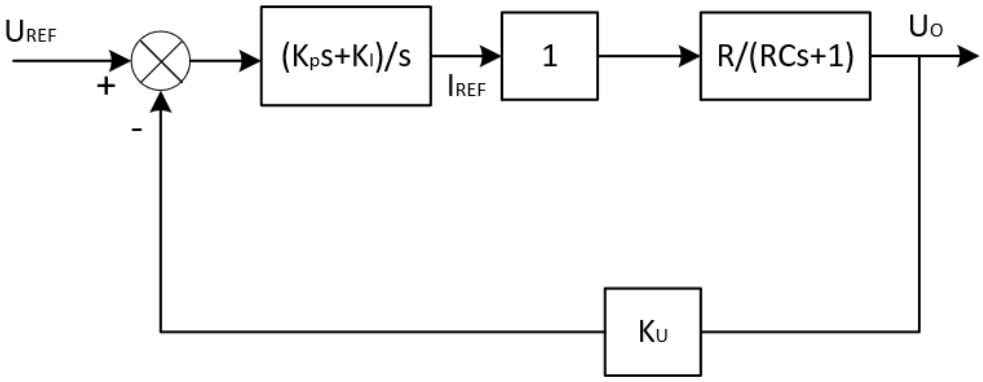

Figure 2.17 Simplified voltage outer loop block diagram

Before the voltage outer loop is added to the PI regulator, the open loop transfer function G_{UO} of the voltage outer loop is:

$$G_{UO} = \frac{K_U R}{RC_s+1} \tag{2.14}$$

To enable the system to obtain better dynamic performance and eliminate the steady-state error of the output voltage U_O, a PI regulator is introduced for compensation, and its open-loop transfer function $G_{UO}{}'$:

$$G_{UO}{}' = \frac{K_{ps}+K_I}{s}\frac{K_U R}{RC_s+1} = \frac{K_U R(K_{ps}+K_I)}{s(RC_s+1)} \tag{2.15}$$

Added the voltage closed-loop transfer function G_{UC} of the PI controller:

$$G_{UC} = \frac{\frac{K_U R(K_{ps}+K_I)}{s(RC_s+1)}}{1+\frac{K_U R(K_{ps}+K_I)}{s(RC_s+1)}} \tag{2.16}$$

2.3.3 Active load sharing techniques

2.3.3.1 Master slave control

In master slave control, the master inverter regulates the voltage and frequency and other inverters become slaves. In other words, the master module acts as a voltage source while the slaves operate as current sources. In general, this control technique achieves good current sharing and stability. There are some variants to this control technique, which depend on the selection of the master module. In a dedicated scheme, one fixed module is selected as the master unit. There is also a rotating scheme in which the master is arbitrary chosen. In another variant, the module that produces maximum rms current is selected as the master module [30].

In [31], the reference current for slave inverter was source from the power distribution center while in [32], output current from the master module was used as reference current for the slave module. The authors in [33] introduced a phase control algorithm into the conventional master slave technique to enable precise current sharing even if the modules have different ratings. *P* and *Q* share buses that are driven by the inverter that has the highest output power (master inverter), was proposed in [34]. In this approach, slave inverters calculate the difference between their output power and the power in the shared buses and adjust in the output voltage frequency and amplitude. Another variant of the master control strategy is current limitation control [35]. In this technique, there is a master module that controls the load voltage and the slave modules only supply and share the load current with the master module. A slave module receives a reference current command from the previous

module which has limited amplitude, resulting in no sinusoidal output current from each inverter.

2.3.3.2 Circular chain control (3C)

In the 3C technique [36, 37], successive inverter modules track the current of the previous inverter to achieve equal current distribution. The first module tracks the last to form a circular chain connection. Each inverter regulates its output voltage based on the common reference voltage. However, a problem occurs when there is a damaged or failed inverter in the loop. If this is not detected and isolated quickly, it will impact the performance of the overall system and in the worst case, can cause total system failure. Two lines are usually used for communication to achieve bidirectional communication and to increase reliability.

2.3.3.3 Centralized control

In this technique, the central controller regulates the load voltage in an outer loop and sends reference current to each inverter. The reference current is determined by adding the output of voltage controller and the average load current (total load current divide by number of inverters). The current controller in each inverter processes the difference between the reference current and its output current. This control technique produces excellent current sharing but lacks reliability and redundancy. The need to measure load current renders this control unsuitable for system with distributed loads.

2.4 Summary

In this chapter, the previous part mainly introduces the classification, structure, and operation mode of the inverter, and determines the inverter type used in this project. The second part mainly introduces the control methods used in different operation modes of the inverter, such as droop control, voltage and current dual-loop control, and active load sharing which provide control theory support for subsequent papers.

Chapter 3 Power flow analysis and circulating current in parallel inverters

3.1 Power flow analysis

In a power system, current or power flows from the power supply through the components of the system and is distributed to the loads. Power flow (or load flow) calculation is a term in power systems, which refers to calculating the state parameters of the network in the steady state under given operating conditions. The required operating state parameters include the voltage amplitude and phase angle of each bus node in the power grid, the active and reactive power distribution of each branch, and the power loss of the network [98]. The given operating conditions normally include power system network topology, component parameters, and the power of each power source and load point in the system, the voltage at the pivot point, the voltage at the equilibrium point, and the phase angle.

Power flow calculation is a very important analysis calculation for power systems to study various problems raised in system planning and operation. For power systems under planning, power flow calculations can be used to verify whether the proposed power system planning solutions can meet the requirements of various operating modes. For power systems in operation, power flow calculations can predict various load changes and assess network structure changes, which determines if the safety of the system is broken, whether the voltage of all buses in the system is within the allowable range, whether various components (lines, transformers, etc.) in the system will be overloaded, and what precautions should be taken in advance when overload may occur. Power flow calculation is also the basis of network loss calculation, static safety analysis, transient stability calculation, small disturbance static stability calculation, short circuit calculation, static equivalent calculation and dynamic equivalent calculation in Power System Analysis Software Package (PSASP) [99].

According to different solution models, power flow calculation can usually be divided into DC power flow and AC power flow. DC power flow ignores line resistance and parallel branches and does not consider the relationship between reactive power and voltage. The mathematical model is a set of linear equations; AC power flow is relatively accurate, and the

mathematical model is a set of nonlinear equations. Although with the development of algorithms and computer technology, AC power flow technology is used in most occasions of power system analysis, DC power flow is still widely used in the safety check of power system day-ahead power generation plan due to its linear expression and rapidity, power market congestion management, safety constraint unit combination and economic dispatch and other occasions. Although DC power flow has been widely used, compared with AC power flow, the analysis of the error of its result and its relationship with network structure and operating status has not attracted enough attention [100, 101]. Details of the calculation of ac power flow and dc power flow can be found in Appendix A [102].

In this thesis, power flow analysis will be used in chapter 6 to analyse the IEEE 14-bus test system and the proposed microgrid integration with IEEE 14-bus test system to verify the stability and rationality of the proposed microgrid during operation. Due to the enormous number of calculations, MATLAB/Simulink is introduced in the section of Chapter 6 to carry out a power flow calculation analysis of the two systems mentioned above. MATLAB/Simulink based power flow calculation enables the computer to play an extremely crucial role in the calculation, analysis, and study of complex power system tide distribution problems, greatly improving efficiency. It makes it possible to transform the power flow calculation from a traditional method to an optimisation algorithm [103].

3.2 Circulating current with parallel inverters

Parallel power supply of multiple modules has become one of the important directions in the development of power supply technology. Using multiple power modules in parallel not only increases the reliability of the power supply and shares the load power, but also reduces thermal and electrical stress, truly redundant power supply and reduces costs. Parallel power supply of multiple modules can flexibly supply loads with different requirements. Modular power supplies can replace serialisation, thus shortening the development and production cycle of power supplies and improving their standardisation and maintainability. Current sharing is one of the most important problems in parallel connection of inverter power supplies. Circulating current and uneven power distribution are the main reasons for parallel failure. For the parallel connection of inverter power supplies, if the circulating current is not restricted, since the impedance of the inverter output leads is very small, the voltage phase,

amplitude, and frequency output by each module cannot be guaranteed to be the same, so a large circulating current may be generated. The parallel connection fails, and the equipment may be burned out in serious cases [104].

Circulating currents can not only damage the power electronic devices and lower the efficiency of the system by introducing some unnecessary currents. In addition, they can even reduce the reliability of the system by imposing too much current stress on the semiconductor devices. Therefore, it is necessary to study the circulating current in a microgrid system with multiple inverters in parallel.

The circulating current may include a DC component and AC components at the fundamental frequency and higher order harmonics. An unneglectable DC circulating current between the inverters caused by a slight unbalance of the control signals, the inner resistances of the inverters and the speed difference of the switching drivers [105]. The fundamental circulating current exists between the parallel inverter units [106] due to the unbalance of parallel connected inverters, such as the gate pulse delay, the pulse width modulator randomness, and the control delay.

For a microgrid system with multiple inverters in parallel, the reasons that can cause circulating current are voltage amplitude difference, frequency difference, phase angle difference and line impedance difference between each distributed source.

In this part, firstly, the calculation method of circulating current for the parallel system of two or more inverters is proposed. Secondly, the simulation analysis of the reasons for each of the above-mentioned circulating currents is conducted out. Finally, the overall circulation of the microgrid system in this subject is conducted out. Simulation to analyse whether the control theory proposed in the subject can solve the circulation problem in the system.

3.2.1 Circulating current in two parallel connected inverter system

In the distributed power generation system, the circulating current between the inverter power sources is formed due to the output voltage difference of each inverter power module. Only when the inverter-based power sources of the parallel cases share the load current without generating circulating current, the parallel system can work normally and efficiently. To eliminate the circulating current between the inverters, the cause and characteristics of the

circulating current must be analysed in detail. To simplify the analysis, let's take two inverters running in parallel as an example. Without considering the influence of the output filter. Since the line resistance in the actual system is much larger than the line inductive reactance, the influence of the line inductive reactance can be ignored. The equivalent schematic diagram is shown in Figure 3.1.

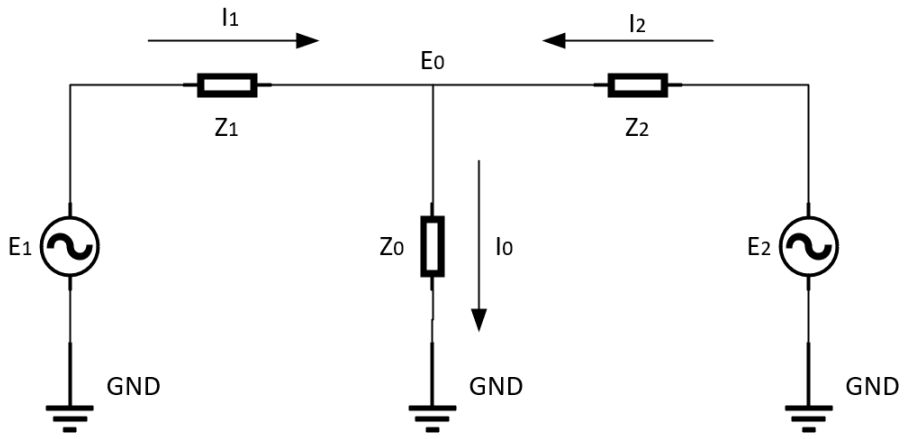

Figure 3.1 Two-parallel inverters distributed power generation system

It is assumed that the output voltage waveforms of each inverter power supply in the steady state are standard sine waves, and the effect of waveform distortion is not considered. In the figure, Z_0 is the load impedance, and Z_1 and Z_2 are the line impedances. E_1, I_1, E_2, I_2 and E_0, I_0 respectively represent the output voltage and current vector of the No. 1 and No. 2 inverter power supplies and the parallel system. Then

$$\begin{cases} \dot{I}_1 = \frac{\dot{E}_1 - \dot{E}_0}{Z_1} \\ \dot{I}_2 = \frac{\dot{E}_2 - \dot{E}_0}{Z_2} \\ \dot{I}_0 = \dot{I}_1 + \dot{I}_2 \end{cases} \tag{3.15}$$

Circulating current for No.1 inverter (E1 in Figure 3.1) is:

$$\dot{I}_H = \frac{\dot{I}_1 - \dot{I}_2}{2} \tag{3.16}$$

If:

$$Z_1 = Z_2 = Z \tag{3.17}$$

So:

$$\dot{I_H} = \frac{\dot{E_1} - \dot{E_2}}{2Z} = \frac{\Delta \dot{E}}{2Z} \tag{3.18}$$

Then:

$$\begin{cases} \dot{I_1} = \frac{\dot{I_0}}{2} + \dot{I_H} \\ \dot{I_2} = \frac{\dot{I_0}}{2} - \dot{I_H} \end{cases} \tag{3.19}$$

As can be seen from the above formula: When two inverter-based power supplies are operated in parallel, the output current of each unit consists of two parts: one is the current provided to the load, and the other is the circulating current I_H flowing between the two parallel power supplies. For parallel units, the load is evenly divided, and the presence of the circulating current causes the difference in the output current of the parallel units. When the circulating current presents different load characteristics to the output voltage of each unit, the output power of each unit also changes accordingly, making the load on each inverter power supply unbalanced. Because the line impedance R is very small, if the phases of the output voltages of the parallel units are not completely equal, even a small difference will produce a loop flow that is much larger than the rated current of the system, and this current does not pass through the load, rather flow between two inverter power supplies. At this time, if two voltage closed-loop controlled inverter power supplies are simply connected in parallel without any treatment, the system is equivalent to a short circuit, which is very dangerous. Current sharing measures must be taken between the inverters operating in parallel to ensure uniform distribution of power stress and thermal stress among power devices and to prevent one or more power supplies from operating at the current limit state.

3.2.2 Circulating current in a multi parallel inverter system

There are *N* parallel inverters,

$$\begin{cases} \dot{I_k} = \frac{\dot{E_k} - \dot{E_0}}{Z_k} (k = 1,2, \dots, N) \\ \dot{I_0} = \sum_{n=1}^{N} \dot{I_n} \end{cases} \tag{3.20}$$

The circulating current seen by each inverter is defined as the difference between its output current and the average current. For inverter No. k, the circulating current is:

$$\dot{I_{Hk}} = \dot{I_k} - \frac{\dot{I_0}}{N} = \frac{N\dot{I_k} - \sum_{n=1}^{N} \dot{I_n}}{N} (k = 1,2, \dots, N) \tag{3.21}$$

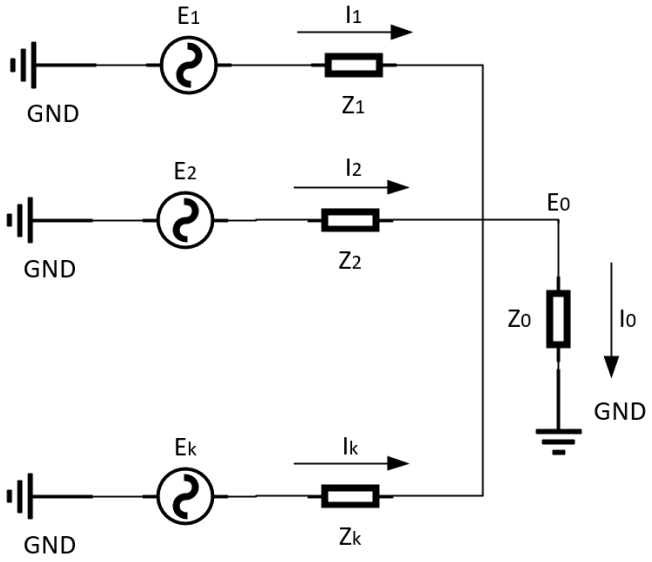

Figure 3.2 N-parallel inverters distributed power generation system

3.3 Simulation for circulating current in multi parallel inverters system

In this simulation part, the number of power sources (N) is set at 3, which means that three inverter-based generation systems are connected in parallel to supply energy to the loads. Five different simulation tests are carried out with different system parameters as shown in Table 3-1. For all tests, the load value is 20 kW plus 6 kVAr. In Test 1, the output voltage of all the three inverters is assumed to have the same amplitude, frequency, and phase. The output line impedances of all the three inverters are also set the same at $0.128\,\Omega + 2.64\,mH$. This test is used as a benchmark for the other four tests which include variations in system parameters. This allows the comparison of simulation results showing the impact of different generator voltage, frequency and phase and line impedance on the circulating current in a power system with parallel generators.

In Test 2, the output voltage amplitudes of Inverter 2 and Inverter 3 are adjusted to 385 V and 375 V, respectively, to discuss the impact of different output voltage amplitudes on the circulating current. In Test 3, the output frequency of Inverter 2 and Inverter 3 are set at 50.05

Hz and 49.95 Hz, respectively, to discuss the influence of different output frequencies. In Test 4, the angles of the output voltage phase A of Inverter 2 and the Inverter 3 are adjusted to be 2° and -2°, respectively, to discuss the influence of different output voltage phase angles. In Test 5, the output line impedance of the Inverter 2 and Inverter 3 are adjusted to $0.15\,\Omega + 3\,mH$ and $0.1\,\Omega + 2.4\,mH$, respectively, to discuss the influence of different output line impedances on the circulating current between parallel inverters.

Table 3-1 SYSTEM PARAMETERS

		Test 1	Test 2	Test 3	Test 4	Test 5
E1	A1(V)	380	380	380	380	380
	f1(Hz)	50	50	50	50	50
	α1(°)	0	0	0	0	0
E2	A2(V)	380	385	380	380	380
	f2(Hz)	50	50	50.05	50	50
	α2(°)	0	0	0	2	0
E3	A3(V)	380	375	380	380	380
	f3(Hz)	50	50	49.95	50	50
	α3(°)	0	0	0	-2	0
Line impedence	R1(Ohms)	0.128	0.128	0.128	0.128	0.128
	X1(H)	2.64E-03	2.64E-03	2.64E-03	2.64E-03	2.64E-03
	R2(Ohms)	0.128	0.128	0.128	0.128	0.15
	X2(H)	2.64E-03	2.64E-03	2.64E-03	2.64E-03	3.00E-03
	R3(Ohms)	0.128	0.128	0.128	0.128	0.1
	X3(H)	2.64E-03	2.64E-03	2.64E-03	2.64E-03	2.40E-03

The following are the simulation results of tests 1 to 5 by MATLAB/Simulink. Circulating current measurement model can be found from Figure C.10 in Appendix C. I_{gabc1}, I_{gabc2}, I_{gabc3} are the measured output currents of inverter 1, 2 and 3, I_0 is the sum of the output currents of the three inverters, so the circulating current of each of the three inverters can be calculated as I_{H1}, I_{H2}, I_{H3} according to the Formula 3.21.

3.3.1 Test 1: Ideal system without circulating current

Figure 3.3 shows the output currents (the red lines) and the circulating currents (the blue lines) of the three parallel-connected generators. Since the test parameters of the three parallel inverters are all the same, the output current values of the three inverters are identical, and there is no circulating current generation. This test is used as a comparison test for the later tests.

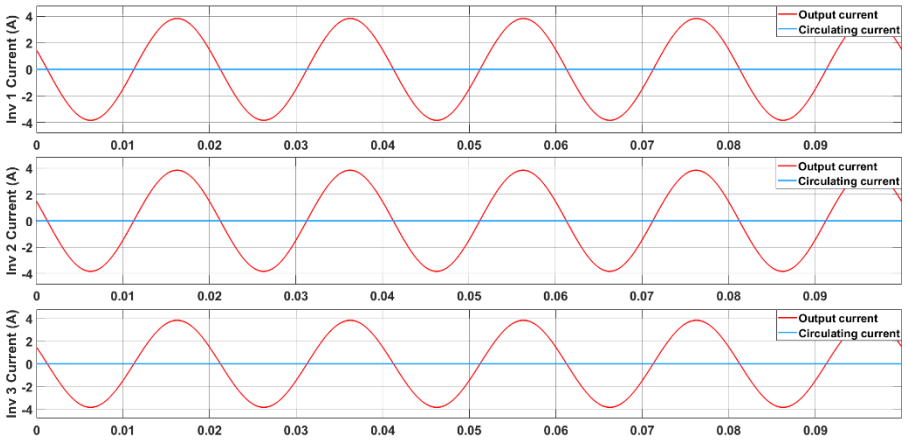

Figure 3.3 Phase a current and circulating current for inverters 1, 2 and 3

3.3.2 Test 2: Circulating current due to voltage amplitude difference

In Test 2, the output powers from all voltage sources are all positive but with different magnitude. This indicates that there are no net active or reactive power exchanges among inverters. For this case, the only negative impact of circulating current in the system is the extra active and reactive power losses in the line impedances due to unequal current from each voltage source. The circulating currents that cause the system extra power losses.

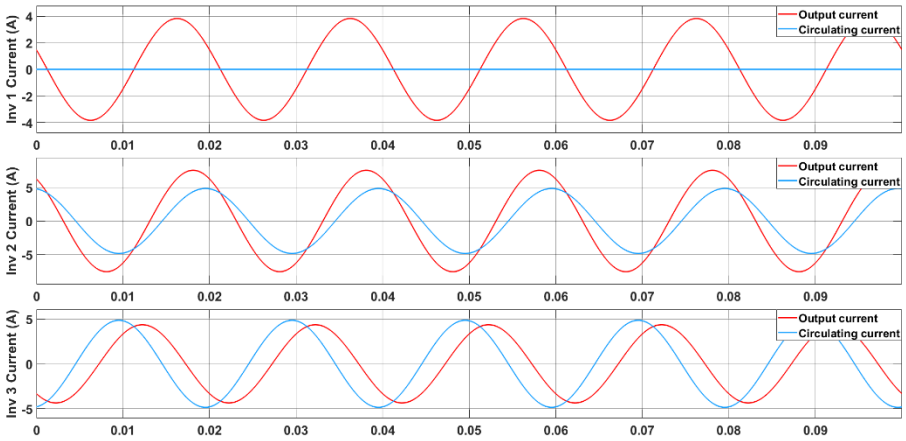

Figure 3.4 Phase a current and circulating current for inverters 1, 2 and 3

3.3.3 Test 3: Circulating current due to frequency difference

In this part, the effect of frequency difference among parallel voltage sources on the circulating current is investigated. In Test 3, circulating currents exist when there is frequency difference among parallel connected voltage sources. There is no net power exchange among voltage sources as all produce positive active and reactive power. However, due to the circulating current, there are extra power losses in the line.

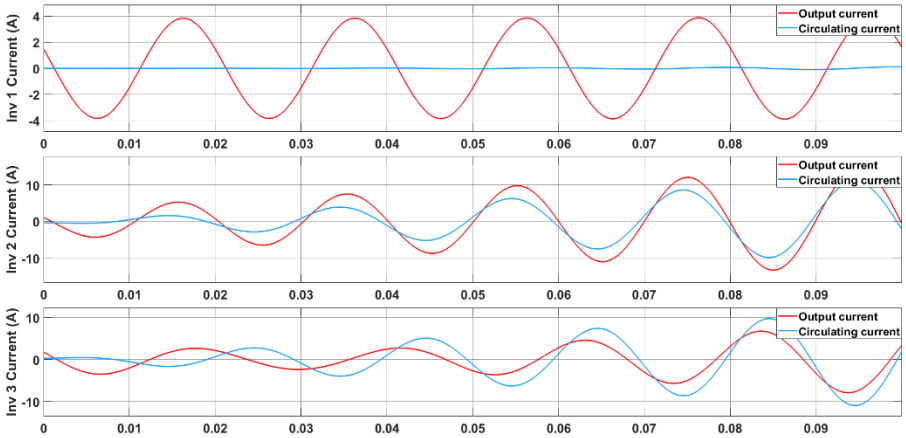

Figure 3.5 Phase a current and circulating current for inverters 1, 2 and 3

3.3.4 Test 4: Circulating current due to phase angle difference

In this section, Test 4 aims to show the effect of differences in voltage phase angle between parallel voltage sources on the circulating current. When the phase angle of the voltage sources connected in parallel differ from each other, there is a circulating current in the system. In terms of power flow, there is no net power flow between the voltage sources, but the circulating current generates additional power losses in the line impedance.

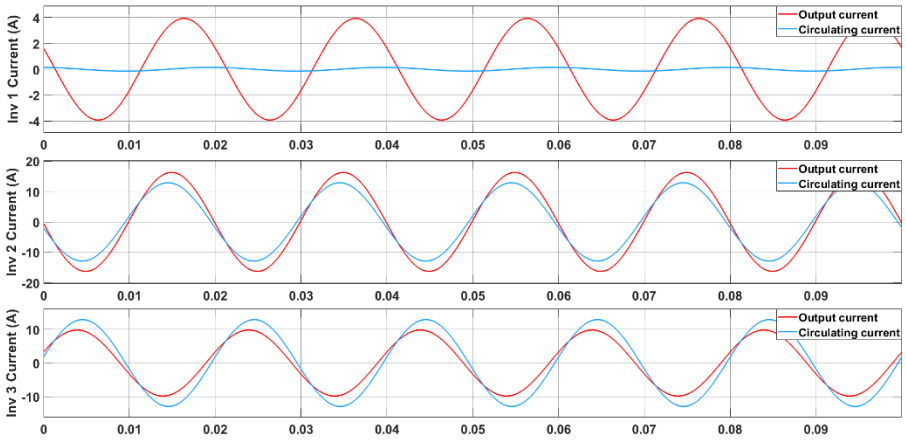

Figure 3.6 Phase a current and circulating current for inverters 1, 2 and 3

3.3.5 Test 5: Circulating current due to different line impedance

In this part, the Test 5 focus on the circulating current between parallel connected voltage sources due to different line impedances. From Figure 3.7, the current phase for each inverter is the same, but the current amplitude for each inverter is totally different. Also, the circulating current seen from each inverter are different.

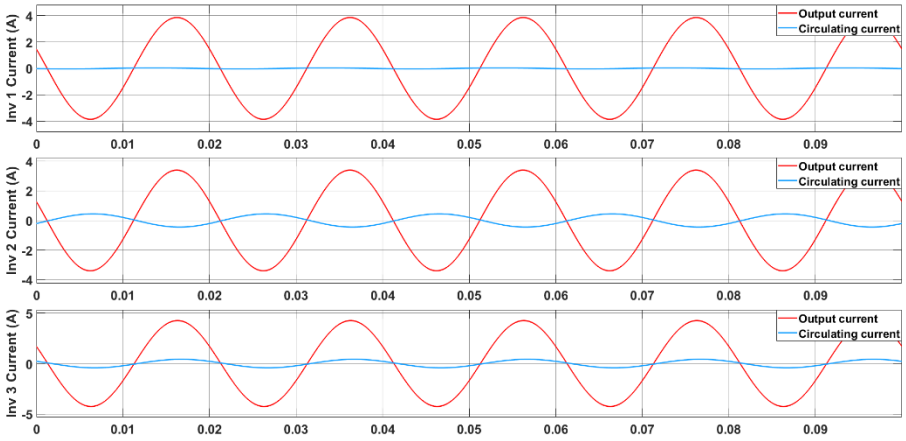

Figure 3.7 Phase a current and circulating current for inverters 1, 2 and 3

3.4 Circulating current for study cases

In this section, circulation current is analysed for the microgrid system used in this project, to explore whether the proposed control theory can prevent large and unacceptable circulating current and reduce its impact on system normal operation.

Divided into five case studies based on the different line impedance ratio and system operation mode. The first two cases are the output line impedances ratio of the three inverters are 1:1:1, and the system is in island operation case 1 and grid-connected operation case 2, respectively; For case 3 and case 4, the output line impedance ratio of the three inverters are 2:1:3, and the system is in island operation and grid-connected operation respectively; For case5, the capacity ratio of the three inverters is 3:2:1, the output line impedance of three inverters are 2:1:3, and the system running in grid-connected mode.

3.4.1 Case 1: Similar line impedance and islanded mode

In this case, since the output line impedance of each inverter is 1:1:1 and the system are operating in island mode, the output current of the three inverters is the same, as well as for the circulating current, which is 0. During 2s to 3s, the output current waveform is increased and decrease due to load 2 connected and disconnected to the system,

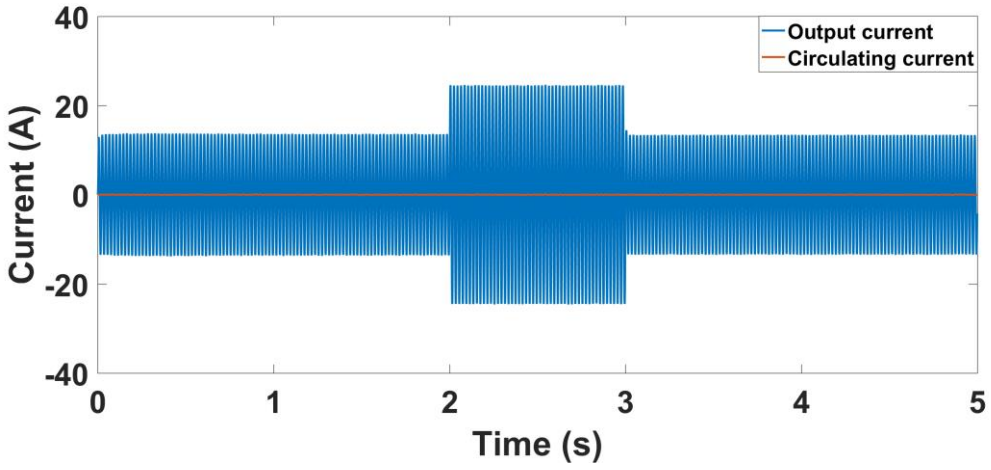

Figure 3.8 Output current and circulating current for inverters 1, 2 and 3 in case 1

3.4.2 Case 2: Similar line impedance and grid connected mode

The difference between this case and case 1 is that the system is running in grid-connected mode. The system starts pre-synchronization control at 0.5 s, and the output current of each inverter increases and gradually returns to the stable value. At 2 s, load 2 is connected to the system, at 3 s, load 2 is disconnected from the system, it caused some fluctuations in the output current of each inverter, but they were all within the acceptable range. The circulating current of each inverter was the same; there were some small fluctuations from 3s to 4s, overall, it was maintained at 0 A.

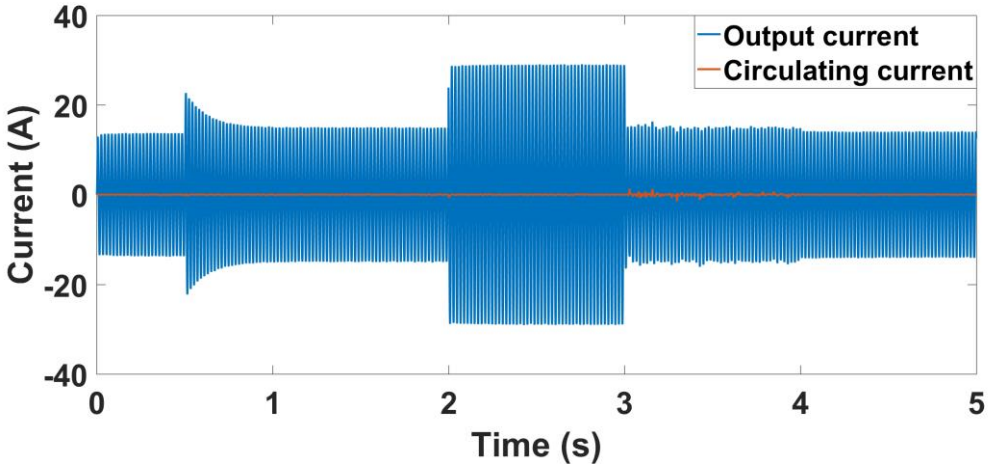

Figure 3.9 Output current and circulating current for inverters 1, 2 and 3 in case 2

3.4.3 Case 3: Different line impedance ratio and islanded mode

In this case, the output line impedance ratio of inverters is 2:1:3, and the system is running in islanded mode. From the result diagrams below, it can be seen that the circulating current of each inverter has a small value difference, but they are all within the acceptance range, it reflects that there is no big difference in the output current of each inverter, which ensures that the power sharing can be achieved when the line impedance of each inverter is different.

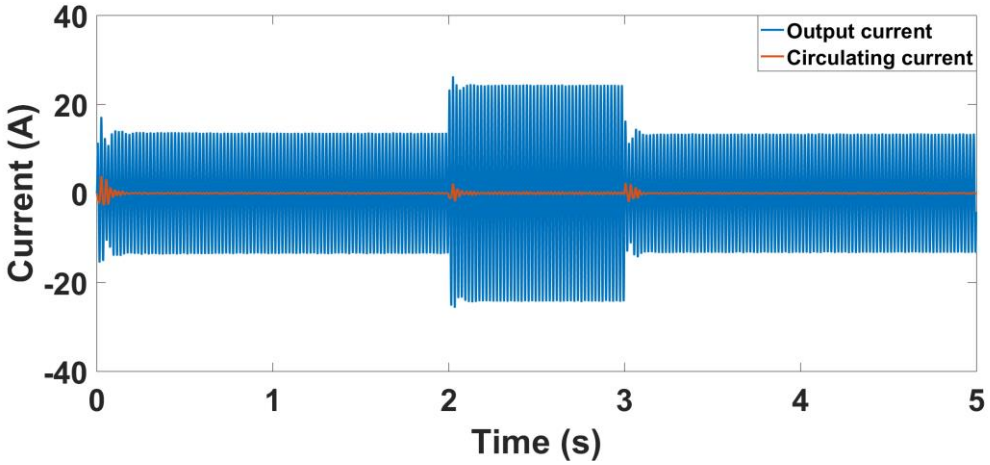

Figure 3.10 Output current and circulating current for inverter 1 in case 3

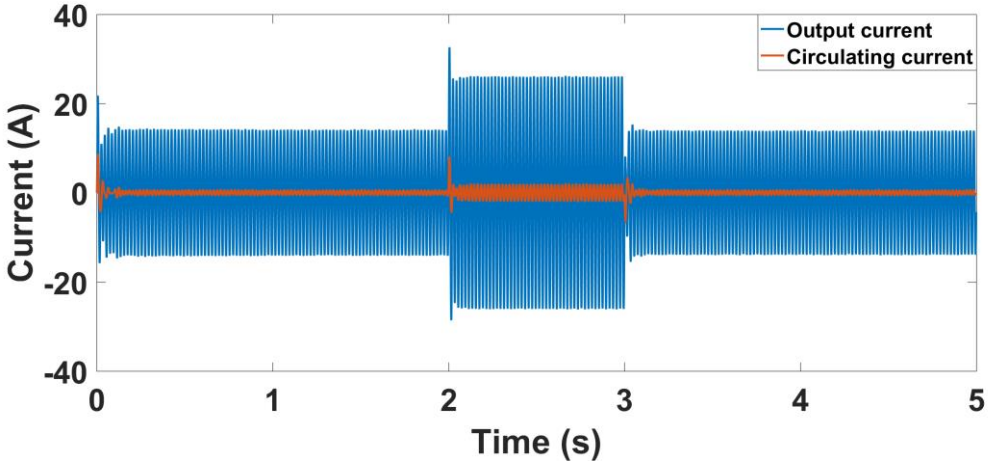

Figure 3.11 Output current and circulating current for inverter 2 in case 3

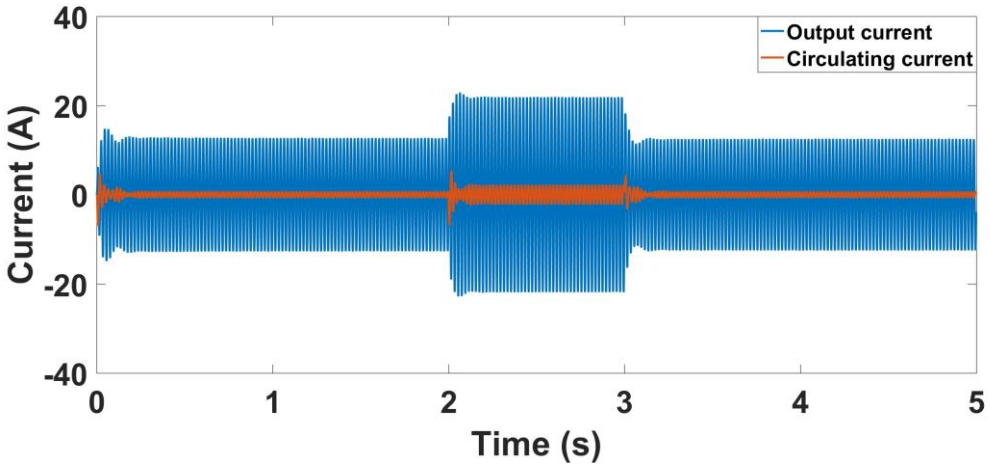

Figure 3.12 Output current and circulating current for inverter 3 in case 3

3.4.4 Case 4: Different line impedance ratio and grid connected mode

The difference between this case and case 3 is that it runs in grid-connected mode. Whether it is in the pre-synchronization control period or the grid-connected operation period, the circulating current of each inverter has no significant impact, same with case 3. Except at 0.5s, there is some fluctuation at the beginning of pre-synchronization, but it can quickly return to a position close to 0 A.

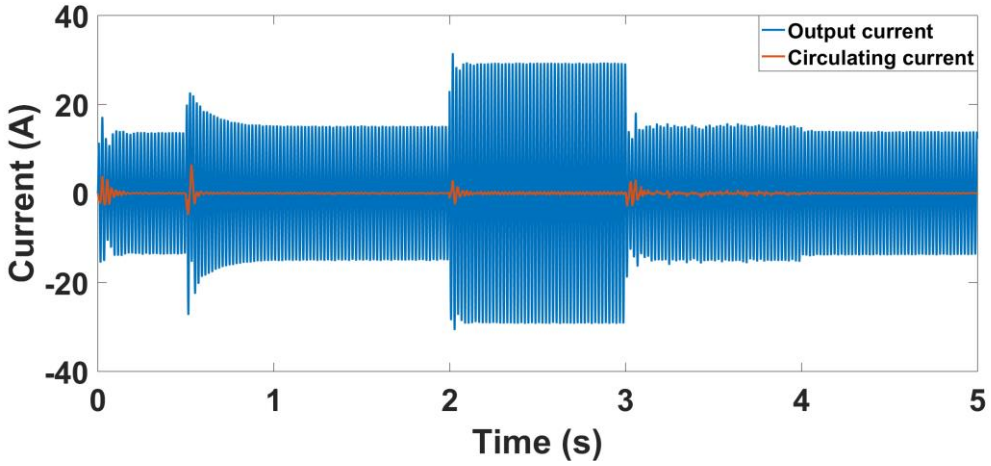

Figure 3.13 Output current and circulating current for inverter 1 in case 4

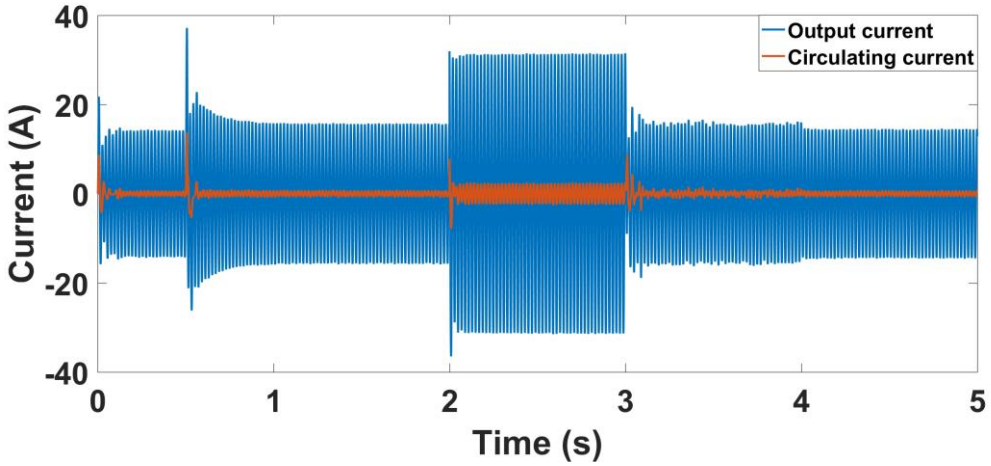

Figure 3.14 Output current and circulating current for inverter 2 in case 4

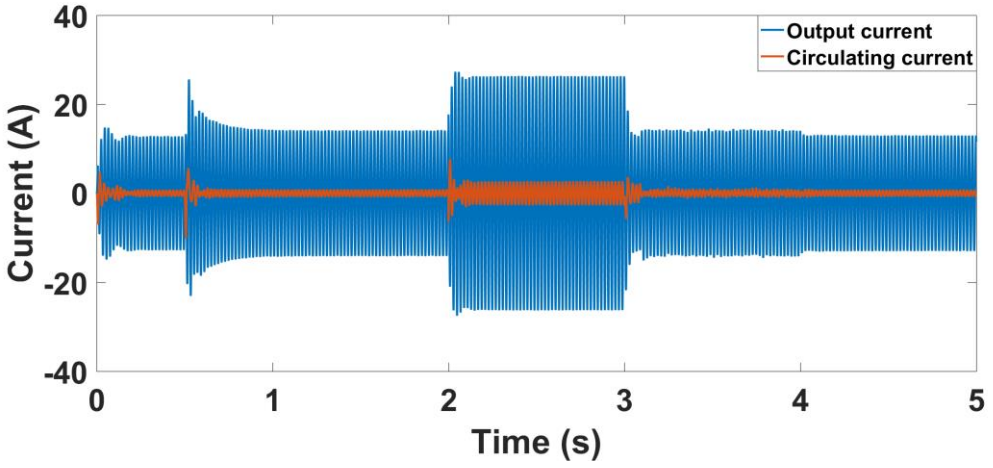

Figure 3.15 Output current and circulating current for inverter 3 in case 4

3.4.5 *Case 5: Different ratio of inverter capacity and line impedance, grid connected mode*

In this case, the capacity ratio of each inverter is set to 3:2:1, and the output line impedance ratio is set to 2:1:3, to compare with the previous four cases. It can be seen from the simulation results that the output current ratio of each inverter is also 3:2:1, which means the system achieves the purpose of power sharing for each inverter according to the capacity ratio. At the same time, the circulating current ratio of each inverter is very different, which is caused by the circulating current calculation method of each inverter, please refer to Section 3.2.2.

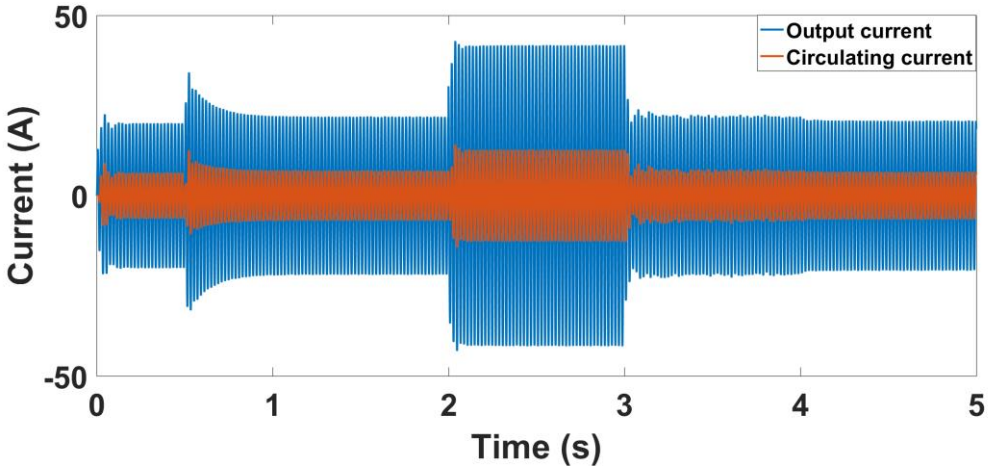

Figure 3.16 Output current and circulating current for inverter 1 in case 5

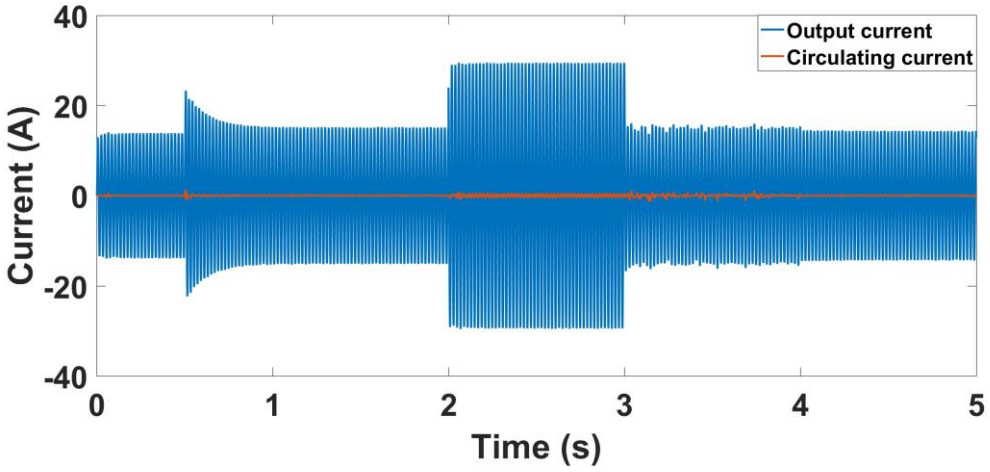

Figure 3.17 Output current and circulating current for inverter 2 in case 5

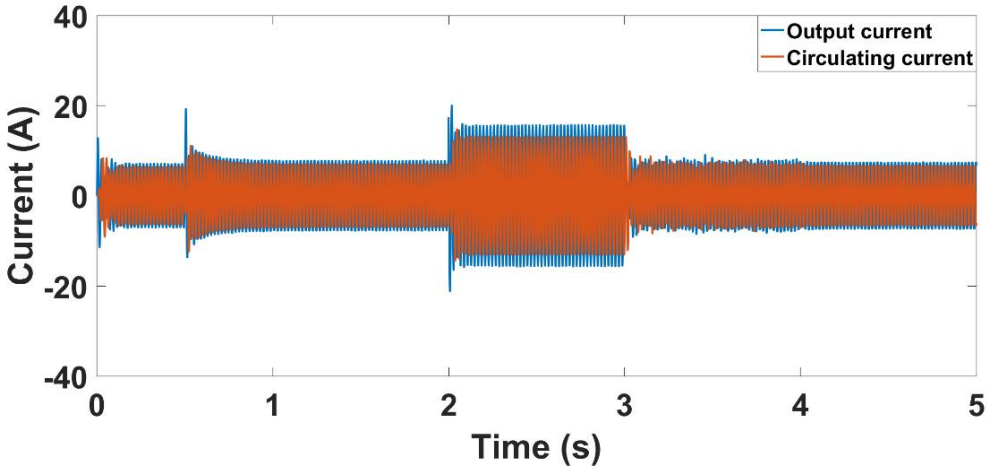

Figure 3.18 Output current and circulating current for inverter 3 in case 5

3.5 Summary

In this chapter, the first part discussed the power flow concept. The DC power flow calculation and the AC power flow calculation process are introduced in detail. It is also shown that this thesis uses the MATLAB/Simulink platform to replace the traditional tidal wave calculation process, making the analysis process more accurate and efficient. For the second part, circulating current was defined for a multiple parallel connected inverter to the same PCC. Several simulations were performed to visualize the circulating currents phenomenon due to the phase, amplitude, frequency, and line impedance differences among parallel connected inverters. Through the circulating current analysis of the microgrid system with three parallel inverters proposed in this subject, the conclusion can be drawn as follows:

In a parallel inverter system, when the output impedance of each inverter is different, the proposed control theory can not only realize the distribution of power according to the capacity of each inverter, but also prevent the generation of relatively large circulating current, which will have a negative impact on the operation of the system.

Chapter 4 An improved droop control method for parallel inverter systems

Power inverters are the most important part in a grid-connected microgrid that integrate conventional distributed generation (DG) units, energy storage systems and renewable energy sources to form a smart grid configuration [107, 108]. These inverters are often connected in parallel. Therefore, achieving stable parallel operation and a reasonable load power sharing has become a serious problem [109]. In the first section of this chapter, droop control with secondary control loop is introduced for power sharing control in the microgrid. A microgrid is simulated with the proposed secondary loop droop control and the virtual impedance droop control and results are compared. In the second section of this chapter, a pre-synchronization control is developed for the microgrid in order to achieve smooth grid connection regardless of the amplitude and phase difference between the microgrid and the main grid before the grid connection.

4.1 Droop control with secondary control loop

4.1.1 Structure of secondary control loop

The proposed droop control with secondary control loop method includes two important parts; one is the traditional droop control loop discussed in Section 2.3.1 in Chapter 2 and the other is a secondary control loop used for power sharing. The reference signals to the droop control are generated by the secondary control loop. In this thesis, the secondary control loop collects output active power and reactive power data from every working inverter, calculates total active and reactive power output from all inverters, calculates the average loading factor considering inverters' power ratings, and then calculates the active and reactive power reference signals to the droop control to maintain equal inverter loading, as shown in Figure 4.1. When inverters have equal power ratings, inverters can output equal active power and reactive power, no matter the line impedance values of themselves.

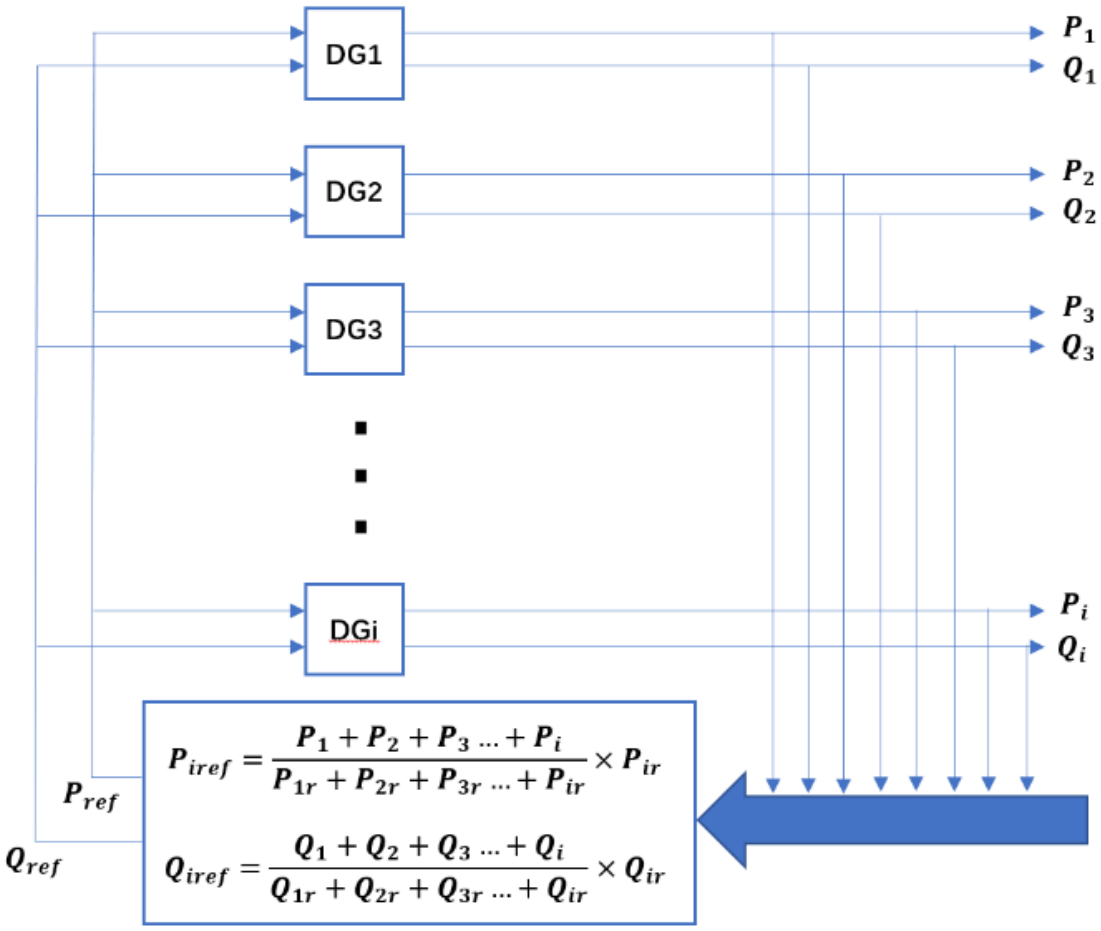

Figure 4.1 Secondary control loop

4.1.2 Simulation results

The microgrid considered in this paper comprises three parallel inverters, two loads and is connected to the main grid. The three parallel inverters have totally different line impedance values to simulate the different distance from the micro source to PCC. One of the two loads is 2 kW active power while the other is 2 kW active with 600 VAr inductive reactive power. For the grid, the phase-to-phase voltage is 380V and the frequency is 50Hz. The different parameters of the system are summarized in Table 4.1.

Table 4-1 PARAMETER OF THE SYSTEM

	Parameters	Value
DG units	Inverter switching frequency	10 kHz
	DC bus voltage	800 V
	Nominal bus frequency	50 Hz
	RMS line voltage	380 V
	Line impedance (DG1)	2.64 mH, 1.642 Ω
	Line impedance (DG2)	1.32 mH, 0.821 Ω
	Line impedance (DG3)	5.28 mH, 3.284 Ω
Load	Load 1	2000 W
	Load 2	2000 W+600 VAr
Grid	Phase to phase voltage	380 V
	Frequency	50 Hz

In the normal operation mode, all parallel inverters and the resistive load are always connected to PCC. Another inductive load is connected to PCC at 0.5 s and disconnected at 1.5 s. The grid is connected to PCC from 1s to 2 s, then disconnected from the system, as shown in Table 4-2.

Table 4-2 OPERATION STATES

Time	Operation
0.5s to 1.5s	Load 2 connected to the system at 0.5s and disconnected at 1.5s.
1.0s to 2.0s	Utility grid connected to the system at 1.0s and disconnected at 2.0s.

Three different cases' simulation results are shown, they are: virtual impedance droop control, the same inverter rated capacity with proposal method, and the different inverter rated capacity with proposal method. For the concept of virtual impedance sag control theory and the principles of control, please refer to Section 2.3.1.3.

a) Virtual impedance droop control

Figures 4.2-4.4 show the simulation results when the virtual impedance droop control method is used when the line impedances are kept constant at the actual island mode values. As the output impedance of the three inverters is almost the same using the virtual impedance control method, the waveforms produced by the three inverters are essentially the same, and only the output power waveform plot of one inverter is selected here to show, the waveform plots of the remaining two inverters are the same as this one. When grid-connected, the total line impedance will not match and the active and reactive power of the inverters will exceed the rated value.

Figure 4.2 shows that when the grid is connected (at 1 s) the line frequency remains stable, but there is a slight droop. Figure 4.3 shows the simulation results for active power. As shown in the figure, power sharing is achieved both before and after grid connection. Before grid connection, the load power was equally distributed among the three inverters. However, after the grid is connected to the system, all three inverters produce a large output active power in excess of their rated values. This was due to the use of a constant line impedance, which became incorrect after grid connection. This shows how sensitive the inverter control is to the accuracy of the line impedance estimate. Similarly, reactive power sharing was achieved, but a significant increase in reactive power was observed after grid connection, as shown in Figure 4.4. Therefore, for virtual impedance drop control, although the same power output can be maintained between inverters, the system performance is very sensitive to the accuracy of the line impedance estimation. Using inaccurate line impedance values will result in incorrect virtual impedance calculations and may lead to system instability and violation of the inverters' healthy operating boundaries.

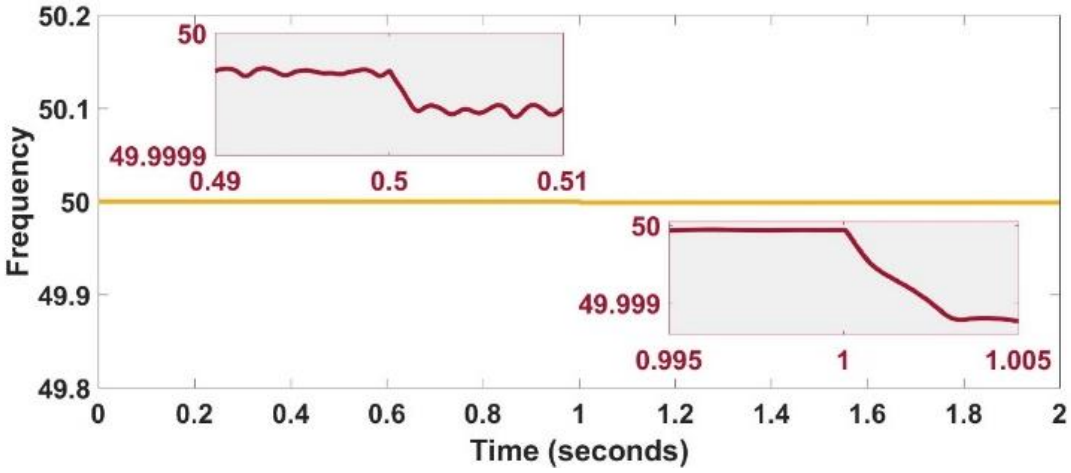

Figure 4.2 The frequency of 3 inverters by using virtual impedance droop control

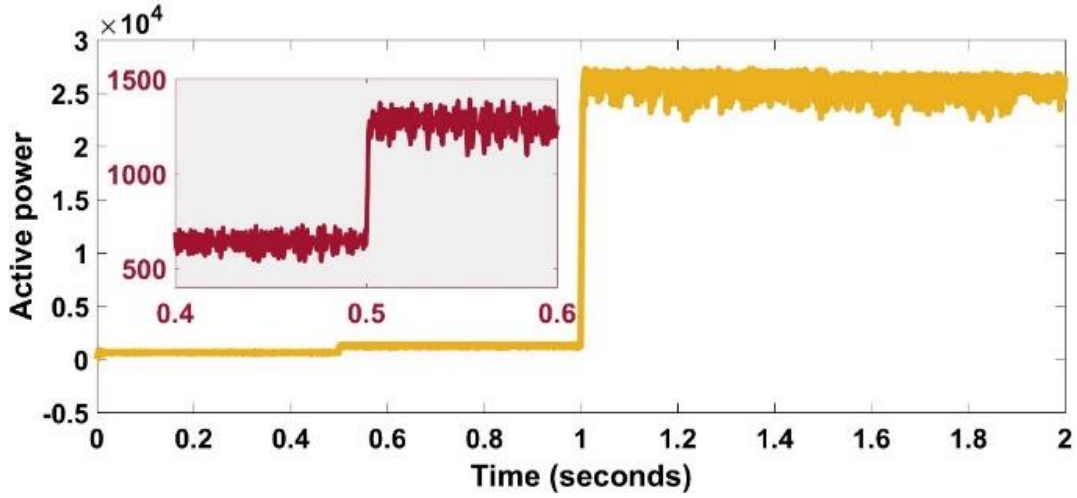

Figure 4.3 The output active power of 3 inverters by using virtual impedance droop control (all three inverters are same)

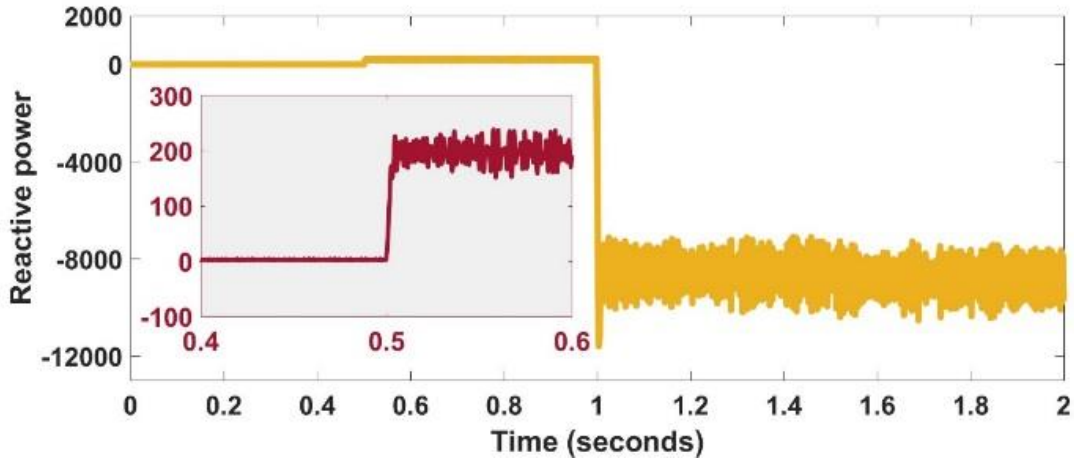

Figure 4.4 The output reactive power of 3 inverters by using virtual impedance droop control (all three inverters are same)

b) Proposed control with equal inverter power ratings

The proposed control method is examined with equal and unequal inverter ratings. The results shown in Figures 4.5-4.8 are for the equal power rating case. Figures 4.5 shows that the frequency of all the three inverters remains stable with 0.1 Hz maximum deviation from 50 Hz when the microgrid is switched between islanded and grid-connected operation or subjected to a step load variation. Figure 4.6 shows the output phase voltages of the three inverters are well stable at 311 V maximum voltage. For the currents of DG1, DG2 and DG3 shown in Figure 4.7, all have the same steady state value with an increase between 0.5 s to 1.5 s, due to the connection of the second load (the inductive load). When the grid is connected, the load current is shared between the inverters and the grid resulting in a

reduction in inverter currents. Figure 4.8 shows that the three parallel inverters, although they have different line impedances from each other, have equal output active power and reactive power, which track the load changes. As the parameters of the system change at certain points in time, whether due to the connection of load 2 or whether the system is connected to the grid or not, the voltage and frequency in the system change over a short period of time, so ripples occur at these points in time and the system is able to adjust and return to a stable value very quickly.

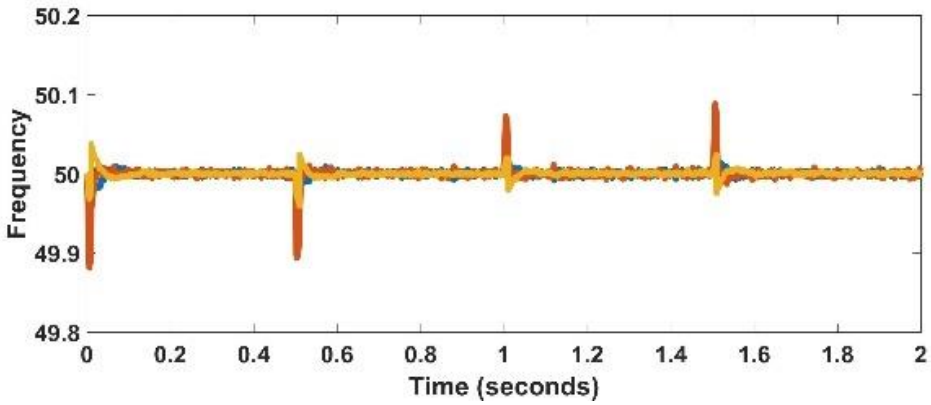

Figure 4.5 Frequency of the 3 inverters with the proposed control

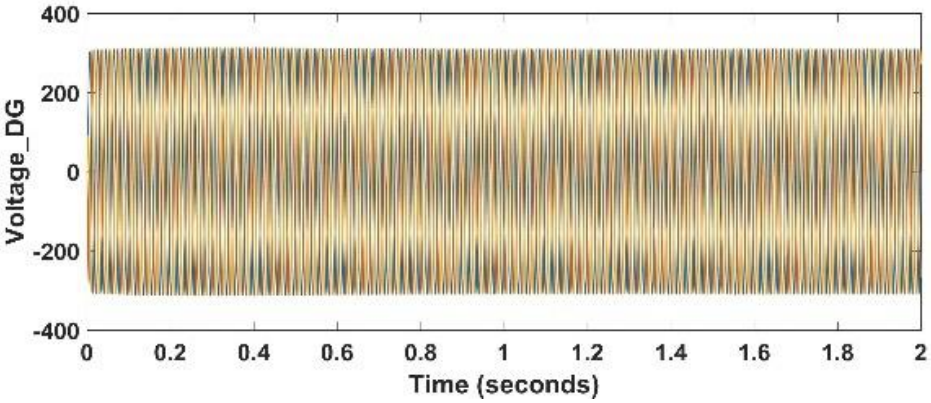

Figure 4.6 Output voltages of the 3 inverters with the proposed control

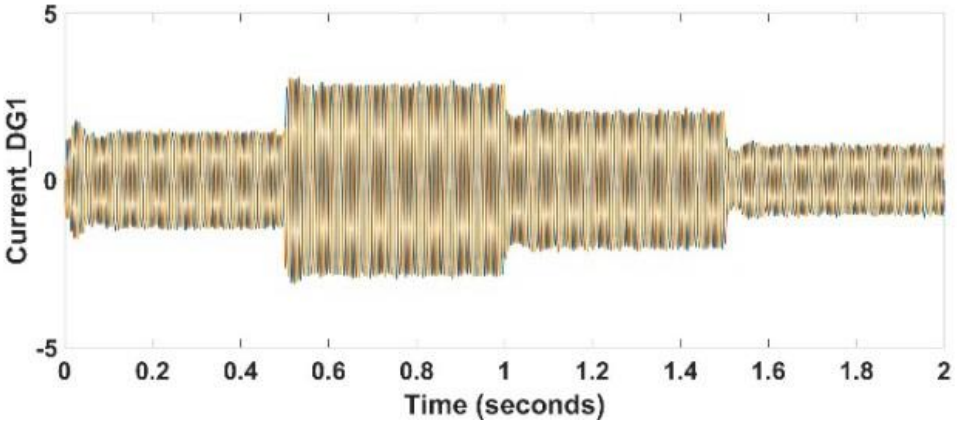

(a)

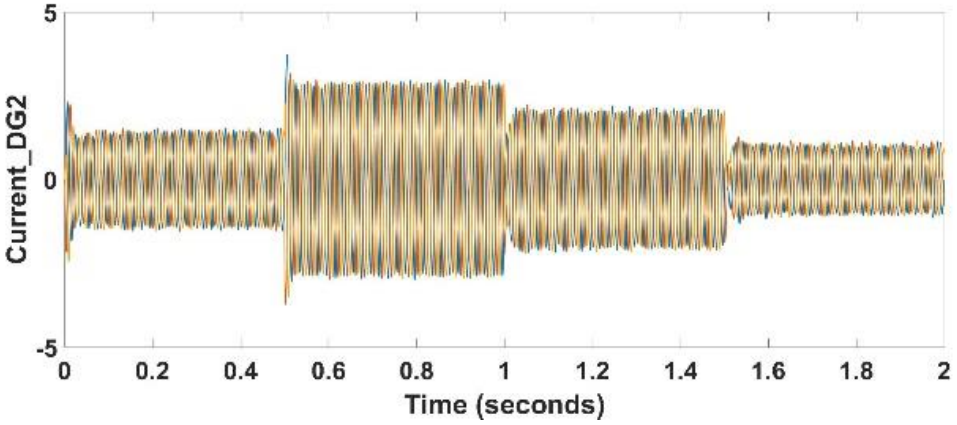

(b)

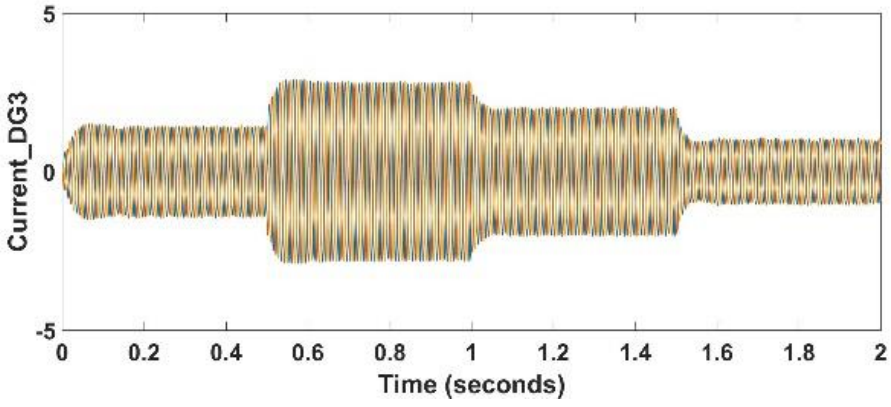

(c)

Figure 4.7 Output currents of the 3 inverters with the proposed control: (a) current of DG1, (b) current of DG2, (c) current of DG3

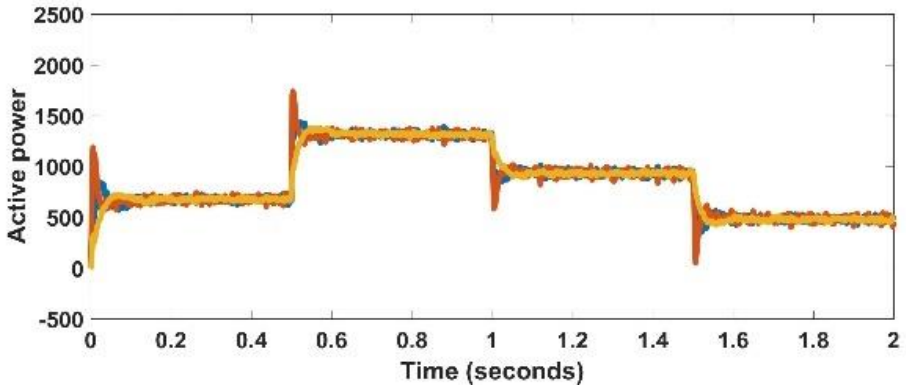

(a)

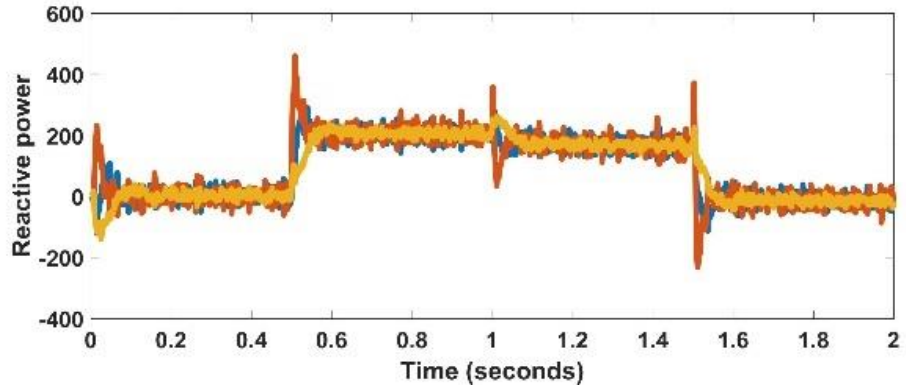

(b)

Figure 4.8 Output active power and output reactive power of 3 inverters by using proposed control: (a) active power, (b) reactive power

c) Proposed control with unequal inverter power ratings

The results shown below are for the unequal power rating case. In this case, it is assumed that the inverter capacity proportion is DG1: DG2: DG3=3:2:1.

As can be seen from these figures, with different power ratings of the inverter, the output frequency of the three inverters has not changed and remains in about 50Hz. The output voltage also did not change and was always stable at 311V maximum voltage. The output current, shown in Figure 4.11, is proportional to the rated capacity of the inverter, i.e. I_DG1: I_DG2: I_DG3=3:2:1. As a result, the output active and reactive power of the three inverters is also kept in this ratio, and a stable output is achieved following the capacity ratio of the inverters, whether there is a new load connection or disconnection, or a change of operating

mode (from islanding to grid-connected operation) (Figure 4.12). Therefore, compared with the common virtual impedance droop control method, the proposed improved droop control method in this thesis has a greater advantage, and the load power can be distributed according to the capacity of the inverter under different situations.

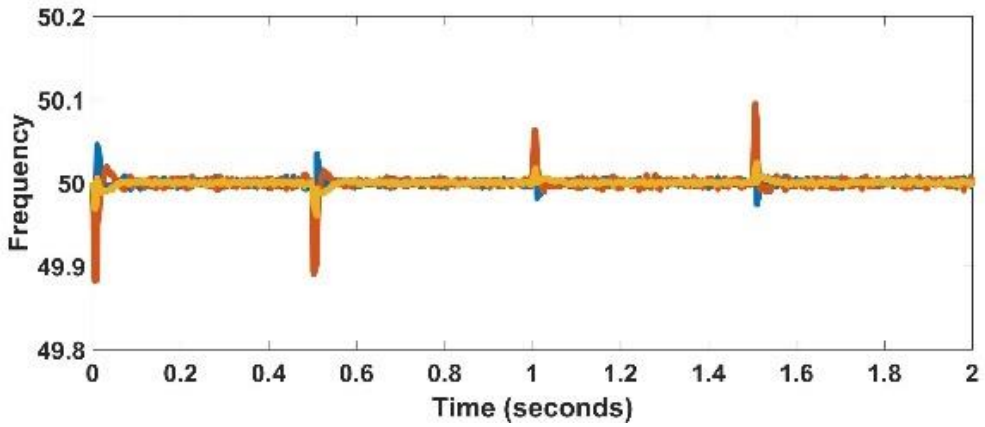

Figure 4.9 Frequency of 3 inverters by using proposed control

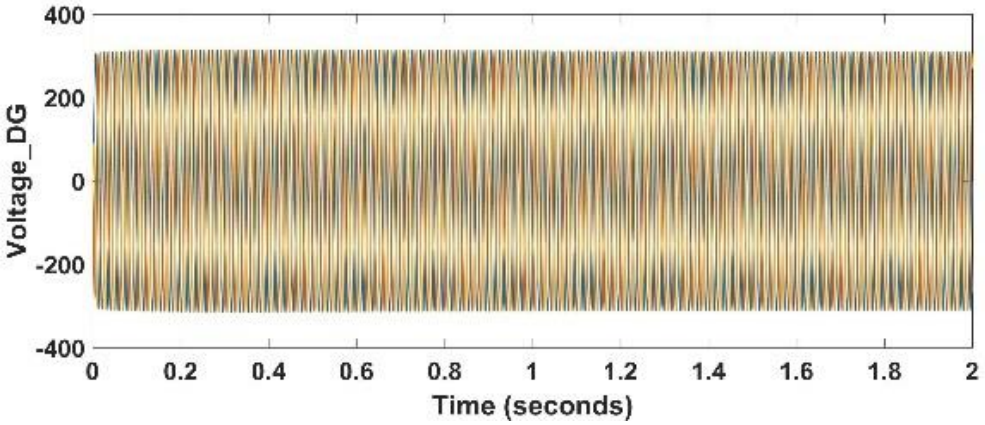

Figure 4.10 Output voltage and output current of 3 inverters by using proposed control

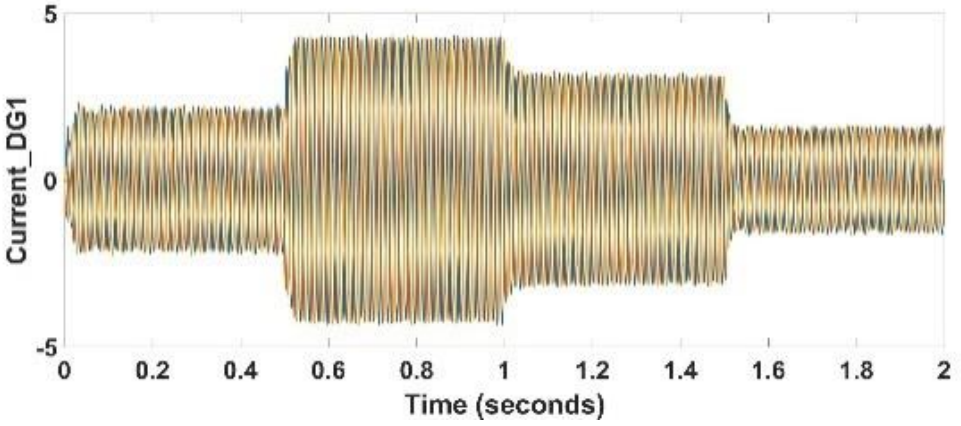

(a)

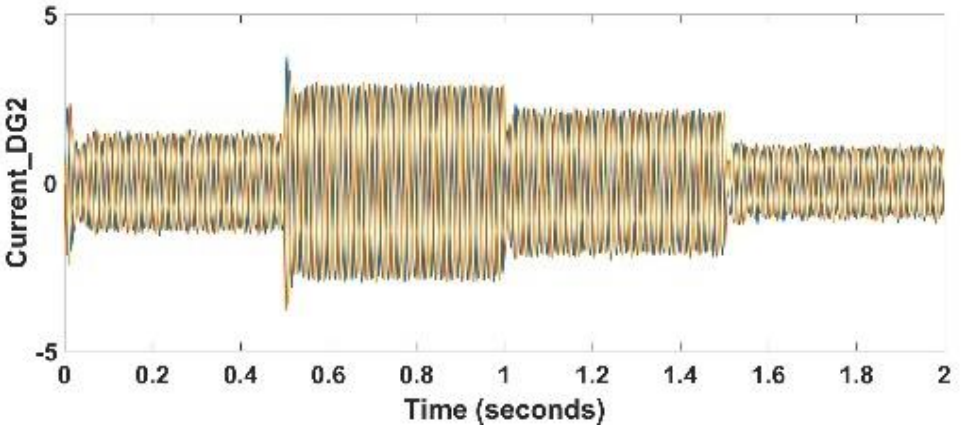

(b)

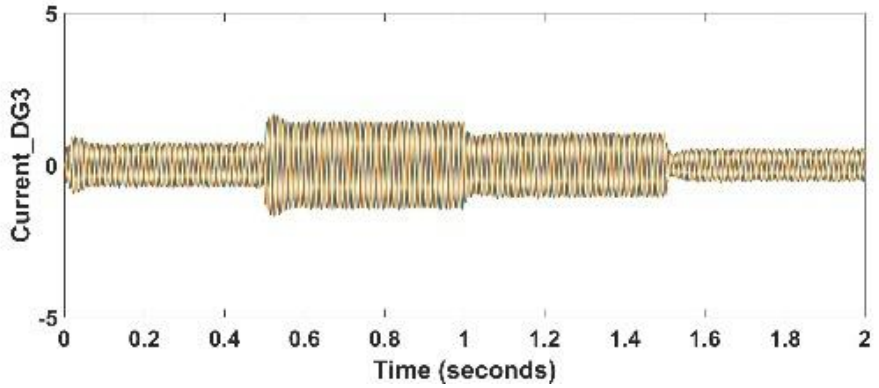

(c)

Figure 4.11 Output current of 3 inverters by using proposed control: (a) current of DG1, (b) current of DG2, (c) current of DG3

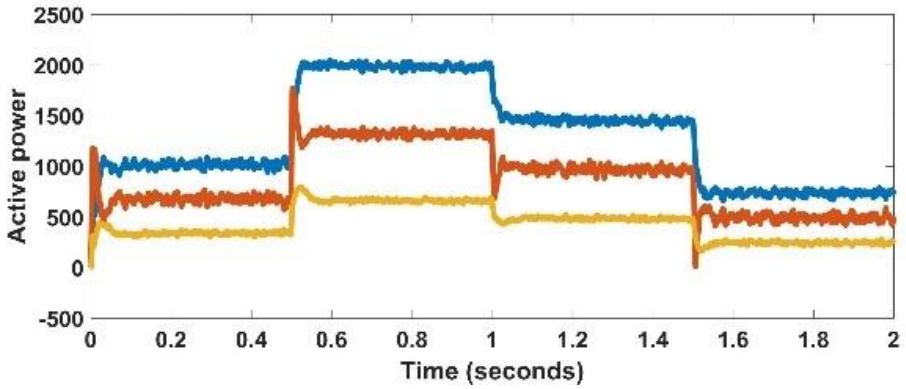

(a)

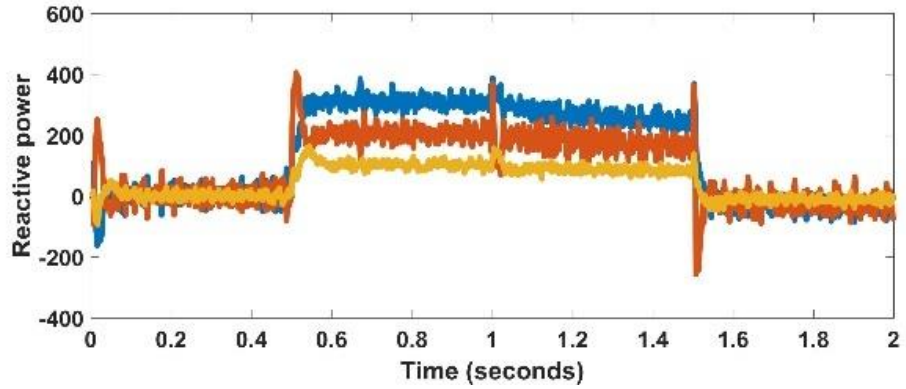

(b)

Figure 4.12 Output active power and output reactive power of 3 inverters by using proposed control: (a) active power, (b) reactive power

4.2 Pre-synchronization control with SSRF-SPLL

Before the microgrid is ready to be connected to the grid, it is necessary to start the grid-connected pre-synchronization control unit, which includes a phase regulator and a voltage amplitude regulator. This enables smooth control of the integration of the microgrid into the grid, eliminating damage to the power electronics and the grid due to mismatches in the voltage characteristics between the two systems.

4.2.1 Design of pre-synchronization control with SSRF-SPLL

As shown in Figure 4.13, the two SPLLs are mainly used to measure the real-time amplitude and phase of the PCC side voltage and the grid side voltage. The difference

between the two measured phase values, or frequency values, is fed to the phase correction module (Figure 4.14 (a)) of each inverter droop control through a PI controller, which can make the phase of the microgrid track the phase of the grid without a static difference. Similarly, the difference between the two measured d-axis voltage values is fed to the voltage correction module (Figure 4.14 (a)) of the inverter voltage and current dual-loop control through a PI controller. This enables tracking the voltage amplitude and phase of the microgrid without a static difference.

The switching signal for grid connection is generated as shown in Figure 4.15. As shown, when the phase difference between the PCC voltage and the grid voltage is less than a threshold value (i. e. phase is synchronized) and the amplitude difference is less than a threshold value (i. e. amplitude is synchronized) the switching signal is generated to connect the microgrid to the main grid. The breaker is closed only when the phase and voltage amplitude are synchronized at the same time. In the control theory proposed in this thesis, the thresholds used for frequency difference and voltage amplitude between microgrid and main grid are 0.01 Hz and 0.3 V respectively. These figures were chosen after several attempts and when both thresholds are satisfied at the same time, there is no negative impact caused by the mismatch of voltage characteristics between the microgrid system and the main grid. Figure 4.16 shows the flowchart of the pre-synchronization control system.

By pre-synchronising the voltage and frequency control of the microgrid with the main grid, transient current surges generated during the grid connection process are effectively suppressed. Since the microgrid is composed of many DGs and inverters, in order to achieve a reasonable distribution of the output power of each inverter during the pre-synchronization process, it is necessary to start the pre-synchronization control for each inverter.

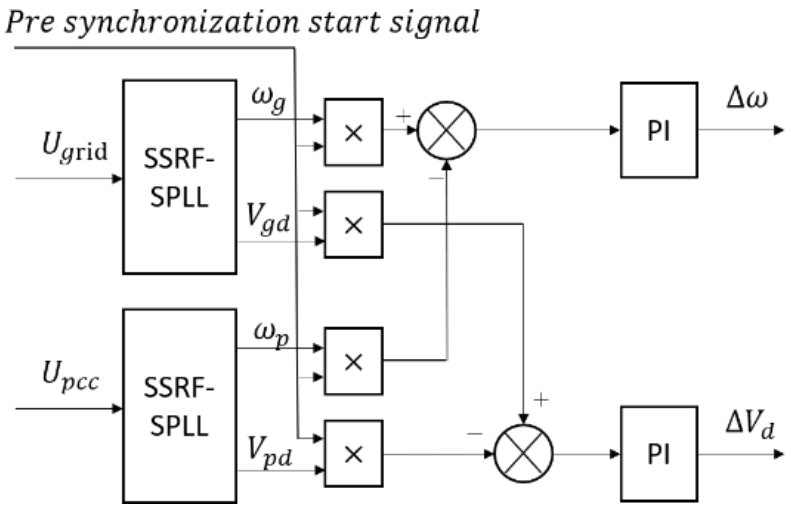

Figure 4.13 Calculation of frequency difference and voltage amplitude difference between grid voltage and PCC voltage

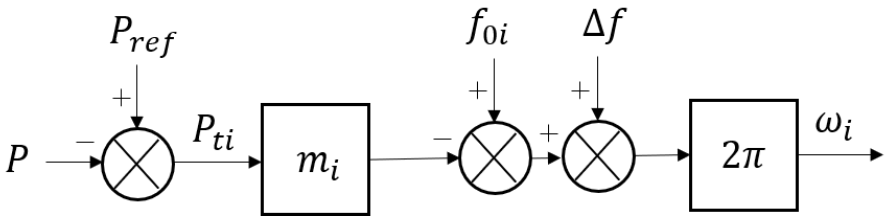

(a)

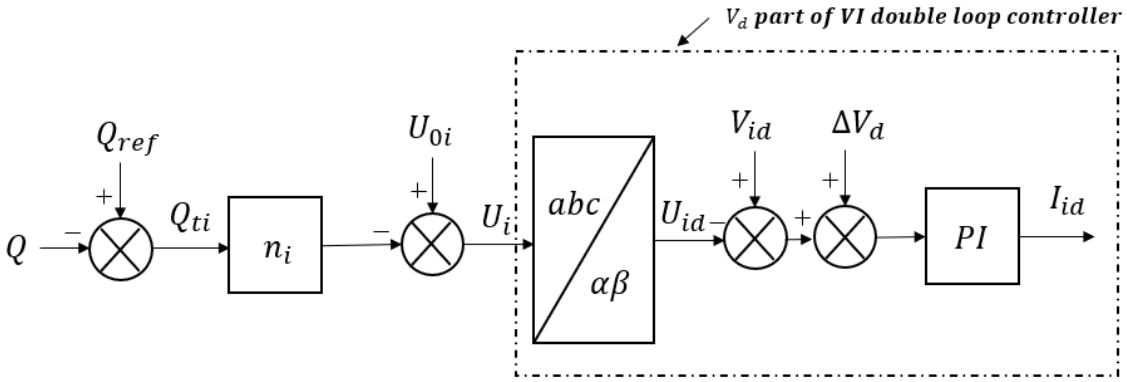

(b)

Figure 4.14 Block diagram of (a) frequency adjustment and (b) voltage amplitude adjustment in pre-synchronous control

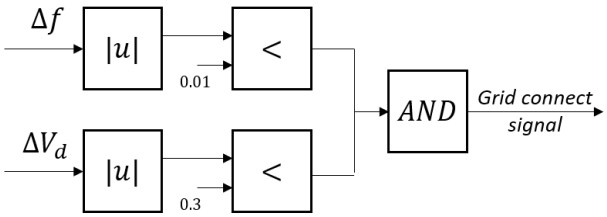

Figure 4.15 Grid-connected signal generation diagram

The impact of different line impedances between parallel inverters is minimized with the proposed control strategy that combines enhanced droop control and pre-synchronization. Not only the output power of the parallel inverters is equally shared, but also the microgrid system can maintain stability under the conditions of island operation and grid-connected operation, protecting the system components from being damaged.

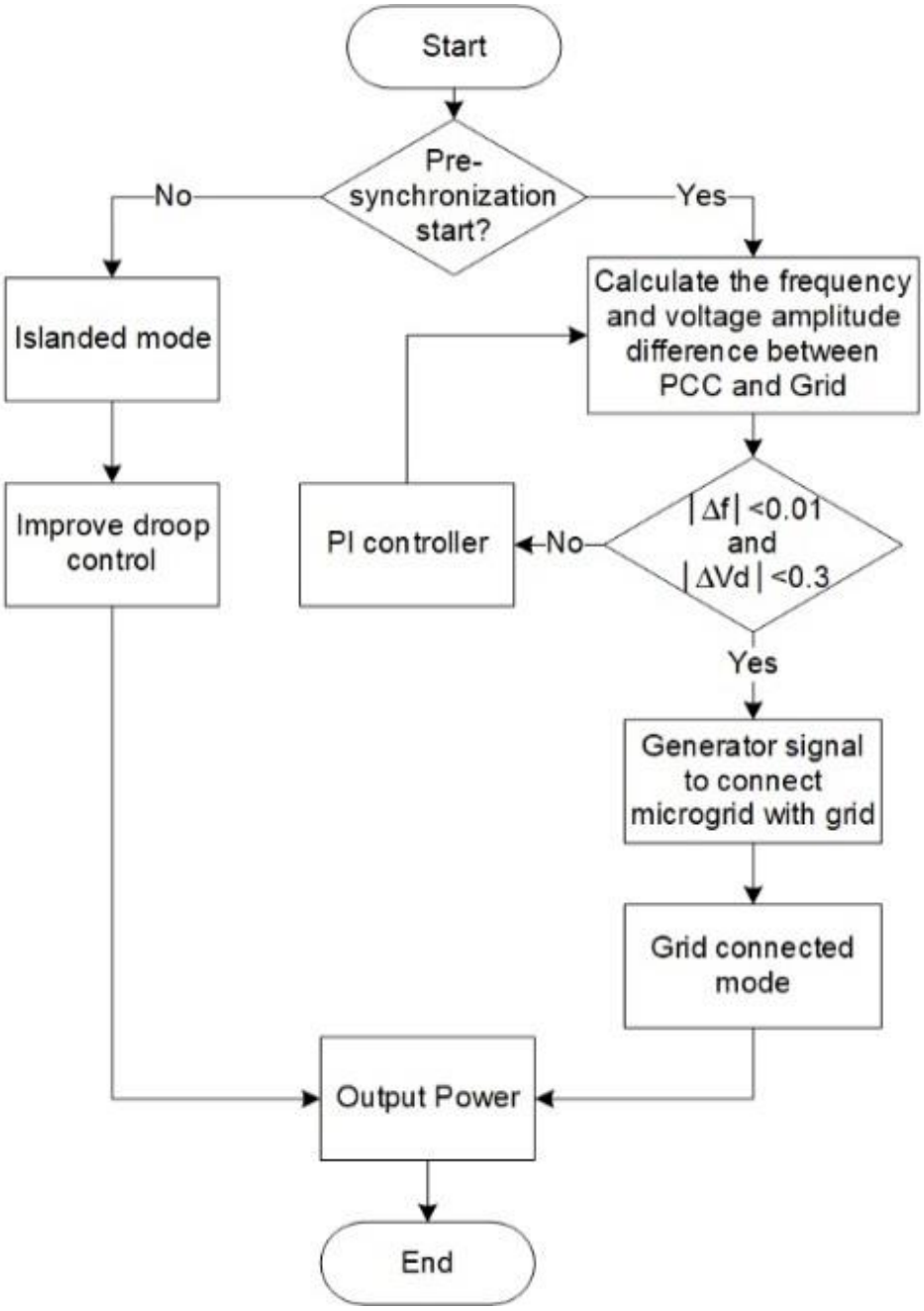

Figure 4.16 Pre-synchronization control flow chart

4.2.2 Simulation results

The microgrid considered in this paper comprises two parallel inverters, one load and can be connected to the main grid. The two parallel inverters have totally different line impedance values to simulate the different distance from the micro source to PCC. The different parameters of the system are summarized in Table 4-3.

Table 4-3 PARAMETER OF THE SYSTEM

	Parameters	**Value**
DG units	Inverter switching frequency	10 kHz
	DC bus voltage	800 V
	Nominal bus frequency	50 Hz
	RMS line voltage	380 V
	Line impedance (DG1)	2.64 mH, 1.642 Ω
	Line impedance (DG2)	1.32 mH, 0.821 Ω
Load	Active power	10 kW
	Inductive reactive power	4 kvar
Grid	Phase to phase voltage	380 V
	Line impedance (Grid)	2.64 mH, 1.642 Ω
	Frequency	50 Hz
	Phase angle of phase A	180°

In the normal operation mode, both parallel inverters and the load are always connected to PCC. With no pre-synchronization (case 1), the grid is connected to PCC at 0.1 s. With pre-synchronization (case 2), the pre-synchronization process starts at 0.1 s and the breaker is closed to automatically connect to the grid when the pre-synchronization is achieved.

Case 1. Grid Connection without Pre-synchronization

In this case, the microgrid with power sharing control is directly connected to the grid without synchronization. Due to the uncertainty of the grid connection time of the microgrid and the phase deviation of phase A of the grid in practice, there may be voltage amplitude differences and phase differences between the PCC side and the grid side. It can be seen from Figure 4.17 that after closing the breaker (at 0.1 s), the microgrid is merged into the main grid, and there is great fluctuation in both active and reactive power which will clearly exceed the generator ratings in a practical system. The fluctuation during the transient is not identical for both generators due to the different line impedance. This means that power sharing is not working during the transient time. At about 0.4 s, both reactive power and active power reach the steady state. However, the active power is maintained at -7.7 kW, the reactive power is maintained at -200 VAr, assuming that no protection is used to stop reverse power flow to the

distributed generators. The load power, in this case, comes from the grid. Figure 4.18 shows that the output fundamental frequencies of DG1 and DG2 significantly deviate from the 50 Hz value during the transient time (from 0.1 s to 0.4 s) and the frequency of both DGs return to 50 Hz after the transient time.

Figure 4.19 shows the one-phase voltage waveforms at the PCC terminal and at the grid terminal. Before connection to the grid, the voltages are out of phase and have different amplitudes. As there is no pre-synchronisation control, the PCC voltage drops significantly after the system is connected to the main grid. After the transition time the two voltages are synchronised in phase, but the voltage amplitudes are not synchronised, which is caused by the network side line impedance between the PCC voltage measurement points on the PCC side and the grid side.

Figure 4.20 shows the three-phase voltage and current waveforms on the grid side. Figure 4.21 shows the output power at the grid terminal. As shown, due to the failure to adopt reasonable synchronous control, the two DGs in the microgrid not only failed to supply the demand of the loads but also needed to continuously absorb power from the grid, which is impossible to happen in a practical system. Significant current is absorbed from the grid during the transient, which means that the microgrid system will fail.

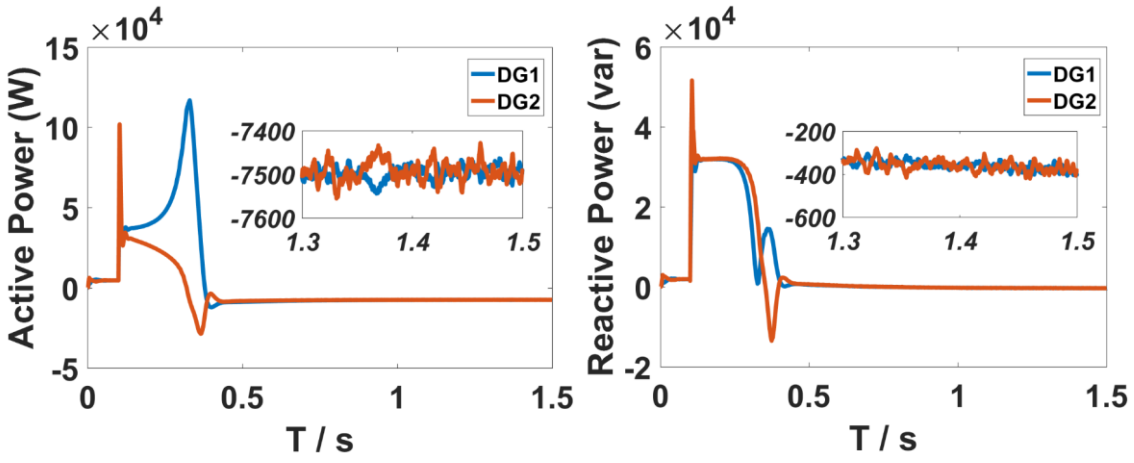

Figure 4.17 Power of DG1 and DG2

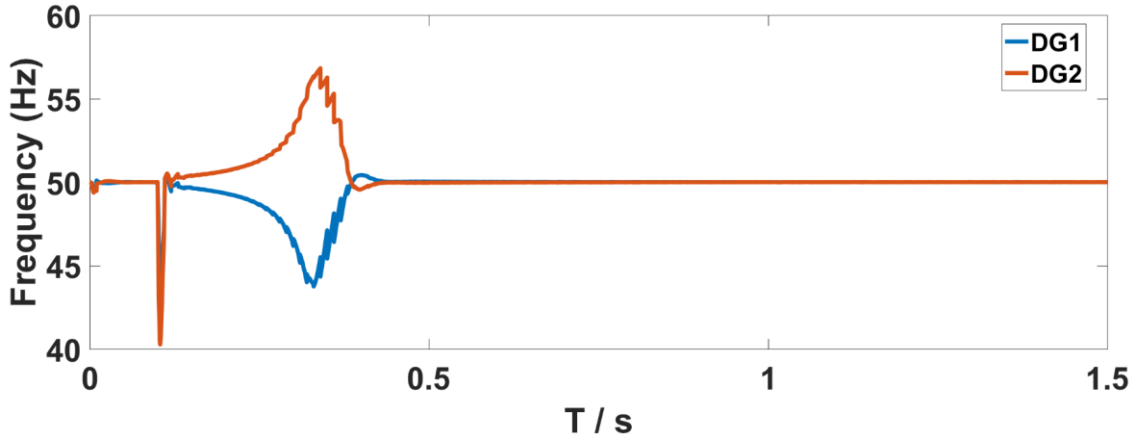

Figure 4.18 Frequency of DG1 and DG2

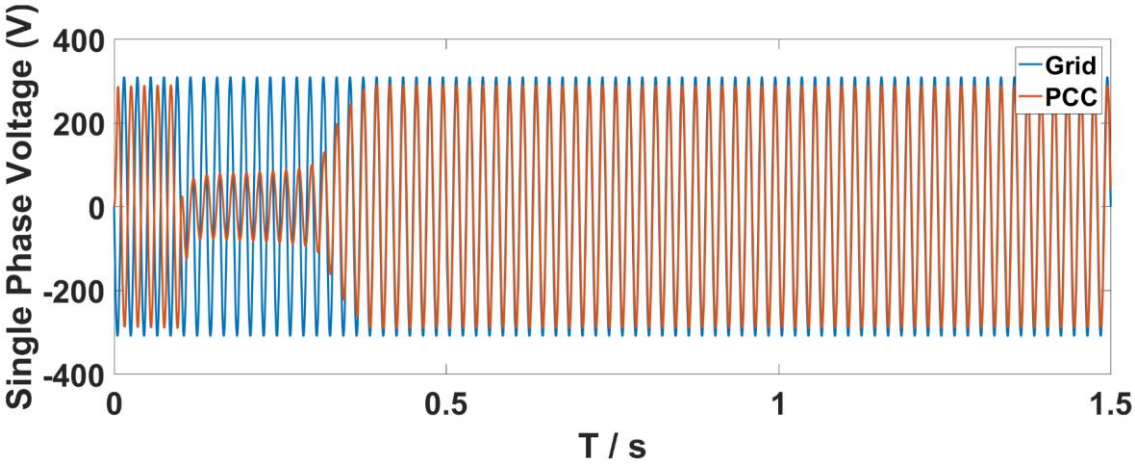

Figure 4.19 Single phase voltage of PCC and grid side

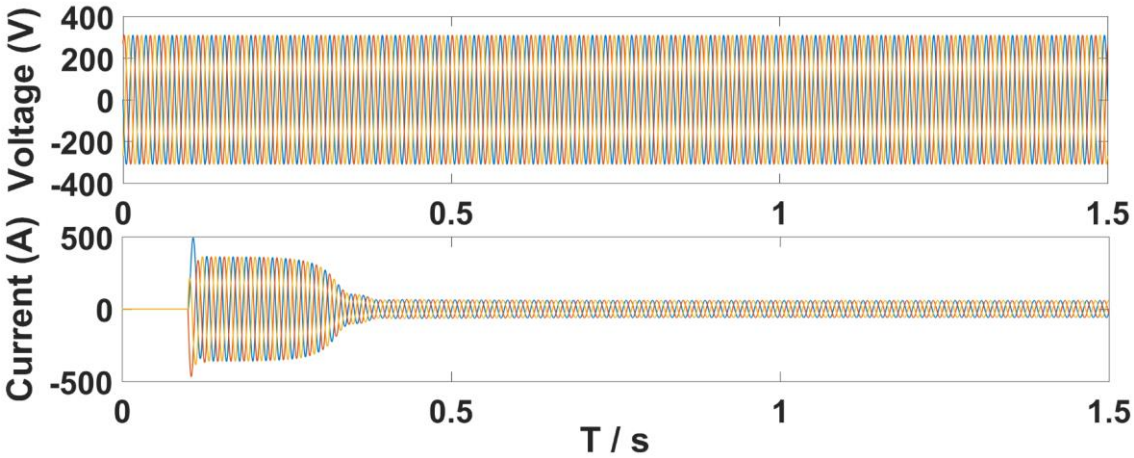

Figure 4.20 Voltage and current of grid side

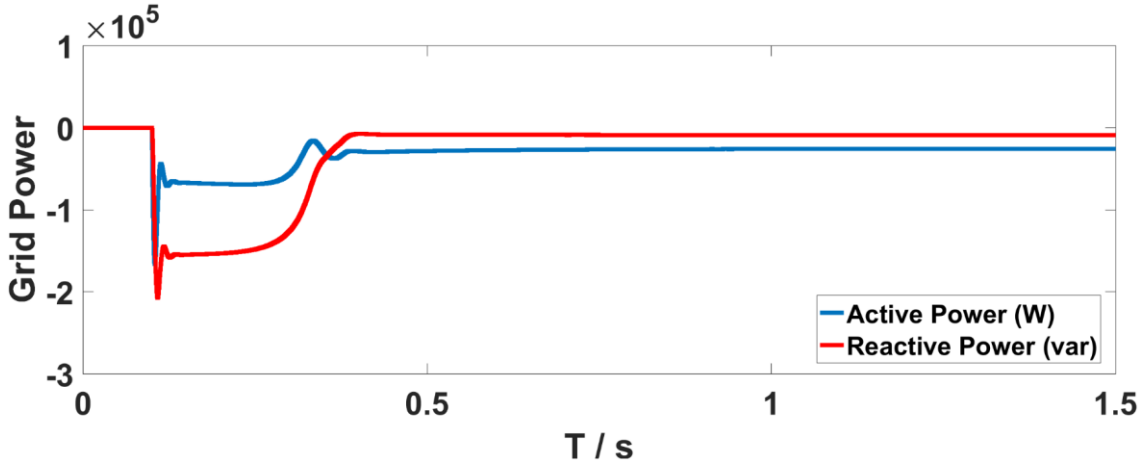

Figure 4.21 Power of grid side

Case 2. Grid Connection with Pre-synchronization

a. Phase Synchronization Only

Under the same conditions as Case 1, frequency/phase pre-synchronization control is added in this case. Different from Case 1, at 0.1 s, the microgrid is not directly connected into the grid, but the frequency pre-synchronization control module is activated to synchronize the microgrid with the grid and the switch is closed after synchronisation is achieved according to the flowchart in Figure 4.16. As shown in Figure 4.22, synchronisation is achieved, and the switching signal is activated at 0.62 s. Figure 4.23 shows that power sharing is achieved with a short-time disturbance at the instance of closing the switch. The frequency is deviated before closing the switch (Figure 4.24) to minimise the difference in phase/frequency between the grid and PCC voltages. Figure 4.25 shows one phase PCC terminal voltage and grid voltage. When the frequency pre-synchronization control is started, the phase difference between the two waveforms quickly shrinks to the same phase. As for the voltage amplitude, although it is not synchronized, same as Case 1, the voltage at the PCC terminal is more stable and less fluctuating.

Figures 4.26 and 4.27 show the current and power exchange with the main grid with the positive sign means that the power is injected to the grid. As shown, the generators generate more power after the grid connection which is fed the local load and the excess in active power is injected to the grid. It worth mentioning that no power limits are applied to the generators, in the simulation, to better understand the effect of line impedance of the

generators and grid. In a practical system, the control will limit the output power of the generators to their power ratings. Because of the amplitude difference between the PCC and grid voltages, due to the grid impedance, significant reactive power is absorbed from the grid.

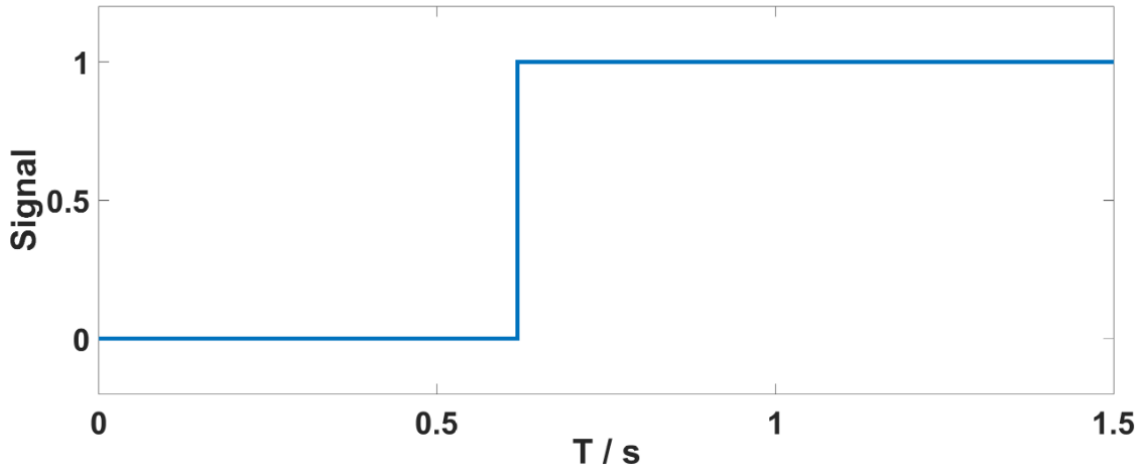

Figure 4.22 Switching signal (Pre-synchronization finish time)

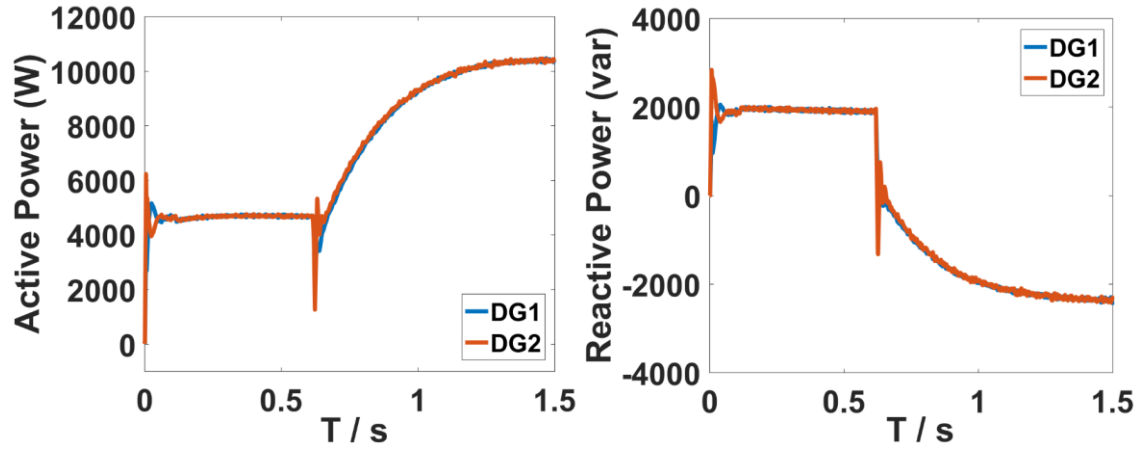

Figure 4.23 Power of DG1 and DG2

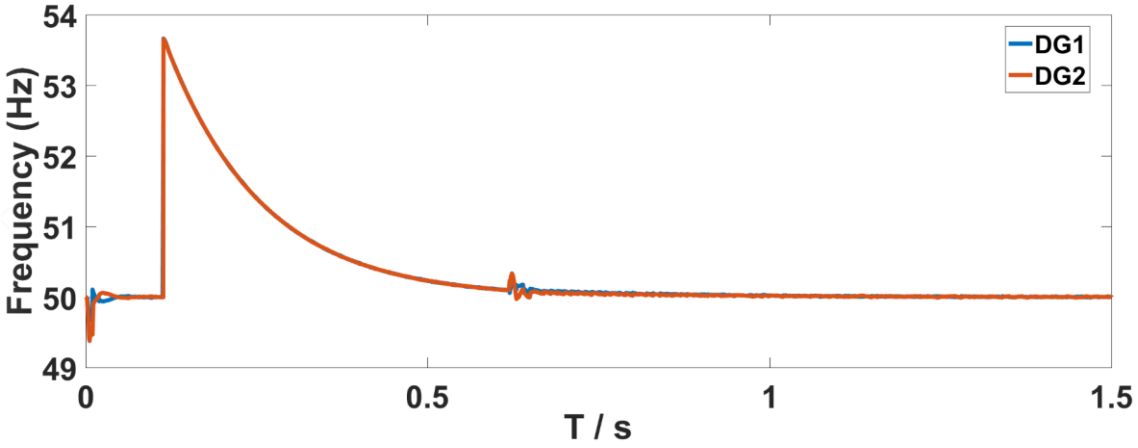

Figure 4.24 Frequency of DG1 and DG2

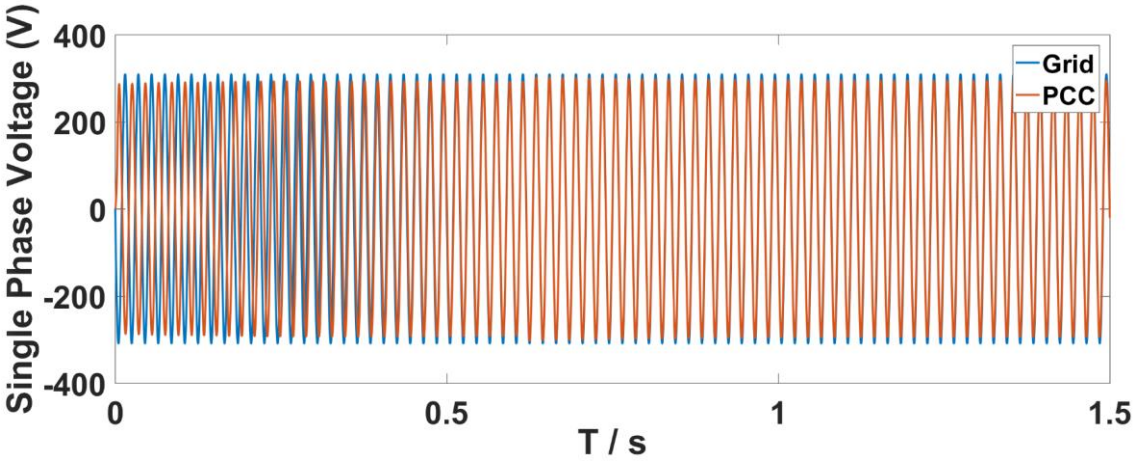

Figure 4.25 Single phase voltage of PCC and grid side

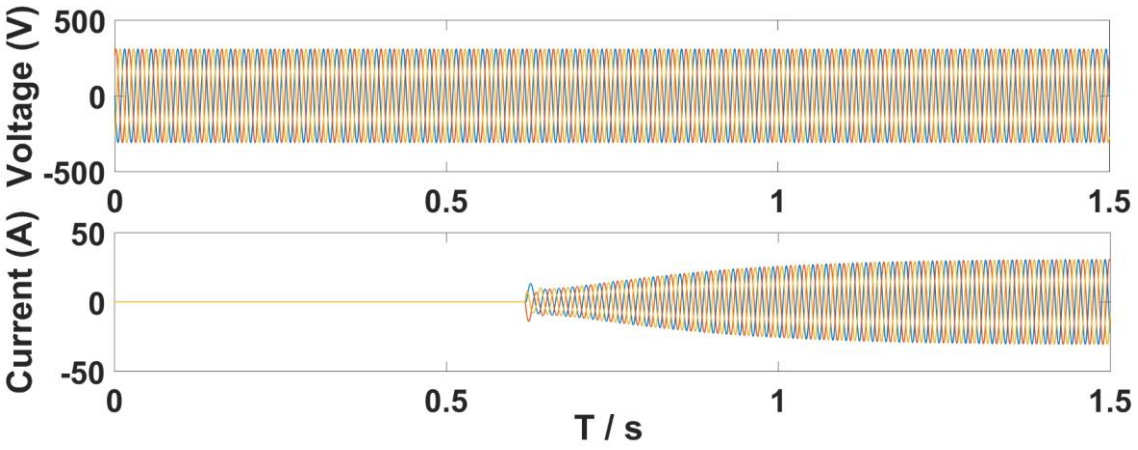

Figure 4.26 Voltage and current of grid side

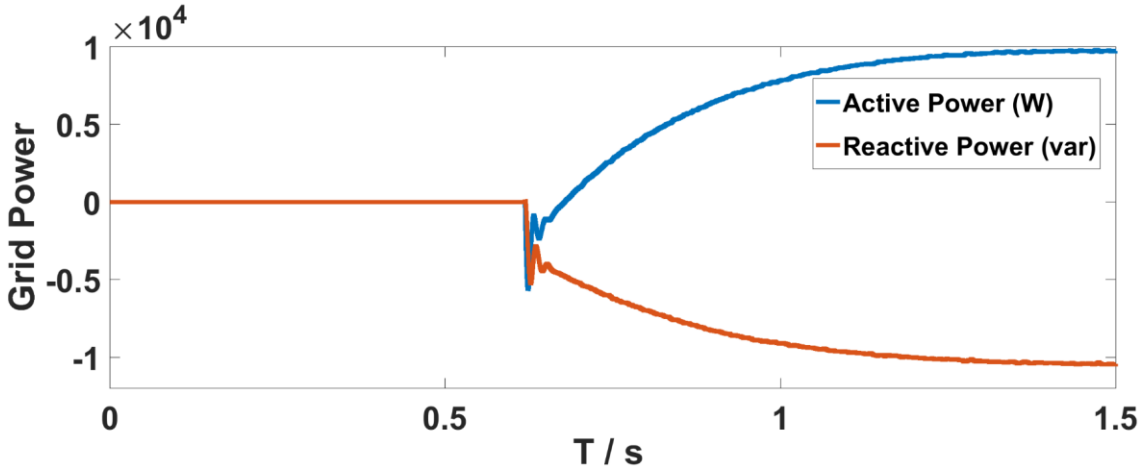

Figure 4.27 Power of grid side

b. Phase and Voltage Synchronization

In this case, voltage pre-synchronization control is added at the same time together with the phase/frequency pre-synchronization. Similar to the previous case, the pre-synchronization starts at 0.1 s. As shown in Figure 4.28, the pre-synchronization process is completed and the grid is connected at 0.63 s. Figure 4.29 shows the output active and reactive power waveforms of the two DGs. Although the output line impedance of the two DGs is different, they can still output power according to the rated power ratio, with less oscillation at the grid connection instant compared to Case 2.a. No significant change in generators reactive power magnitude/ sign compared to the previous case due to the matching amplitude of the PCC and grid voltages. The change in generator frequency before and after grid connection is similar to Case 2.a but with less oscillation due to grid connection.

Figure 4.31 shows the phase A voltage values of PCC and grid. At the beginning, the phase difference between the two waveforms is set at 180°. Due to the load, there are also some voltage amplitude differences. Between 0.1 s and 0.63 s, the two waveforms steadily approach until they completely coincide. At this time, the phase difference and amplitude difference are nearly 0 and the pre-synchronization process is completed. From 0.63 s to 1.5 s, the two waveforms are completely coincident. Unlike Figure 4.25, the amplitudes of the PCC and grid voltage is nearly the same. This ensures a smoother and more stable operation.

Figures 4.32 and 4.33 show the voltage/current waveforms and the output power waveforms at the grid side, respectively. Similar to Case 2.a, the excess in generated power is

injected to the grid. However, much smaller reactive power exchange is achieved due to the voltage amplitude synchronization.

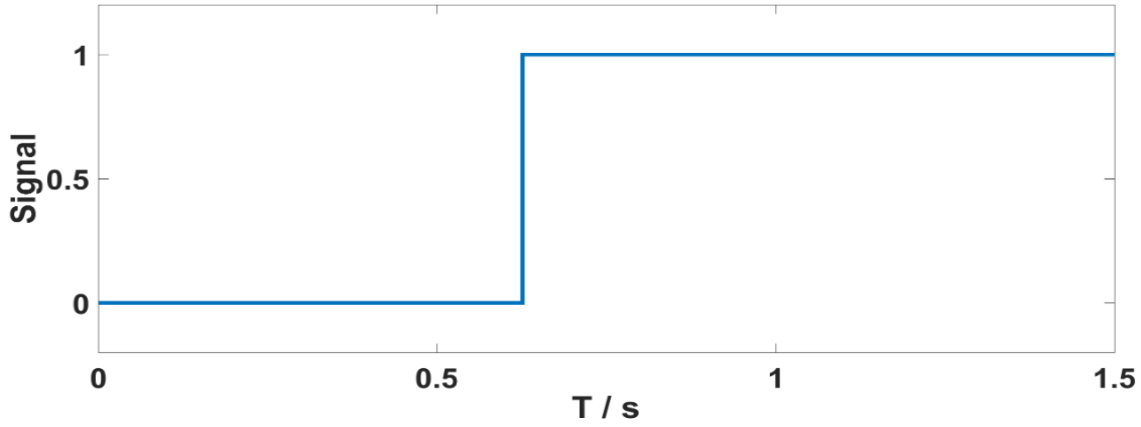

Figure 4.28 Switching signal (Pre-synchronization finish time)

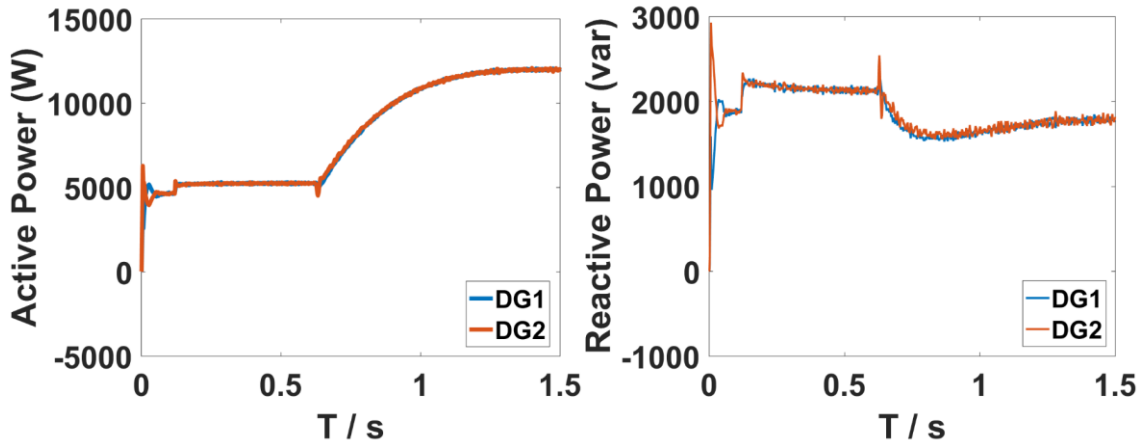

Figure 4.29 Power of DG1 and DG2

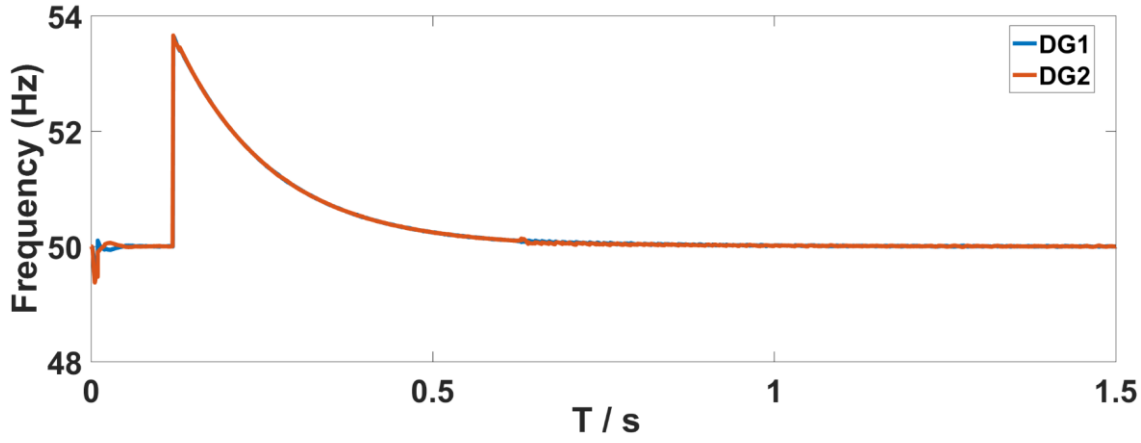

Figure 4.30 Frequency of DG1 and DG2

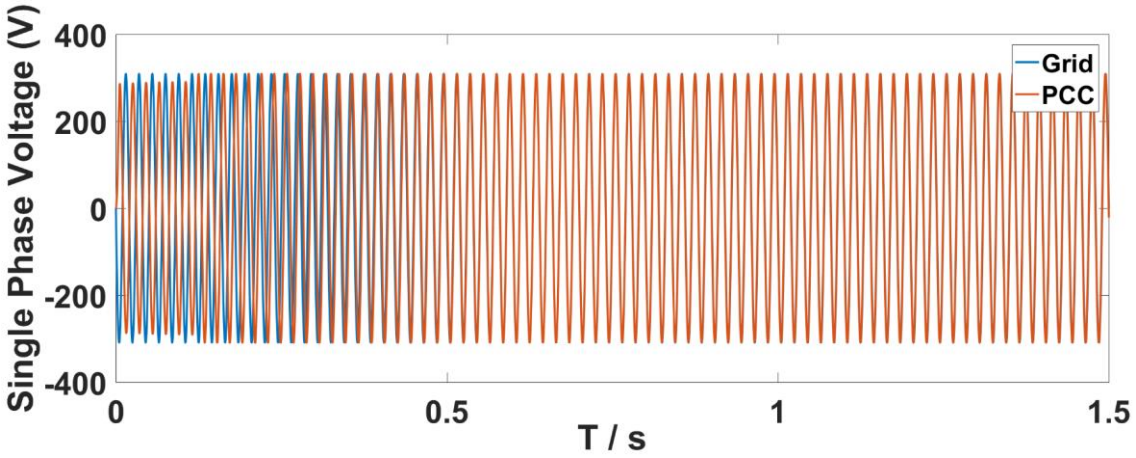

Figure 4.31 Single phase voltage of PCC and grid side

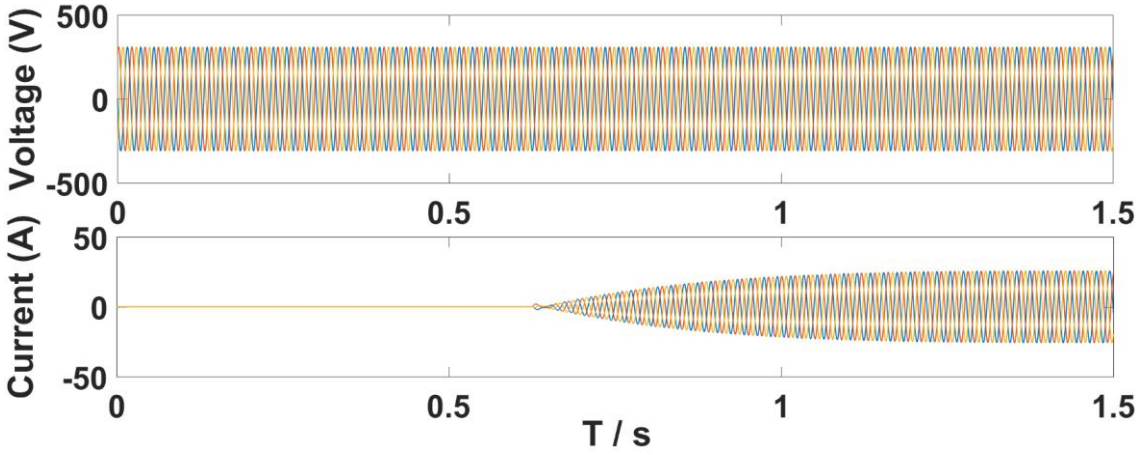

Figure 4.32 Voltage and current of grid side

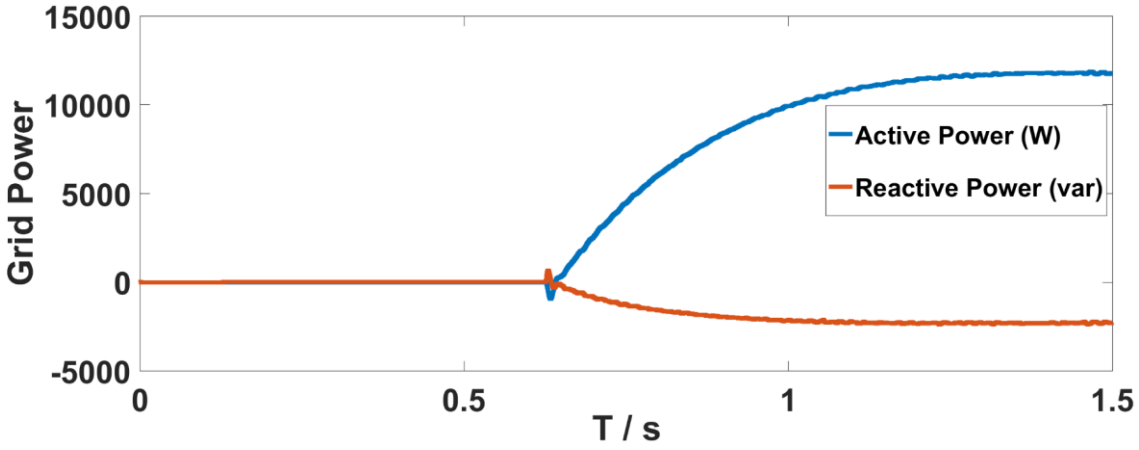

Figure 4.33 Power of grid side

4.3 Summary

In the first part of this chapter, the problem of power sharing between parallel grid-connected inverter is solved by the proposed droop control with a secondary control method. Firstly, the traditional droop control method was discussed and their disadvantage in parallel grid connected inverter is highlighted. Then, a popular control method named virtual impedance droop control is analysed and its drawback compared to the proposed control method is discussed. A simulation model was built to analyse the performance of the proposed control method, and to compare with the simulation of the virtual impedance control method. The results show that the droop control with the secondary control loop has much better performance than virtual droop control method.

In the second part of this chapter, proposes a control method combining droop control and pre-synchronization control under the situation that the line impedance of each micro source in the microgrid is different. In addition to achieving power sharing between micro-power sources, a smooth connection when the microgrid is connected to the main grid is also achieved, which improves the stability of the system operation. Finally, the method is verified by simulation using Matlab/Simulink.

Chapter 5 System performance evaluation by proposed power sharing control method

In this chapter, the proposed improved droop control method is applied to a multi-inverter power system to verify that the method is not only suitable for simple parallel connection of two inverters, but also applicable for multi-inverters parallel connection system. Similar to the operating principle of the dual inverter parallel system described in Chapter 4, in a parallel multi-inverter system with inconsistent line impedance at the inverter output, each inverter sends the output active power and output reactive power information to the system control module. After calculations, and according to the rated output power ratio of each inverter, the system control module feeds back to each inverter a reference for power output according to the obtained data. In this chapter, to verify that the improved droop control method can be used under different operating conditions, the entire system operation is analysed under islanded operation, grid-connected operation and when switching between these two modes of operation.

To represent the multi-inverter parallel system operation, a three-inverter parallel system is considered in this chapter. The circuit diagram is shown in Figure 5.1. As shown, the system includes three inverter modules, two loads, and switches for connecting and disconnecting the loads and main grid. The system parameters are shown in Table 5-1.

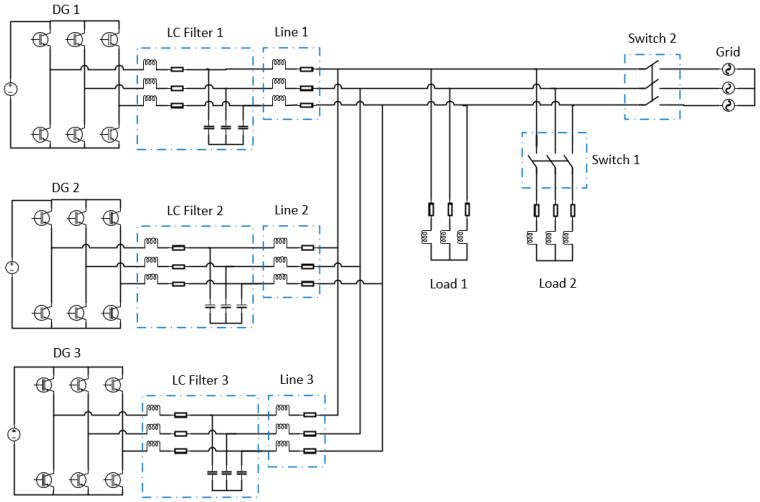

Figure 5.1 Circuit diagram of test system

Table 5-1 PARAMETER OF THREE INVERTERS PARALLEL CONNECTION SYSTEM

	Parameters	Value
DG units	Inverter switching frequency	10 kHz
	DC bus voltage	800 V
	Nominal bus frequency	50 Hz
	RMS line voltage	380 V
	Line impedance (DG1) / 5 km	1.71 mH, 1.37 Ω
	Line impedance (DG2) / 2.5 km	0.855 mH, 0.685 Ω
	Line impedance (DG3) / 10 km	3.42 mH, 2.74 Ω
Load 1	Active power	20 kW
	Inductive reactive power	6 kVAr
Load 2	Active power	20 kW
	Inductive reactive power	0 kVAr
Grid	Phase to phase voltage	380 V
	Frequency	50 Hz
	Phase angle of phase A	0°/180°

Because the distance from the output terminal of each inverter in the parallel inverter system to the load is different, the line impedance is different. In the simulation, the ratio of inverter output line impedances is set at 2:1:4 and the 70 mm^2 single core XLPE/PVC cable is used in impedance calculation as detailed in Appendix B. For the two loads in the system, Load 1 is 20 kW active power plus 6 kVAr reactive power, and Load 2 is 20 kW active power with no reactive power. To verify that the microgrid can successfully be synchronised with the main grid, prior to the grid-connection, regardless of the uncertainty of when the two systems are connected, the system operation is simulated with 0 degrees and 180 degrees initial phase shifts i.e., when the two systems are in phase and totally out of phase, respectively.

5.1 Case study for proposed system

Four different scenarios covering islanding and grid connected operation of the microgrid with equal and different generators power rating are simulated in this chapter. Table 5-2 shows the timing of the main network events assumed in the simulation of these four scenarios. In all the four cases, switch 1 is closed at 2 s to connect Load 2 to the PCC terminal and is opened to disconnect it at 3 s. In the islanding operation (cases 1 and 2), Switch 2 remains open. In the cases with grid connection (cases 3 and 4), the pre-synchronization process, which was explained in Chapter 5, starts at 0.5 s and Switch 2 is closed after pre-synchronization is achieved. Switch 2 is opened again at 4 s to examine the impact of grid disconnection on microgrid's operation.

All detailed information of the simulation models used in this thesis is provided in Appendix C.

Table 5-2 TIMING OF NETWORK EVENTS IN DIFFERENT TEST CASES

Network Event	Time	Microgrid operation scenario
Connection of Load 2	2 s	All cases
Disconnection of Load 2	3 s	
Start of pre-synchronisation	0.5 s	Cases with grid connection
Connection to grid	After pre-synchronisation	
Disconnection from grid	4 s	

5.1.1 Case 1: Islanding mode with equal generator power ratings

In case 1, the power ratings of the three parallel inverter-based DG systems are the same ($DG1: DG2: DG3 = 1: 1: 1$). Figure 5.2 shows the operating frequencies of the three inverters. As shown, the frequencies include fluctuations at the starting of the system, Load 2 connection (at 2 s) and Load 2 disconnection (at 3 s). An increase in load will cause a temporary drop in frequency, while a break in load will cause a temporary increase in frequency. In both cases, the control was able to bring the frequency back to 50 Hz within a short period of time. Similarly, as shown in Figure 5.3 and Figure 5.4, the output active power and reactive power of the three inverters are slightly different during the starting transient and at the load connection (at 2 s) and disconnection (at 3 s). However, the output powers of the inverters are quickly re-shared which evidence the fast response of the power sharing algorithm. This clearly shows that, in the case of island operation of the microgrid, the control algorithm can achieve power sharing between the inverter-based DG systems despite the different line impedances.

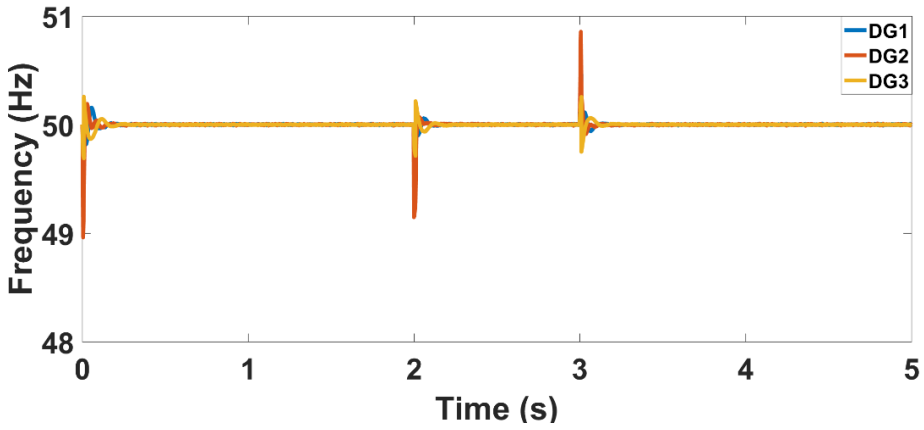

Figure 5.2 Frequency of DG1, DG2 and DG3

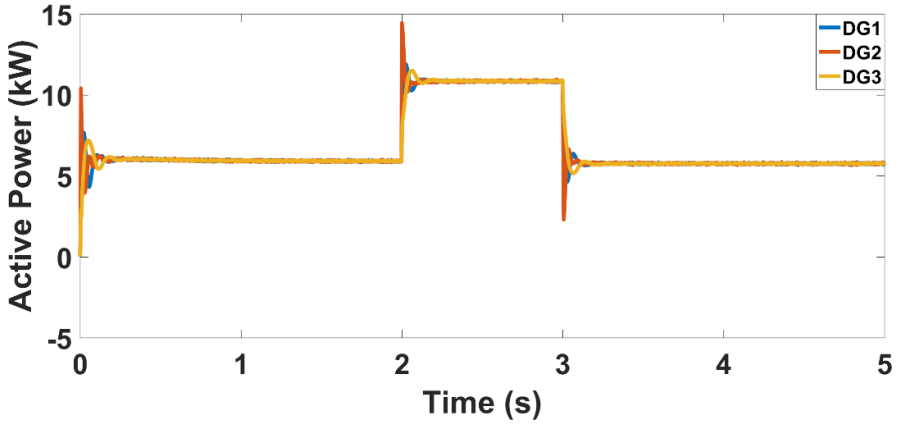

Figure 5.3 Active power of DG1, DG2 and DG3

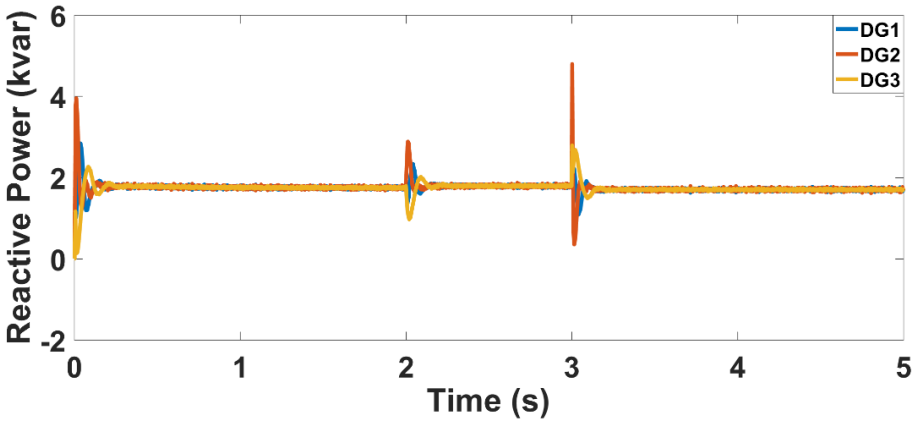

Figure 5.4 Reactive power of DG1, DG2 and DG3

5.1.2 Case 2: Islanding mode with different generator power ratings

In this case, the capacities of the three parallel inverters are different ($DG1: DG2: DG3 = 3: 2: 1$). It can be seen from Figure 5.5 that the operating frequencies of the three inverters are not different from those obtained in Case1. The inverter control is able to quickly stabilise the frequency back to 50 Hz after the starting transient and transients due to load connection and disconnection. Figures 5.6 and 5.7 show the active power and reactive power of the three inverters, respectively. As shown in Figure 5.6, the active powers of DG1, DG2 and DG3, after the starting transient, are 9 kW, 6 kW and 3 kW, respectively. Therefore, the ratio between the output powers of the generators is 3:2:1, which is consistent with the ratio of the rated capacity. In the steady state after the connection of Load 2, the active powers of DG1, DG2 and DG3 increase to 16.8 kW, 11.2 kW and 5.6 kW, respectively, maintaining the 3:2:1 ratio.

One point to note is that since the reference output power of each inverter in the control theory proposed in this thesis is the calculated value and the actual output power is the measured value, there will be a certain difference between the calculated value and the measured value, and these power differences are actually consumed by the output line impedance of each inverter, resulting in a certain difference between the actual output power sum of each inverter and the load sum in the system. However, the main point of power output of the parallel inverters by capacity ratio is fully valid. It is also present in all subsequent Cases.

Similarly, as shown in Figure 5.7, after the starting transient, the reactive powers of DG1, DG2 and DG3 are settled at 2.7 kVAr, 1.8 kVAr and 0.9 kVAr, respectively. After connecting Load 2, the reactive powers of DG1, DG2 and DG3 increase to 2.76 kVAr, 1.83 kVAr and 0.92 kVAr, respectively. The slight increase in reactive power is due to increased voltage drops across line impedances, taking into account that the added load (Load 2) is assumed to have no reactive consumption. Again, the reactive power is shared with the ratio between the generator's capacities (3:2:1) at different loading conditions. Therefore, it can be concluded that when the output line impedance is inconsistent, each inverter can output power according to the rated capacity ratio when employing the proposed power sharing control algorithm. Therefore, multiple parallel inverters can cooperate well to provide the required energy supply for the loads.

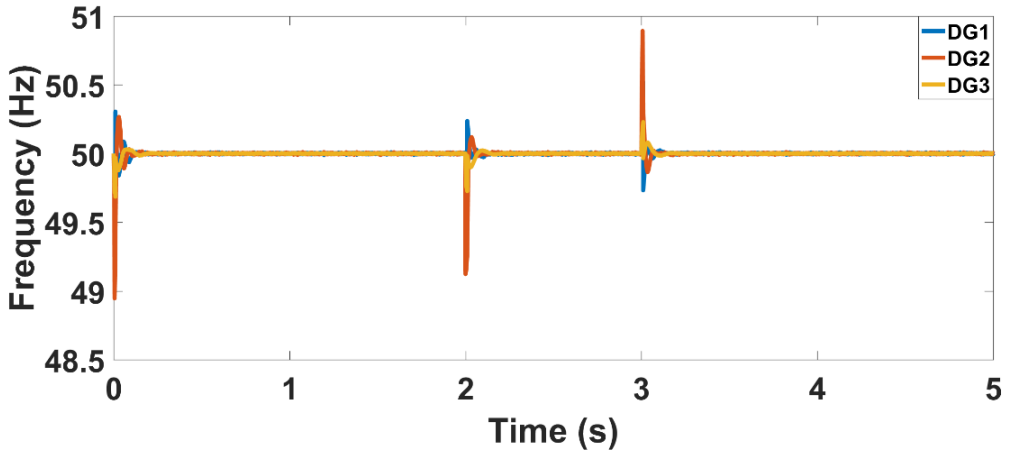

Figure 5.5 Frequency of DG1, DG2 and DG3

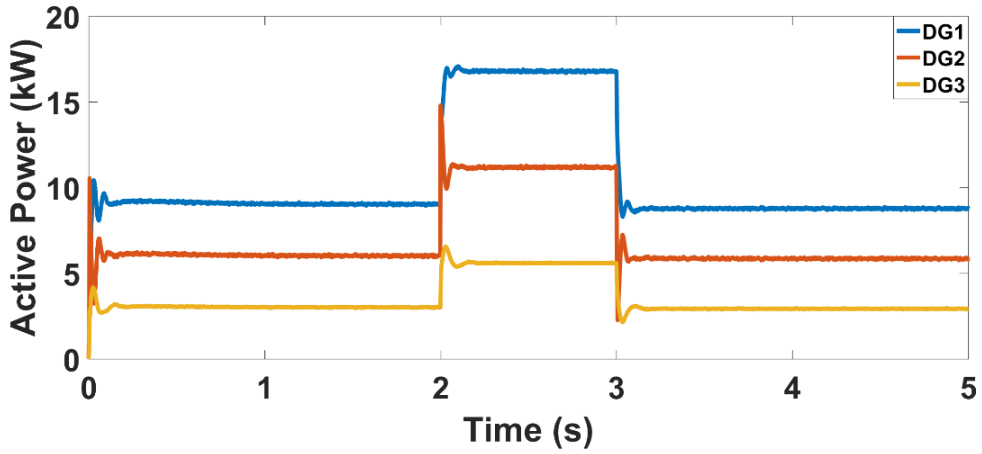

Figure 5.6 Active power of DG1, DG2 and DG3

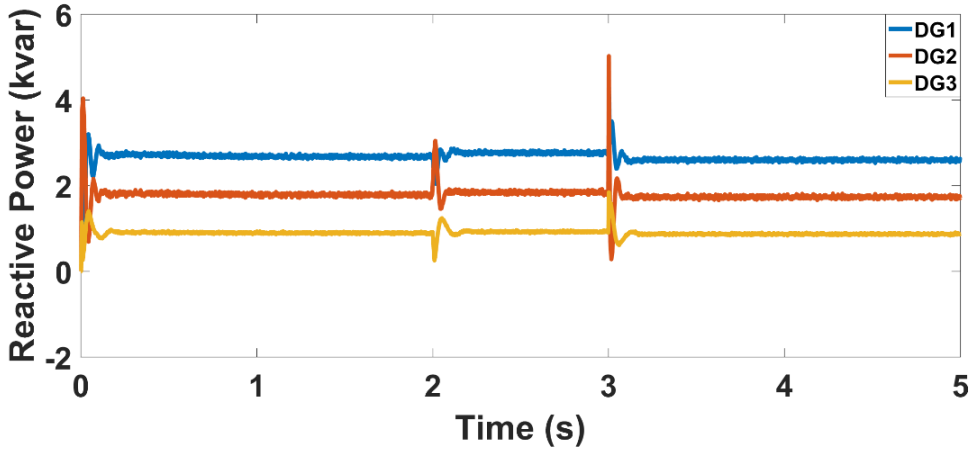

Figure 5.7 Reactive power of DG1, DG2 and DG3

5.1.3 Case 3: Connection to grid at 0° voltage phase difference

In this case, the microgrid system is started in the islanding mode and then the connection to the grid is started when the microgrid is in phase with the grid. After operating under grid-connected conditions for some time, the microgrid is disconnected from the grid to make sure that it will remain stable when switching between grid-connected and islanded operation. In this case, the three parallel inverters in the microgrid are assumed to have the different rated capacity ($DG1: DG2: DG3 = 3: 2: 1$), and the microgrid is assumed to be in phase with the grid at the start of pre-synchronisation process. The connection to grid command is received at 0.5 s and consequently pre-synchronization control is started. Switch 2 is closed after pre-synchronisation is achieved and opened again to disconnect the grid at 4 s. Figure 5.8 shows the switching signal for Switch 2 which connects the microgrid to the grid.

Since there is no phase difference between the grid voltage and the microgrid voltage, the pre-synchronization process will only eliminate the voltage amplitude difference and therefore is completed quickly, at about 0.6 s as shown in Figure 5.9. At this time, the microgrid is merged into the main power grid, and it starts to operate in grid-connected mode. In Figure 5.10, similar to islanding conditions, the operating frequency of each inverter includes small fluctuations at 0 s, 0.5 s, 0.6 s, 2 s and 3 s, which attenuates in short time and the frequency settles back at 50 Hz.

For the output power of each inverter, as can be seen in Figures 5.11 and 5.12, although there are transients at each of the above time points, the output power of each inverter is distributed according to the rated capacity ratio, which is 3:2:1 in this case. This means that for the active power in Figure 5.11, from 0 s to 0.5 s, the output of the three inverters is 9 kW, 6 kW and 3 kW, same as in island operation. At 0.6 s the system completes pre-synchronization control and starts to operate in the grid-connected mode. Before connecting Load 2 at 2 s, the output powers of the three inverters are stable at 11 kW, 7.3 kW and 3.65 kW which are increased to 23.4 kW, 15.5 kW and 7.8 kW, respectively after the connection of Load 2, maintain power sharing among parallel inverters before and after the load increase. After the disconnection of Load 2 at 3 s, the output powers of the inverters are reduced to the same levels before connection of Load 2. At 4 s, the microgrid system is disconnected from the grid and continues to operate, in island mode, at the same voltage and frequency as the islanded operation between 0 s to 0.5 s, which means the grid connected mode with almost no impact on the stability of operation of the microgrid.

Similarly, as shown in Figure 5.12 the reactive powers of the three inverters before the start of pre-synchronisation at 0.5 s are the same as the previous islanded case. After grid connection, the reactive power values are increased to 2.75 kVAr, 1.81 kVAr and 0.9 kVAr, respectively; from 0.5 s to 2 s, the output of the three inverters is not The power is stable at 3.2 kVAr, 2.2 kVAr and 1.1 kVAr respectively; in 2 s to 3 s, Load 2 is connected to the system, because it is a resistive load, the output reactive power of the three inverters has not changed much, and they are stable at 3.8 kVAr, 2.3 kVAr and 1.25 kVAr; from 3 s to 4 s, the output reactive power of each inverter returns to the level before Load 2 is connected; when the 4 s grid is disconnected, the microgrid system can still operate stably without impact.

In Figure 5.13, the main grid power change under pre-synchronization and the grid-connected conditions are shown. At each time point, there is power flow between the grid and the microgrid to ensure that the loads can get enough power supply.

In general, in case 3, based on the phase angle of the main grid voltage phase A is 0°, the rated capacity of the three inverters is 3:2:1. Not only in the process of pre-synchronization, also in the system running at grid-connect mode, as well as mode change from islanded mode to grid-connected mode and from grid-connected mode to islanded mode, the proposed control algorithm can support the system to run well.

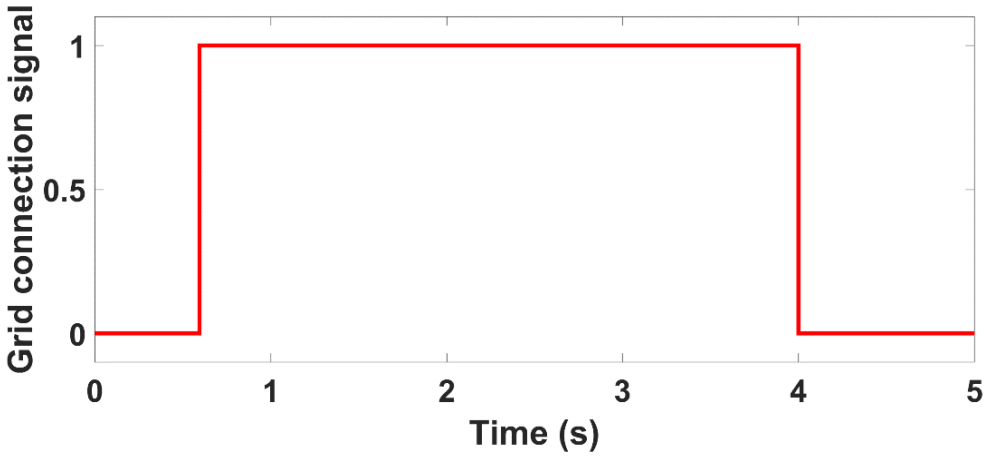

Figure 5.8 Switching signal (Pre-synchronization finish time/Grid connect time)

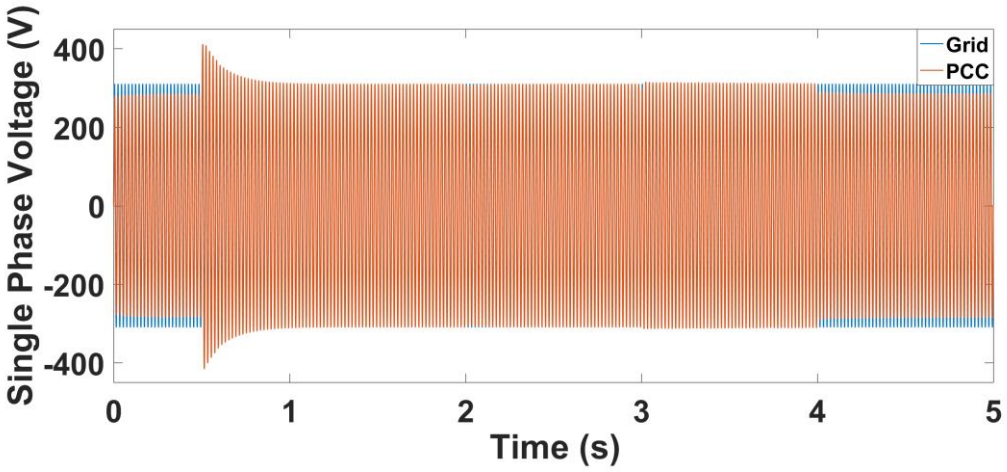

Figure 5.9 Single phase voltage of PCC and grid side

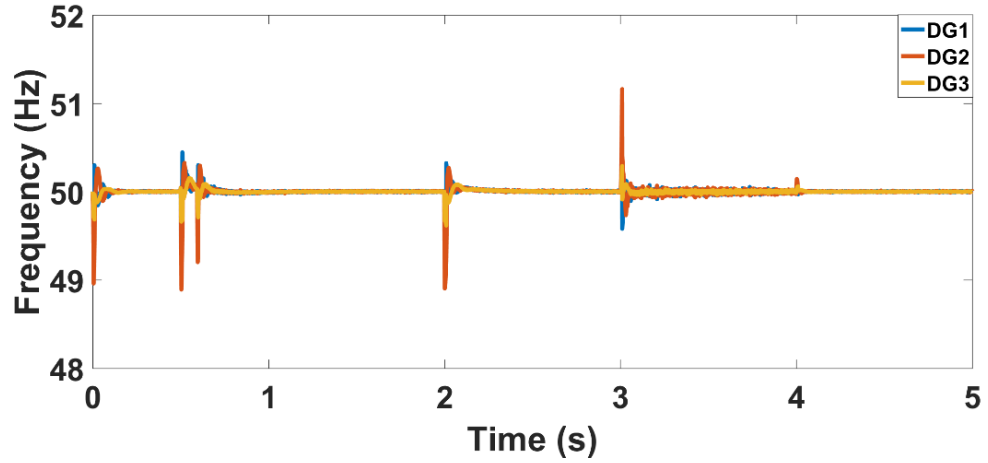

Figure 5.10 Frequency of DG1, DG2 and DG3

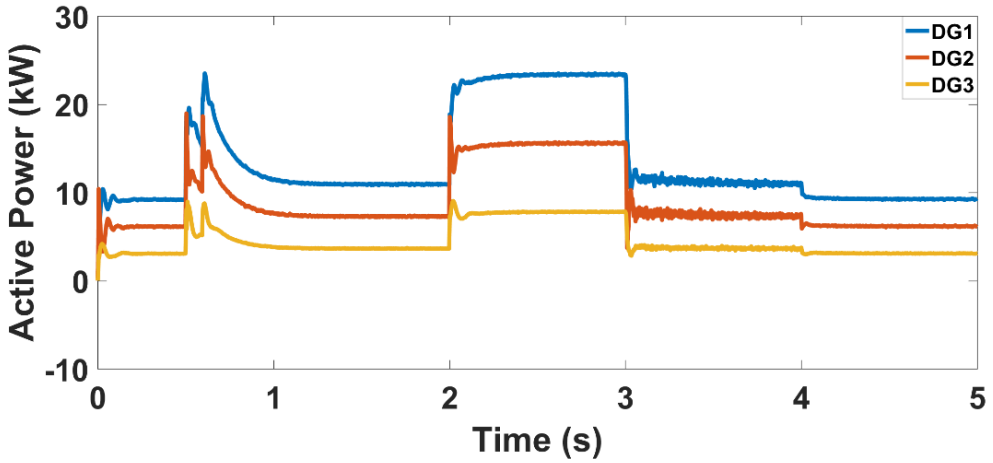

Figure 5.11 Active power of DG1, DG2 and DG3

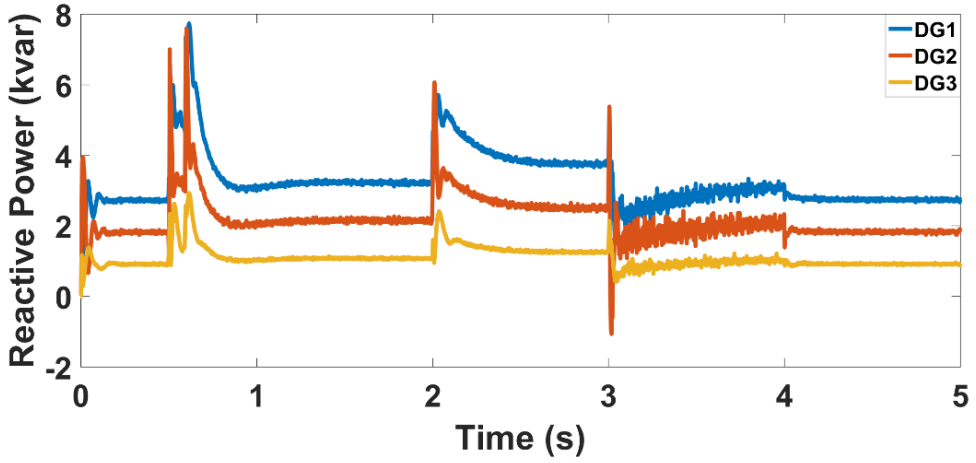

Figure 5.12 Reactive power of DG1, DG2 and DG3

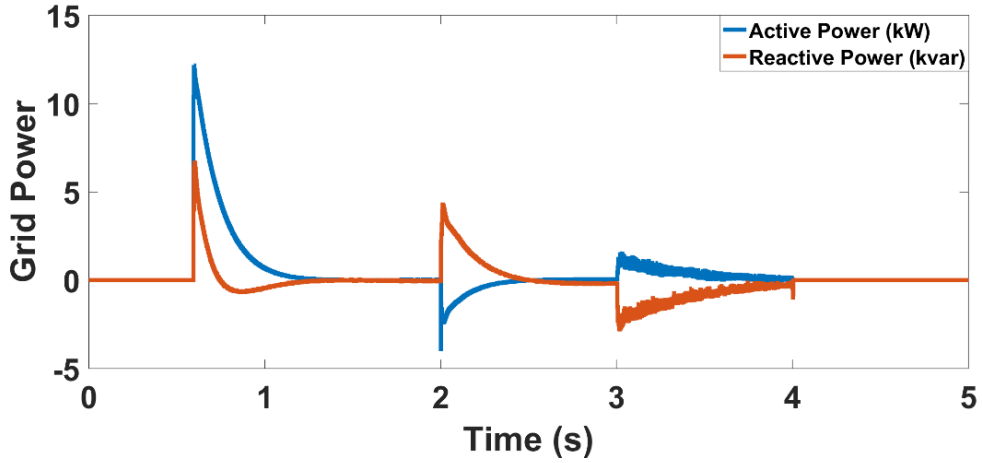

Figure 5.13 Power of grid side

5.1.4 Case 4: Connection to grid at 180° voltage phase difference

In this case, the operation mode is the same as that of Case 3: start the grid-connected pre-synchronization control at 0.5 s; load 2 is connected to the system at 2 s; load 2 is disconnected from the system at 3 s; and the microgrid system disconnected from the grid at 4 s, the microgrid system runs in island mode. Unlike Case 3, there is a 180° phase angle difference between the microgrid and the grid. As can be seen in Figure 5.14 and Figure 5.15, due to the 180° phase angle difference, the grid-connected pre-synchronization control will take longer. The pre-synchronization control is completed at about 1.2 s. At this time, switch 2 is closed and the microgrid system connected to the grid runs in grid-connected mode.

In Figure 5.16, at 0 s, 0.5 s, 0.6 s, 2 s, 3 s and 4 s, the operating frequency of each inverter will fluctuate, but the frequency at all time point can quickly back to 50 Hz. Compared with case 3, at 0.5 s, the frequency fluctuation in case 4 will be larger. This is because at the beginning of the pre-synchronization control, there is not only a difference in voltage value between the microgrid and the grid, but also a big phase angle difference of 180°. The related control theory is mentioned in Section 4.2.

Figure 5.17 and Figure 5.18 respectively show the output active power and output reactive power of the three inverters. For the active power, from 0s to 0.5 s, the same as in case 3, 9 kW, 6 kW and 3 kW, respectively; from 0.5 s to 2 s, the pre-synchronization control is completed and system runs in grid-connected mode, the output active power of each inverter are 11.8 kW, 7.9 kW, 3.9 kW; from 2 s to 3 s, Load 2 is connected to the system, and each

inverter outputs reactive power are 24.2 kW, 16.2 kW, and 8.1 kW; from 3 s to 4 s, Load 2 is disconnected, and each inverter outputs active power returns to the level before Load 2 is connected; from 4 s to 5 s, the microgrid system runs in island mode, and the active power of each inverter are 10.9 kW, 7.3 kW and 3.6 kW. For reactive power, from 0 s to 0.5 s, the reactive power of each inverter are stabilized at 2.7 kVAr, 1.8 kVAr and 0.9 kVAr respectively; from 0.5 s to 2 s, the output reactive power of each inverter is stabilized at 0.6 kVAr, 0.4 kVAr and 0.2 kVAr respectively; from 2 s to 3 s, the output reactive power of each inverter is stable at 1.5 kVAr, 1 kVAr and 0.5 kVAr respectively; from 3 s to 4 s, the output reactive power of each inverter stabilizes at 1.2 kVAr, 0.8 kVAr and 0.4 kVAr respectively; after 4s, the output reactive power of each inverter stabilizes at 3.3 kVAr, 2.2 kVAr and 1.1 kVAr respectively. In general, whether it is active power or reactive power, it can be distributed according to the capacity ratio between the inverters.

Figure 5.19 shows the power change on the grid side. It can be seen that at 1.2 s, 2 s, 3 s and 4 s, due to load changes and operation mode switching, the grid can exchange power with the microgrid system. Provide power support for stable operation.

In general, in case 4, based on the phase angle of the main grid voltage phase A is 0°, the rated capacity of the three inverters is 3:2:1. Not only in the process of pre-synchronization, also in the system running at grid-connect mode, as well as mode change from islanded mode to grid-connected mode and from grid-connected mode to islanded mode, the proposed control algorithm can support the system to run well.

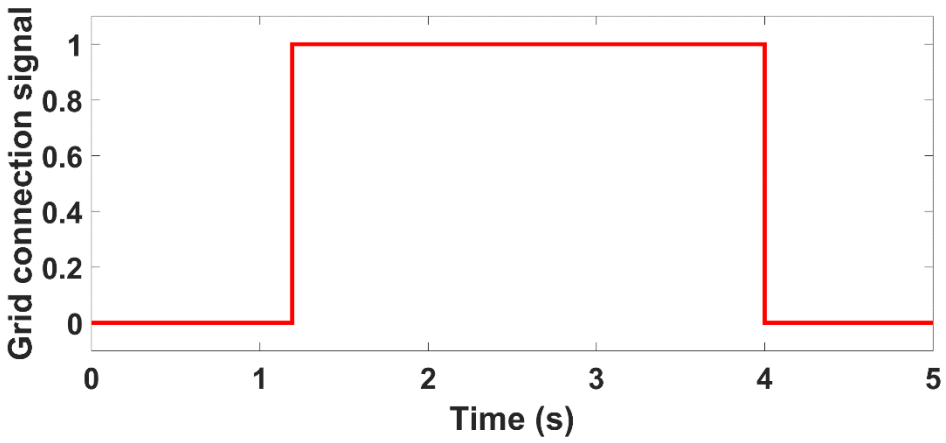

Figure 5.14 Switching signal (Pre-synchronization finish time/Grid connect time)

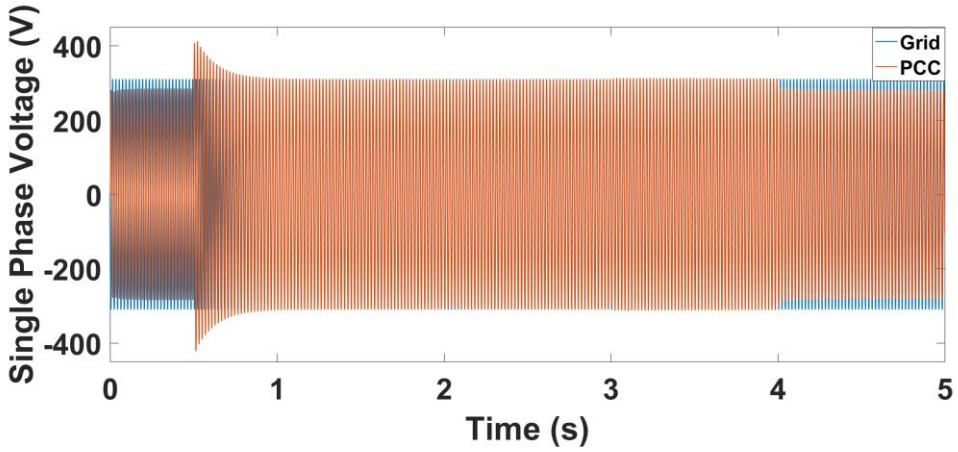

Figure 5.15 Single phase voltage of PCC and grid side

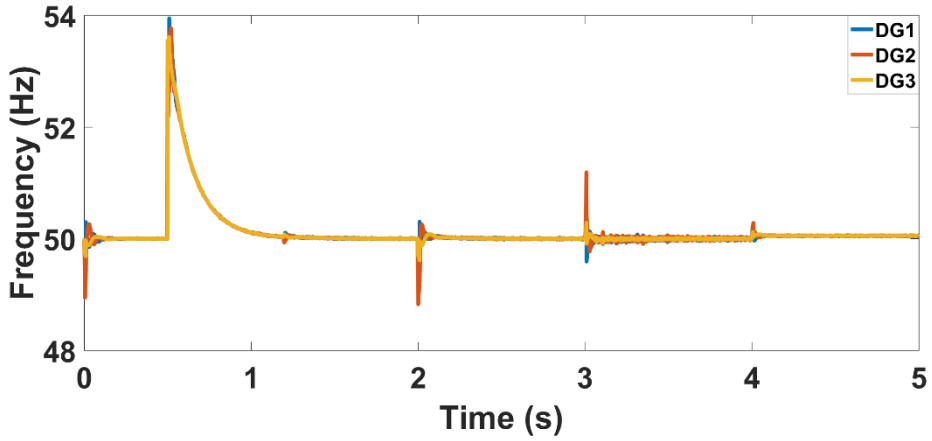

Figure 5.16 Frequency of DG1, DG2 and DG3

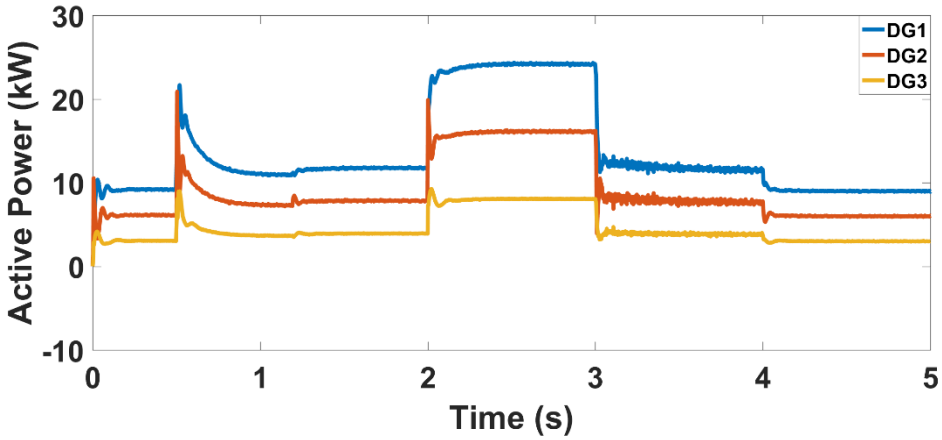

Figure 5.17 Active power of DG1, DG2 and DG3

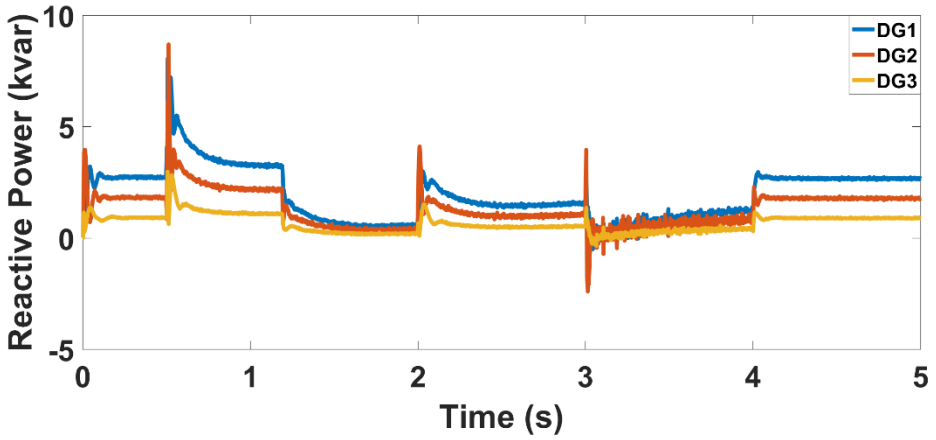

Figure 5.18 Reactive power of DG1, DG2 and DG3

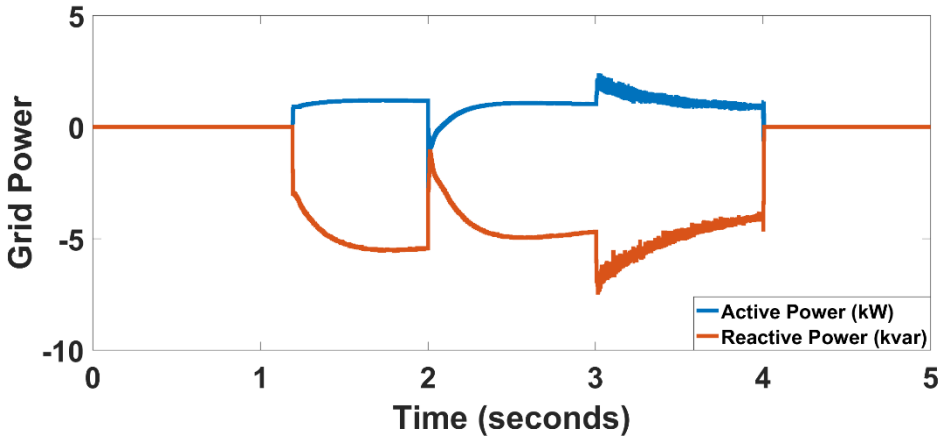

Figure 5.19 Power of grid side

5.1.5 Power exchanges between microgrid and the grid

By comparing Figure 5.13 and Figure 5.19, the power exchange between the microgrid and the grid in case 3 and case 4 is completely different. In order to explain this situation, two other cases are proposed, that is, the initial phase angle difference between the microgrid and the grid is 60 degrees and 120 degrees. By comparing between Figure 5.13, Figure 5.19, Figure 5.20 and Figure 5.21, when the phase angle difference between the microgrid and the grid gradually increases to 0 degrees, 60 degrees, 120 degrees and 180 degrees, the corresponding power exchange value is also gradually increasing. The larger the phase angle difference, the more active and reactive power that the grid needs to output or receive to meet the stable operation of the microgrid after the grid is connected.

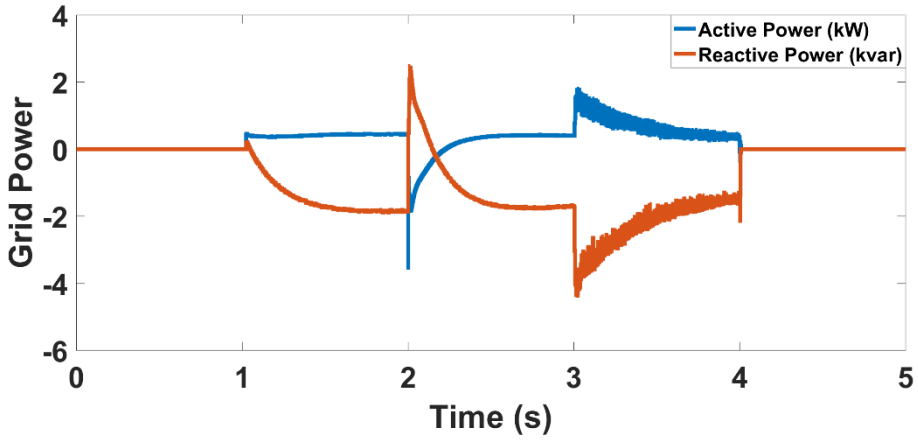

Figure 5.20 Power of grid side when the phase angle difference is 60°

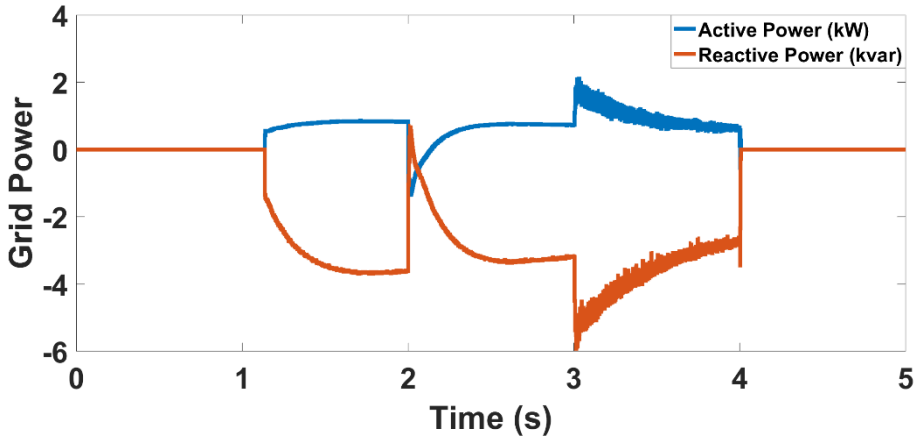

Figure 5.21 Power of grid side when the phase angle difference is 120°

5.2 Case study for proposed system integration with the IEEE 14-bus test system

In this Section, the operation of the microgrid with the proposed control is investigated when the microgrid is connected to the IEEE 14-bus test system. At the same time, a new parameter is investigated which is the response of the microgrid, with the proposed control, to power dispatch commands issued by the main grid to meet its load demand. This means that through these dispatching commands, the input and output power of the microgrid system can be controlled to provide support for the stable operation of the power grid.

Firstly, the IEEE 14-bus test system is introduced, and a detailed data sheet is given for the parameters (Appendix D). Secondly, the concept of demand response is introduced and the

proposed microgrid system is simulated and tested in two cases to determine whether the microgrid system can produce an accurate response to the grid-side dispatch commands. Finally, the IEEE 14-bus test system and the combined microgrid and IEEE 14-bus test system are analysed in the power flow simulation to verify whether the proposed microgrid system, which applies the control method proposed in this paper, can operate with a real-life power system.

5.2.1 IEEE 14-bus test system and test conditions

The topological structure of the power grid is that the power grid associates the busbars, generators, synchronous generators, load points and other components through switch devices such as circuit breakers, abstracts them into nodes, and the power lines connecting these nodes abstract into lines, and then express the relationship between these nodes in the form of a topological graph.

Figure 5.22 shows the grid structure diagram of the IEEE 14-bus test system. The topology diagram represents the power system structure of the Midwestern United States in February 1962. It contains: 14 busbars, 2 generators, 3 synchronous motors, and 11 load points, 20 transmission lines and 40 circuit breakers [110]. The simplified power grid topology can be conveniently applied to power flow calculation, fault diagnosis, dynamic simulation and other simulations. Detailed information on the IEEE 14-bus test system is shown in Appendix D. And the lists of power flow data about the IEEE 14-bus test system in MATLAB/Simulink, is shown in Appendix E, which name is *Summary for ieee_14*.

To test the microgrid proposed in this thesis, which is applied with a combination of improved droop control and pre-synchronous control, can be used in real-life, the proposed microgrid system was connected to bus 9 of the IEEE 14-bus test system, marked with a red arrow in Figure 5.22. The lists of power flow data about power flow analysis of proposed microgrid integrated with IEEE 14-bus test system in MATLAB/Simulink, is shown in Appendix E, which name is *Summary for ieee_14_microgrid_connected*.

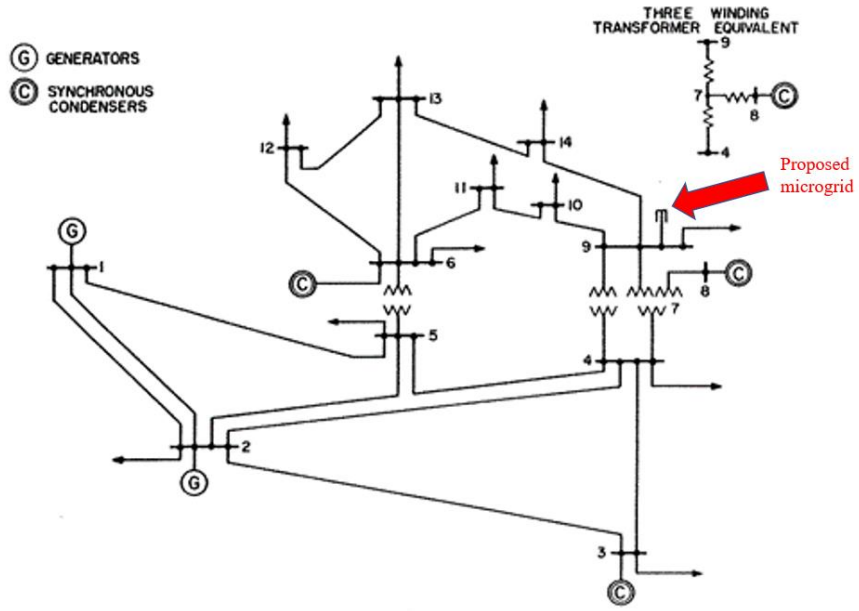

Figure 5.22 Single-line diagram of IEEE 14 feeder bus test system [111]

5.2.2 Power dispatching command from the grid

The reform of the electricity market has brought new challenges to the implementation of demand side management (DSM) in the power industry. The benefits of implementing DSM under the original vertical monopoly system to power companies have been dispersed. Some traditional DSM measures such as load management and energy efficiency has also changed. With the development and improvement of the competitive market, the interests of the power system are gradually diversified, and the role of demand-side resources in the competitive market is being re-understood. Introducing demand response (DR) into the power market competition, increasing the role of the demand side in the market through price signals and incentive mechanisms, and carrying out comprehensive resource planning on the supply side and demand side resources are inevitable requirements to adapt to the development of the power market [112].

Electric energy cannot be stored economically on a large scale, and the supply and demand sides need to ensure real-time balance. These characteristics of the power system require that the power grid must be planned to ensure the reliability of the system operation, and also determine that the power market is not ideal for complete competition for a long period of time. Under the traditional power system, the only way to adapt to the development of the power system is to build more power generation and transmission facilities. After the introduction of DR, since it is based on relaxing retail price controls and increasing demand

elasticity, network problems can be solved with relatively low cost using the available resources and involving distributed power generation.

Despite the above benefits of demand response, there are certain limitations to the corresponding capacity on the demand side. To resolve the imbalance between energy supply and load demand within the main grid, it is particularly crucial that distributed generation units in the microgrid can accept grid dispatch. Power dispatching is an effective management tool to ensure the safe and stable operation of the grid, the reliable supply of electricity to the outside world and the orderly production of all types of electricity. The specific work of power dispatching is based on the data and information returned from various information collection devices or information provided by monitoring personnel, combined with the actual operating parameters of the power grid, such as voltage, current, frequency and load, and taking into account the development of various production work, to make judgments on the safe and economic operation status of the power grid, issue operation instructions through telephone or automatic systems, and command on-site operators or the system can be adjusted by telephone or automatic, commanding the operator or automatic control system to adjust the generator output, adjust the load distribution, cut capacitors, reactors, etc., so as to ensure the continuous safe and stable operation of the grid [113].

In the following sections, two case study, with the same system parameters and test conditions, are considered. In Case study 1, the voltage phase difference between the microgrid and the IEEE 14-bus system is 180°, and the capacity ratio between the three parallel inverters is 1:1:1. Case study 2 is similar to Case study 1 but the parallel inverter capacity ratio is changed from 1:1:1 to 3:2:1, to test whether each inverter can distribute power according to the capacity ratio when the line impedance of each inverter is different. In both cases, positive and negative power dispatch commands are considered where the microgrid increases/decreases the power exchange with the 14-bus system with 2 kW and 1kVAr, as summarised in Table 5-3.

Table 5-4 shows the operating conditions of the system which are the same conditions considered in Table 5-2, but with an added state to enable and disable the microgrid to receive power dispatching commands from the IEEE 14-bus grid system. Power dispatching is initially disabled and the power exchange with the grid is not controlled and normally enforced by network loading and line impedances. Power dispatching is enabled at 1.2 s and

disabled again at 3.5 s. When the dispatching is enabled, the microgrid system starts to receive grid dispatching command to increase/decrease power exchange with a predefined magnitude of active and reactive power; 2 kW and 1 kVAr in the considered cases.

Table 5-3 CASE STUDY CONDITIONS

Number	Grid voltage phase A angle	Inverter capacity ratio	Dispatch command from the Grid	
			Increase 2 kW and 1 kVAr	Decrease 2 kW and 1 kVAr
1	180°	1:1:1	Case 1. a	Case 1. b
2	180°	3:2:1	Case 2. a	Case 2. b

Table 5-4 TIMING OF NETWORK EVENTS IN BOTH TEST CASES

Network Event	**Time**
Connection of Load 2	2 s
Disconnection of Load 2	4 s
Start of pre-synchronisation	0.1 s
Connection to grid	After pre-synchronisation
Disconnection from grid	N/A
Enable dispatch command	1.2 s
Disable dispatch command	3.5s

5.2.2.1 Case 1: Power dispatch with equal generator power ratings

In this case, the phase difference between the microgrid system and the IEEE 14-bus system is 180°, and the capacity ratio between the parallel inverters in the microgrid is 1:1:1. The system starts pre-synchronization control at 0.1 s, as shown in Figure 5.23, the pre-synchronization control is completed at about 0.6 s. At this time, the phase and amplitude between the microgrid voltage and the IEEE 14-bus system voltage at the PCC are consistent, and therefore the microgrid system is connected to the IEEE 14-bus grid test system. Figure 5.27 shows the phase A waveform diagram of the microgrid voltage and the grid voltage. In this figure, the blue waveform is the voltage waveform on the grid side and the orange waveform is the waveform on the microgrid side. Before 0.1 s there is a relatively large difference in voltage magnitude as well as phase difference between the microgrid and the

grid system. After a period of pre-synchronisation control, at around 0.6 s, the synchronisation control is completed, and the microgrid side voltage amplitude and phase values are the same as the grid side voltage amplitude and phase values. At 1.2 s, 2 s, 3.5 s and 4 s, the voltage waveforms change due to changes in the parameters of the grid-connected system, but they stabilise very quickly, allowing the system to continue to operate smoothly. This is explained in more detail in the figures of the other waveform results in this case. Similarly, Figure 5.36 in Case 2 shows the same principle.

a. Positive dispatching command

In Case 1.a, the dispatch command from the IEEE 14-bus system to the microgrid is to increase the active power output of 2 kW and the reactive power output of 1 kVAr from the microgrid system. Figure 5.24 shows the frequency waveform output by parallel inverters. At 0.1 s, due to the start of the pre-synchronization control, the 180° phase difference between the microgrid voltage and the IEEE 14-bus test grid voltage cannot be ignored, resulting in the output frequency of each inverter had a large increase, after adjustment, quickly returned to around 50 Hz. At the same time, in 1.2 s, 2 s and 4 s, due to the changes of the devices operation in the system, the frequency has small change, but it can quickly return to around 50 Hz.

Figure 5.25 and Figure 5.26 are the output active power and reactive power of each inverter respectively, and Figure 5.28 is the power exchange with the grid side. It can be seen that from 0 s to 0.1 s, only load 1 is incorporated into the system, the output power of each inverter is distributed according to the capacity ratio, which is 6.7 kW+2 kVAr; from 0.1s to 0.6s, during the pre-synchronized control operation, due to the mismatch of the voltages between two sides, the output active power and reactive power of each inverter have increased to 7.2 kW+2.4 kVAr; at 0.6 s, the microgrid is integrated into the grid; from 0.6 s to 1.2 s, the power grid and microgrid began to exchange power to maintain stable operation on both sides. At this moment, the output power of each inverter is 8.5 kW+0.55 kVAr, and the power exchange with the grid side is 2.66 kW-5.8 kVAr. On the grid side, the positive value is the direction from which the microgrid flows into the grid, and the negative value is the direction from which the grid flows into the microgrid. At 1.2 s, the microgrid starts to receive grid dispatch commands, and the dispatch command received by the microgrid system in case 1.a is 2 kW +1 kVAr. From 1.2 s to 2 s, the output power of each inverter is

9.8 kW-0.3 kVAr, and the power on the grid side is 4.95 kW-8.5 kVAr. At 2 s, Load 2 is integrated into the microgrid system, and the power required by the load increases. From 2 s to 3.5 s, the output of each inverter increases due to the load increase, which is 18 kW+1.2 kVAr, and the grid-side power is 4 kW-7 kVAr. At 3.5 s, the microgrid stops receiving grid dispatch, and the output power required by each inverter decrease. From 3.5 s to 4 s, the output power of each inverter becomes 16 kW+2.3 kVAr, and the grid-side power is 1.3 kW-2.7 kVAr. At 4 s, Load 2 is disconnected, and the power required by the load is reduced; from 4 s to 5 s, The output power of each inverter is 7.6 kW+1.7 kVAr, and the power of the grid side is 0.9 kW-1.8 kVAr. The output power of each inverter and the power change on the grid side are shown in Table 5-5.

Table 5-5 POWER OF EACH PARALLEL INVERTERS AND GRID SIDE FOR CASE 1.a

Case 1.a		Islanding		Pre-sync		Grid connected									
		0s-0.1s		0.1s-0.6s		0.6s-1.2s		1.2s-2s		2s-3.5s		3.5s-4s		4s-5s	
		P(kW)	Q(kvar)	P(kW)	Q(kvar)	P(kW)	Q(kvar)	P(kW)	Q(kvar)	P(kW)	Q(kvar)	P(kW)	Q(kvar)	P(kW)	Q(kvar)
Inverter (1:1:1)	1 2 3	6.7	2	7.2	2.4	8.5	0.55	9.8	-0.3	18	1.2	16	2.3	7.6	1.7
Grid		0	0	0	0	2.66	-5.8	4.95	-8.5	4	-7	1.3	-2.7	0.9	-1.8

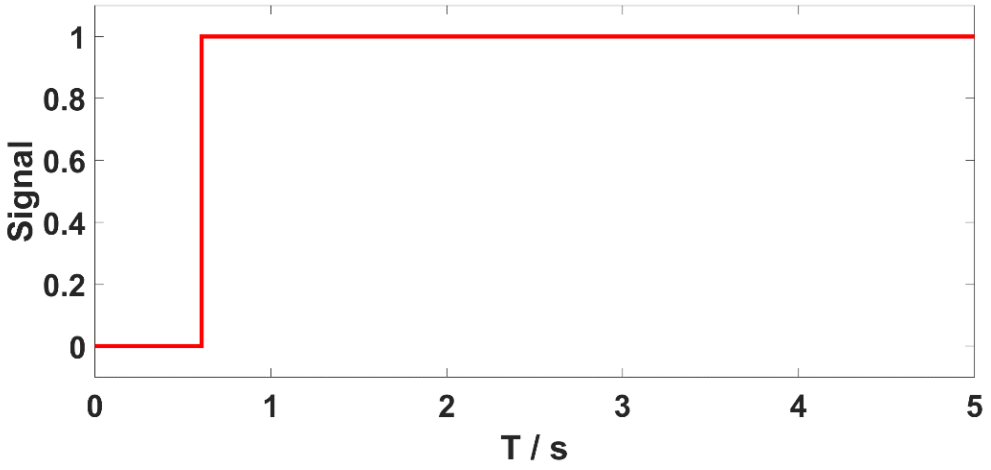

Figure 5.23 Connect signal of Case 1

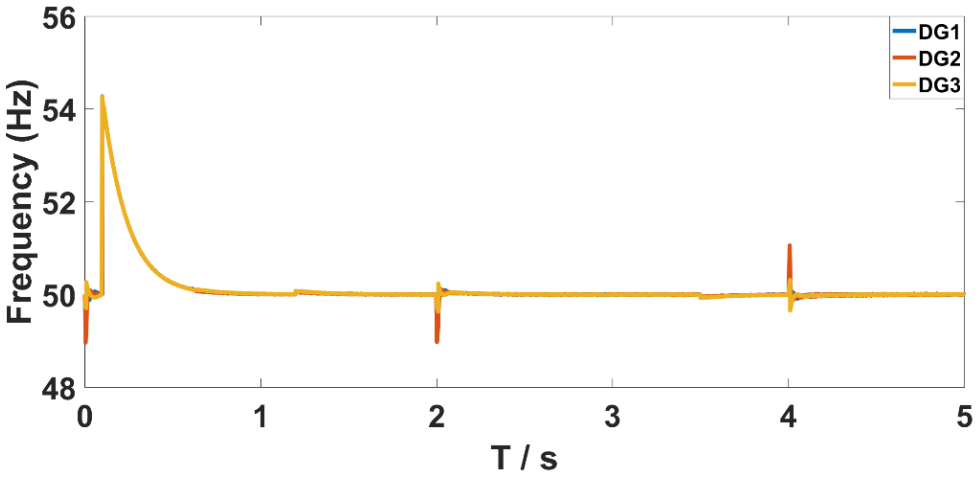

Figure 5.24 Frequency of three inverters for case 1

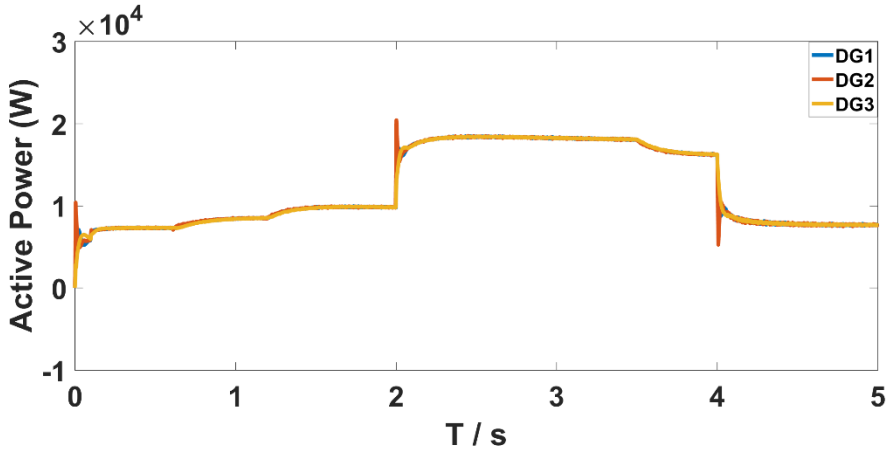

Figure 5.25 Active power output of three inverters for case 1.a

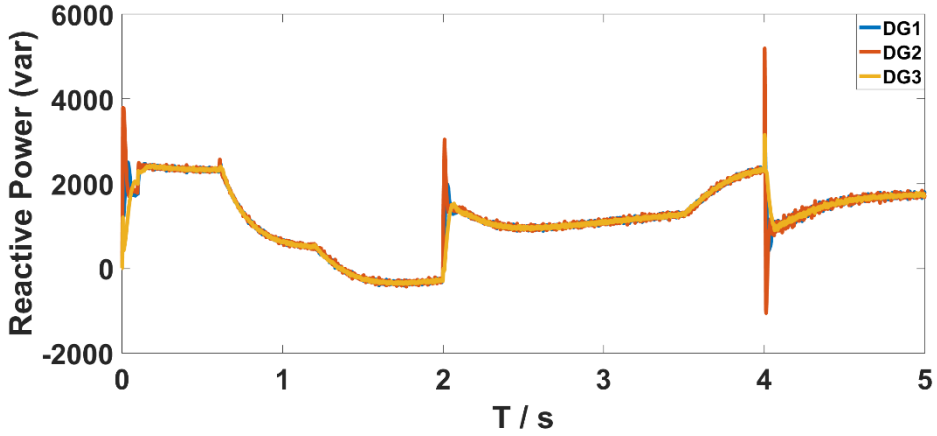

Figure 5.26 Reactive power output of three inverters for case 1.a

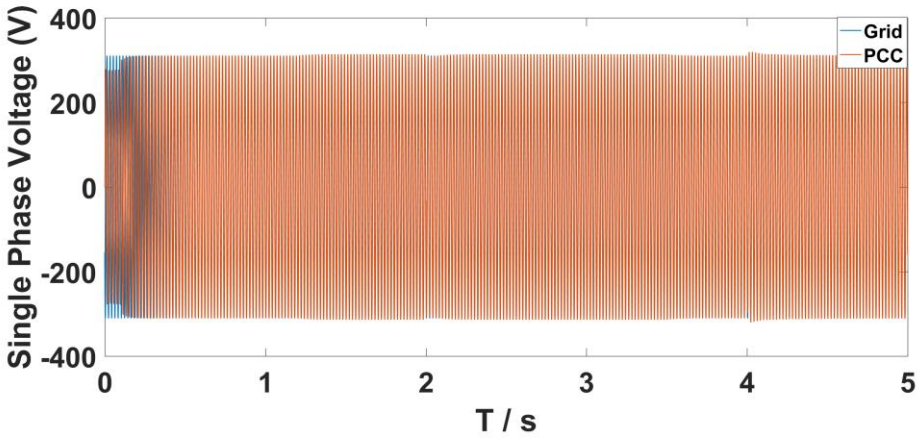

Figure 5.27 Single phase voltage between Grid side and PCC side for case 1

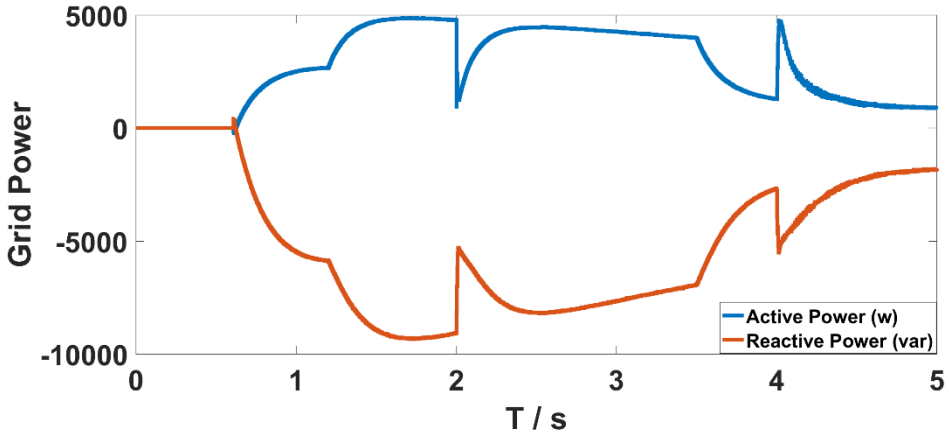

Figure 5.28 Grid side power for case 1.a

b. Negative dispatching command

The difference between Case 1.b and Case 1.a is that the power grid dispatching command changes from 2 kW +1 kVAr to -2 kW -1 kVAr. There is no change to the switch operation mode. Figure 5.29 and Figure 5.30 are the output active power and reactive power waveforms of each inverter respectively, and Figure 5.31 is the power waveform of the grid side. Contrary to the output power waveform of each inverter in case 1.a, after the 1.2 s, microgrid starts to receive grid dispatch, the output power of each inverter decreases from 1.2 s to 3.5 s; after the 3.5 s microgrid stops receiving grid dispatching commands, the output power of each inverter increased from 3.5 s to 5 s, in line with the operating conditions set by the case study. Correspondingly, from 1.2 s to 3.5 s, the power on the grid side also decreases, and

after 3.5 s, the power on the grid side also increases. The output power of each inverter and the power change on the grid side are shown in Table 5-6.

Table 5-6 POWER OF EACH PARALLEL INVERTERS AND GRID SIDE FOR CASE 1.b

Case 1.b		Islanding		Pre-sync		Grid connected									
		0s-0.1s		0.1s-0.6s		0.6s-1.2s		1.2s-2s		2s-3.5s		3.5s-4s		4s-5s	
		P(kW)	Q(kvar)	P(kW)	Q(kvar)	P(kW)	Q(kvar)	P(kW)	Q(kvar)	P(kW)	Q(kvar)	P(kW)	Q(kvar)	P(kW)	Q(kvar)
Inverter (1:1:1)	1 2 3	6.1	1.9	7.3	2.35	8.5	0.55	7.2	1.65	15.2	2.55	16.7	1.7	8.2	0.95
Grid		0	0	0	0	2.6	-5.8	-0.06	-1.8	-0.2	-1.5	2.25	-4.9	2	-4.3

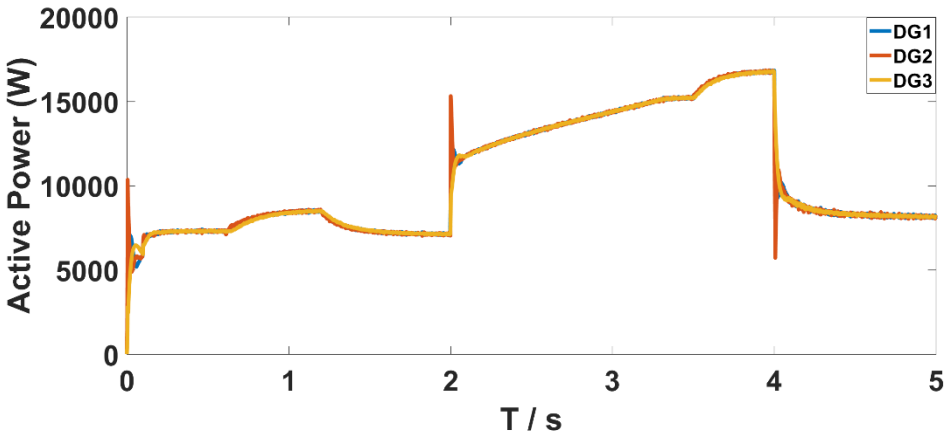

Figure 5.29 Active power output of three inverters for case 1.b

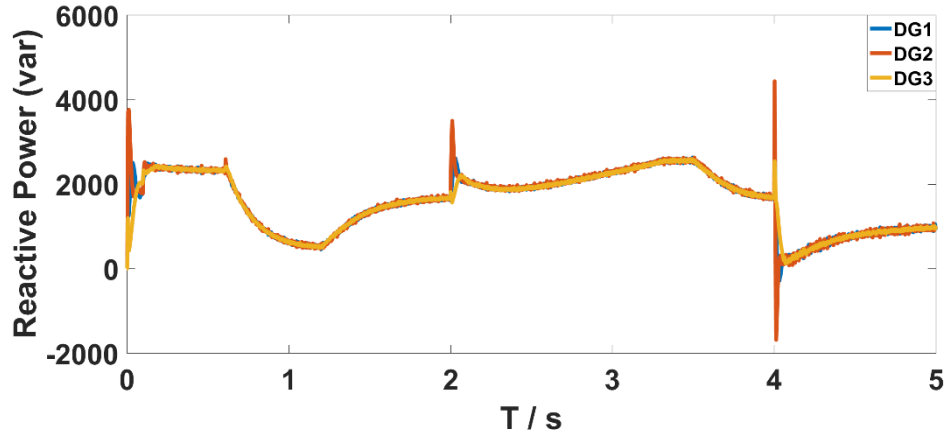

Figure 5.30 Reactive power output of three inverters for case 1.b

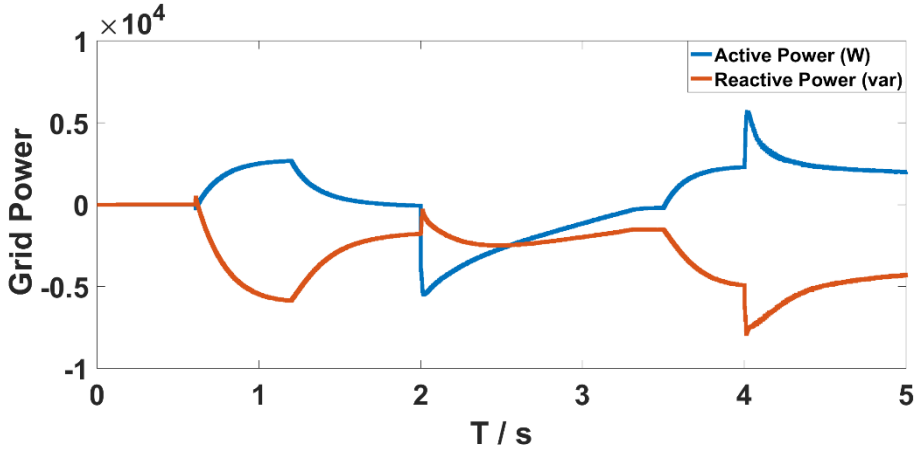

Figure 5.31 Grid side power for case 1.b

c. Summary

In case 1, the capacity ratio of each inverter in the microgrid is 1:1:1. After the pre-synchronization control, the microgrid system is incorporated into the IEEE 14-bus test system. In the case where the output line impedance of each inverter is completely different, each inverter can distribute power according to the capacity ratio of 1:1:1, and can also adjust of the output power based on the dispatching command from the grid, as well as based on the changes of the load. Maintain the stable operation of the microgrid system in both island and grid-connected mode.

5.2.2.2 Case 2: Power dispatch with different generator power ratings

The difference between Case 2 and Case 1 is that the capacity ratio between the inverters is 3:2:1. Other conditions are the same. After the microgrid completed the pre-synchronization control operation, the microgrid system is incorporated into the IEEE 14-bus grid test system, and the angle of the grid side voltage phase A is 180°. At the same time, the output line impedance of each inverter is completely different. The operating conditions of the system are: at 0.1 s, the pre-synchronization control starts to run; at 0.6 s, the pre-synchronization control is completed, the switch 2 is closed, the microgrid is merged into the IEEE 14-bus test system; at 1.2 s, the switch 3 is closed, the microgrid starts to receive the grid-side dispatch commands and make adjustments; at 2 s, switch 1 is closed, load 2 is

merged into the microgrid system; at 3.5 s, switch 3 is opened, the microgrid stops receiving dispatching instructions from the grid side until the end of the test; at 4 s, switch 1 is opened, load 2 disconnected from the microgrid system.

a. Positive dispatching command

In case 2.a, the dispatch command from the grid side to the microgrid side is: +2 kW plus +1 kVAr. Figure 5.32 and Figure 5.36 show the time when the microgrid is integrated into the IEEE 14 buses test grid, and during the whole test, the comparison between phase A voltage of the grid and the phase A voltage of the PCC terminal of the microgrid. The pre-synchronization process can be clearly seen, as well as the voltage operation waveform. Figure 5.33 shows the output frequency waveform of each inverter. Same as Figure 5.24, instantaneous frequency changes occurred at 0.1 s, 1.2 s, 2 s and 4 s, respectively. After a quick adjustment, the frequency returned to around the rated 50 Hz. Figure 5.34 and Figure 5.35 show the output power of each inverter during system operation respectively. At the same time, Figure 5.37 shows the power flow on the grid side during system operation. Due to the capacity ratio between the three inverters is 3:2:1. It can be seen that the output power ratio of the three inverters is maintained at 3:2:1 during operation, and it will not be affected by the completely different line impedances. The output power of each inverter and the power change on the grid side are shown in Table 5-7. On the grid side, a positive value represents the direction of power flowing from the microgrid side to the grid side, and a negative value represents the direction of power flowing from the grid side to the microgrid side.

Table 5-7 POWER OF EACH PARALLEL INVERTERS AND GRID SIDE FOR CASE 2.a

Case 2.a		Islanding		Pre-sync		Grid connected									
		0s-0.1s		0.1s-0.6s		0.6s-1.2s		1.2s-2s		2s-3.5s		3.5s-4s		4s-5s	
		P(kW)	Q(kvar)	P(kW)	Q(kvar)	P(kW)	Q(kvar)	P(kW)	Q(kvar)	P(kW)	Q(kvar)	P(kW)	Q(kvar)	P(kW)	Q(kvar)
Inverter (3:2:1)	1	9	2.9	10.8	3.5	12.6	0.8	15	-0.4	27.3	1.9	24.3	3.4	11.5	2.55
	2	6	1.9	7.3	2.4	8.5	0.52	9.8	-0.4	18	1.25	16.3	2.2	7.7	1.7
	3	3	1	3.6	1.2	4.3	0.27	4.5	-0.4	8.7	0.5	8.05	1.1	3.8	0.85
Grid		0	0	0	0	2.65	-5.9	4.8	-9.1	4	-6.9	1.3	-2.6	0.9	-1.9

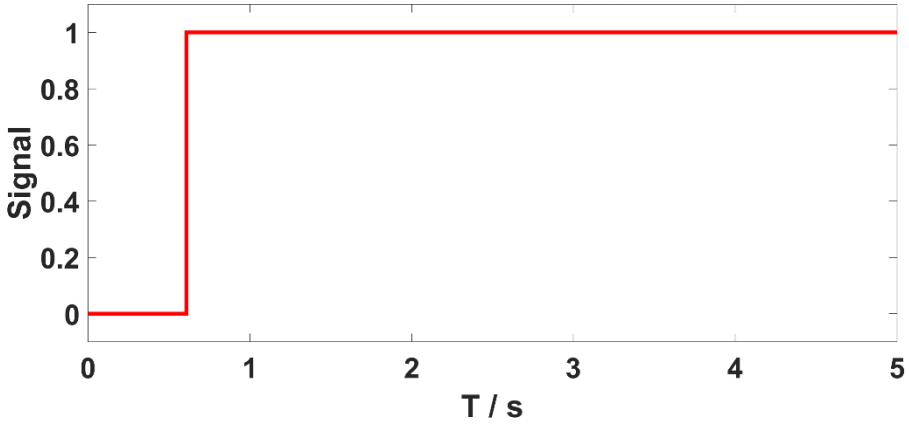

Figure 5.32 Connect signal of case 2

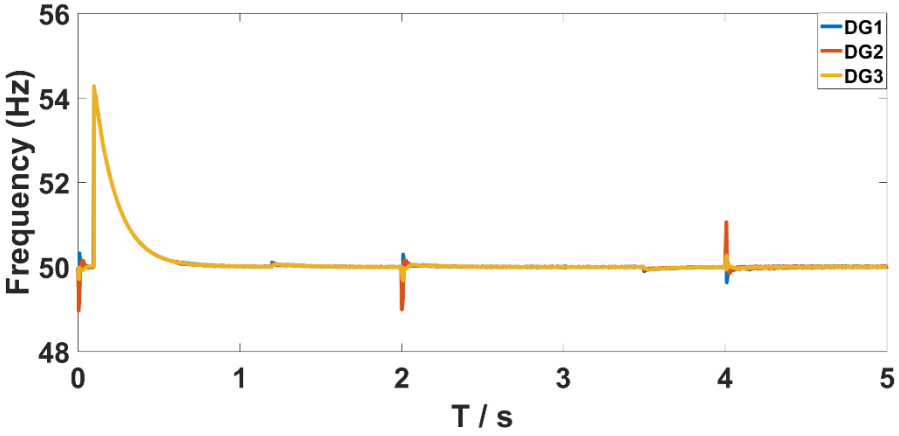

Figure 5.33 Frequency of three inverters for case 2

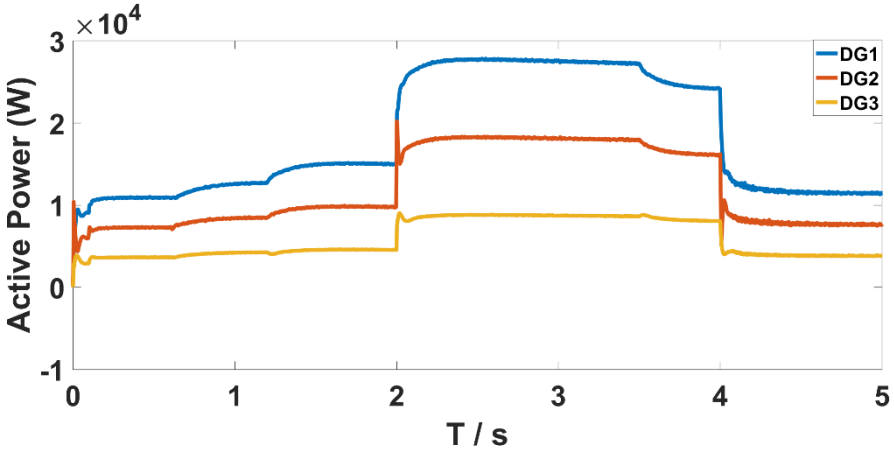

Figure 5.34 Active power output of three inverters for case 2.a

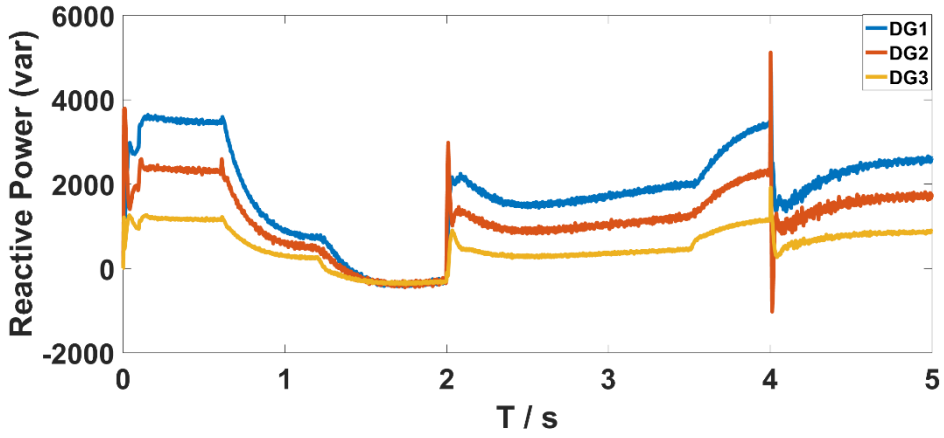

Figure 5.35 Reactive power output of three inverters for case 2.a

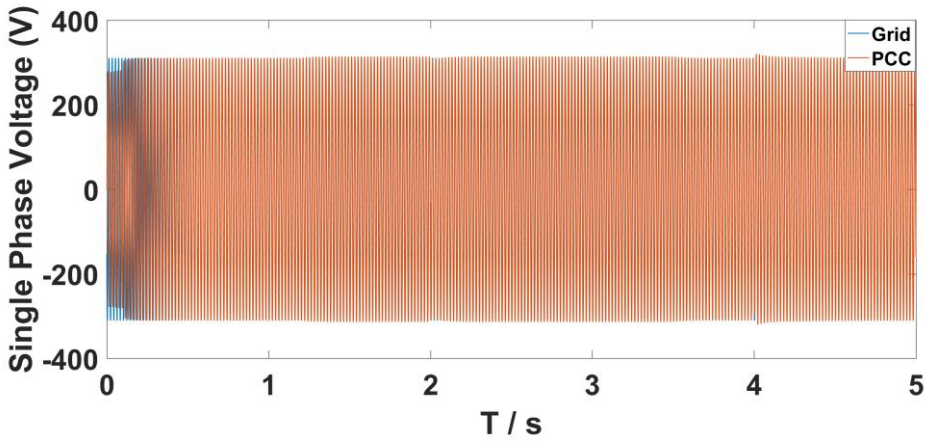

Figure 5.36 Single phase voltage between grid side and PCC side for case 2

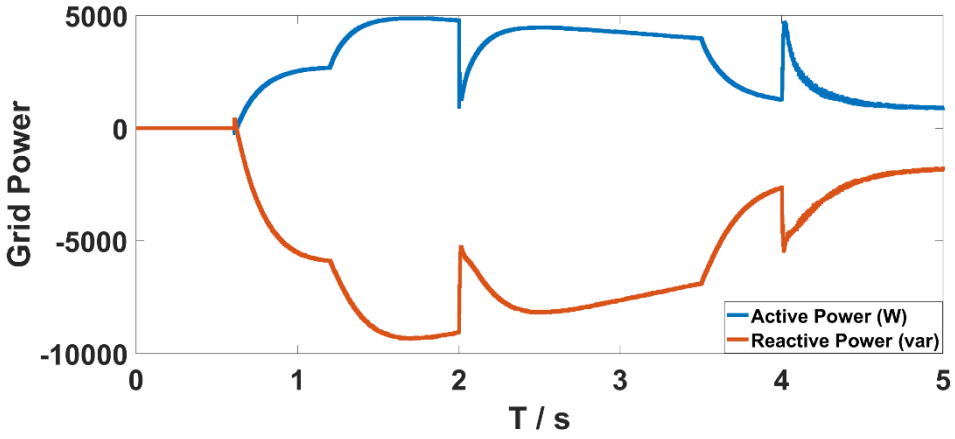

Figure 5.37 Grid side power for case 2.a

b. Negative dispatching command

In Case 2.b, the dispatch command from the grid side to the microgrid side is: -2 kW plus -1 kVAr. Figure 5.38 and Figure 5.39 show the output power of an inverter during system operation, respectively. Figure 5.40 shows the power flow on the grid side during system operation. The same as the result in Case 2.a, the output power of each inverter is output according to the capacity ratio of 3:2:1. Table 5-8 shows the power changes of each inverter and the grid side. On the grid side, a positive value represents the direction of power flowing from the microgrid side to the grid side, and a negative value represents the direction of power flowing from the grid side to the microgrid side.

Table 5-8 POWER OF EACH PARALLEL INVERTERS AND GRID SIDE FOR CASE 2.b

Case 2.b		Islanding		Pre-sync		Grid connected									
		0s-0.1s		0.1s-0.6s		0.6s-1.2s		1.2s-2s		2s-3.5s		3.5s-4s		4s-5s	
		P(kW)	Q(kvar)	P(kW)	Q(kvar)	P(kW)	Q(kvar)	P(kW)	Q(kvar)	P(kW)	Q(kvar)	P(kW)	Q(kvar)	P(kW)	Q(kvar)
Inverter (3:2:1)	1	9	2.8	11	3.5	11.27	0.7	11.03	2.35	22.3	3.51	24.8	2.5	12.1	1.4
	2	6	1.8	7.2	2.3	8.4	0.45	7.1	1.6	15.1	2.48	16.6	1.6	8.2	0.9
	3	3	0.9	3.6	1.2	4.3	0.22	3.9	0.95	7.9	1.4	8.35	0.8	4.1	0.47
Grid		0	0	0	0	2.7	-5.8	-0.08	-1.8	-0.2	-1.5	2.28	-4.92	2	-4.3

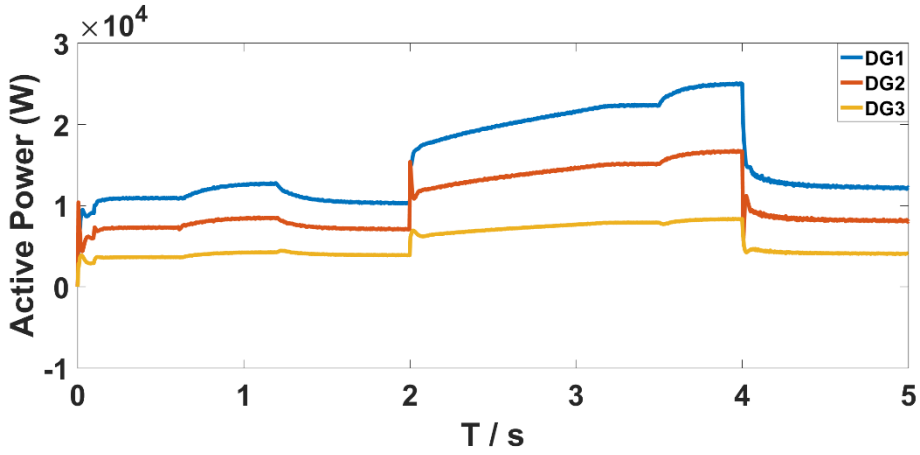

Figure 5.38 Active power output of three inverters for case 2.b

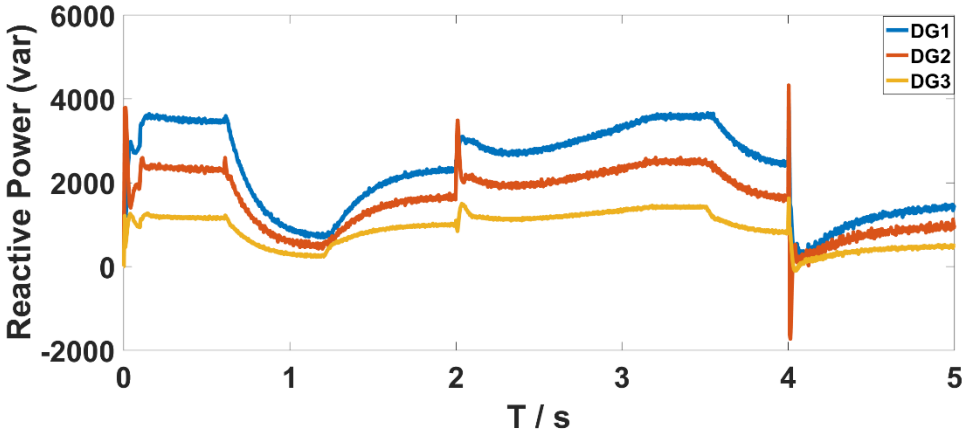

Figure 5.39 Reactive power output of three inverters for case 2.b

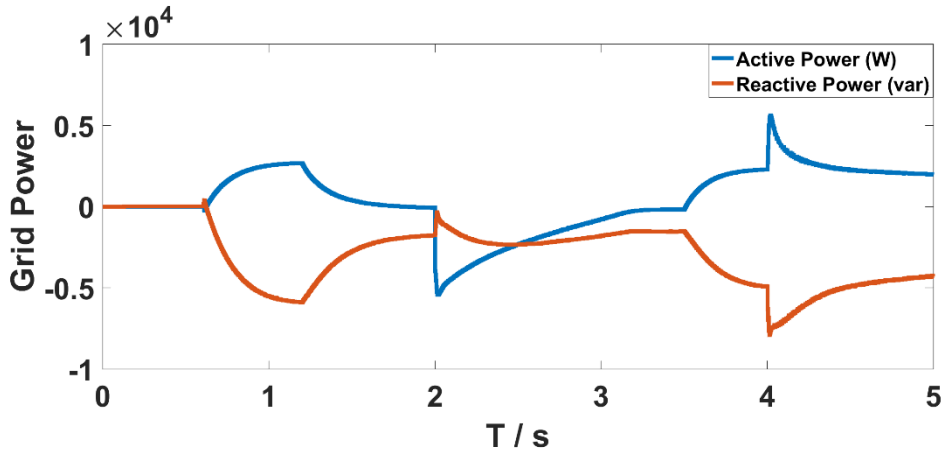

Figure 5.40 Grid side power for case 2.b

c. Summary

In case 2, the capacity ratio of each inverter in the microgrid is 3:2:1. After completed the pre-synchronization control, the microgrid system is incorporated into the IEEE 14-bus test system. When the output line impedance of each inverter is completely different, each inverter can distribute power according to the capacity ratio of 3:2:1, and can also adjust of the output power based on the dispatching command from the grid, as well as based on the changes of the load. Maintain the stable operation of the microgrid system in both island and grid-connected mode.

5.2.3 Power flow analysis of IEEE 14-bus test system and proposed microgrid integrated with the test system

To verify the microgrid proposed in this project, after being integrated with the IEEE 14-bus test system, neither the microgrid nor the IEEE 14-bus test system will be affected. In this part, power flow simulation analysis will be performed on the IEEE 14-bus test system and the merged system in MATLAB/Simulink respectively. As mentioned previously, the power flow data lists for the two systems are attached in Appendix E.

Since there are several different periods of dynamic processes during the simulation of the proposed microgrid integrated with IEEE 14-bus test system, namely the island operation period, the pre-synchronous control period, and the grid-connected operation period. Therefore, one of these periods of steady state operation needs to be selected for power flow analysis. Here, the steady-state data between 2s and 3.5s of case 2.a in Section 5.2.2.2 is selected for analysis using MATLAB/Simulink. As can be seen from Table 5-7, the active power output of each inverter is 27.3 kW, 18 kW and 8.7 kW, and the reactive power output of each inverter is 1.9 kVAr, 1.25 kVAr and 0.5 kVAr respectively during this period. The results can be found in Table C-2 in APPENDIX E. In this table for the proposed microgrid bus, named *BUS_microgrid*, the active and reactive power outputs are 0.054 MW and 0.00365 MVAr respectively, and the PQ loads are 0.04 MW and 0.006 MVAr, and they all match the values and conditions in Table 5-7. As the microgrid is integrated into the IEEE 14-bus test system at Bus 9, a comparison of the values of Bus 9 in the power flow analysis of the IEEE 14-bus test system and the values of Bus 9 in the power flow analysis of the combined system leads to the conclusion that the microgrid system proposed in this thesis can be well connected to the IEEE 14-bus test system and provides support for the application of the proposed control theory in practice life.

5.3 Summary

For the first part of this chapter, firstly, the composition, operating mode, and operating conditions of the test system are proposed; secondly, through the adjustment of the rated capacity of the parallel inverter and the adjustment of the phase angle of the phase A voltage on the grid side, it is shown that under different parameters, the proposed control algorithm has good feasibility and reliability. In case 1 and case 2, the system runs in island mode.

Although the rated capacity ratios of parallel inverters are different, the system can operate stably in both cases, and each inverter performs active power and reactive power according to the rated capacity ratio. In case 3 and case 4, the system runs in grid-connected mode, which is divided into two stages, pre-synchronization control process and grid-connected operation. Also, both in case 3 and case 4, the system switched from grid-connected mode to islanded mode at 4 s and system runs in islanded mode from 4s to 5s. The proposed control algorithm not only enables each inverter to output power according to the rated capacity ratio, also can make the system return to stable operation quickly when the system fluctuates. Therefore, the proposed control algorithm can run well in the test system.

For the second part of this chapter, the IEEE 14-bus test system is introduced first, then the concept of demand-side response and its role in power system operation are introduced. Based on these two concepts, a microgrid with the proposed control method model incorporates into the IEEE 14-bus test system is designed, and by adjusting the dispatching commands issued by the grid side to the microgrid side, it is tested that under different conditions, whether the microgrid can operate stably and respond to dispatching commands on the grid side.

The premise of the simulation test in second part of this chapter is the same as that of first part. when the line impedances of the parallel inverters in the microgrid system are completely different, four different conditions are tested, namely: the capacity ratio between the parallel inverters is 1:1:1, the microgrid is required to have more output and less output power respectively; the capacity ratio between parallel inverters is 3:2:1, the microgrid is required to have more output and less output power respectively. The simulation results show that although the line impedances of the inverters are completely different, the inverters can distribute and output power according to the capacity ratio between the parallel inverters. In tests 1.a and 2.a, the output power ratio between the three inverters is 1:1:1; in tests 1.b and 2.b, the power output ratio between the three inverters is 3:2:1. At the same time, the total output power of the three inverters not only meets the changing load demand in the microgrid system, but also fully responds to the dispatch of the grid to maintain the stable operation of the grid.

Chapter 6 Conclusions

This chapter gives a summary of the work presented in this thesis and some suggestions for further research on the problem of the power output of each inverter not following the rated power ratio of the inverters due to line impedance mismatch in microgrid systems operating in parallel with multiple inverters.

6.1 General conclusions

In recent years, the emphasis on low carbon emissions has led to distributed generation systems and microgrids being studied by researchers worldwide. As an alternative to traditional power grids, microgrids have significant advantages, such as making the way people use electricity more flexible and efficient. However, new problems are constantly emerging in the development of microgrids, one of which is that the flexibility of microgrids makes them more difficult to control due to the increased number of variable parameters in the control process. In this thesis, the focus is on the fact that in microgrids with multiple distributed generation systems operating in parallel, the line impedance is not the same due to the different line lengths of each generation unit, thus making it impossible to distribute the power required by the load equally or in accordance with the rated power ratio of each generation unit using conventional control theory.

The aim of this thesis is to solve the above problem by proposing an improved droop control, which in combination with pre-synchronous control, allows the target microgrid to operate more smoothly, either in islanding mode or in grid-connected mode, and to switch between these two modes, in accordance with the rated power ratio of each generating unit, thus making the target microgrid system operates more efficiently and protects the electrical components.

The first chapter of the thesis discussed background knowledge about distributed generation and microgrids is first presented. For example, the development of distributed generation, the structure and classification of microgrids. Next, some common control methods for microgrids and inverters in microgrids are presented, such as PQ control, V/f control and conventional droop control. Then the control methods for energy coordination in

different types of microgrids are presented. The shortcomings of the existing control methods and the problems currently faced in the operation of microgrids are also presented. Finally, the contribution of the project is given, and an outline of the whole thesis is given.

In chapter 2, the inverter in the microgrid mentioned in the first chapter will be discussed in more detail. Not only the classification and operation mode of the inverter are discussed, but also the droop control used in this subject is introduced in detail as well. Through this chapter, the droop control applicable to this topic is identified so that improvements can be proposed in the subsequent chapters.

In chapter 3, the focus is on the power flow and the circulating current between the parallel inverters. By analysing these two parameters, problems such as the uneven output of each inverter due to inconsistent line impedance are presented for parallel inverters in microgrids. The performance of the improved control methods proposed in this topic can also be evaluated in the subsequent chapters. For example, whether the proposed improved control theory can solve the problem of uneven power distribution among parallel inverters in the microgrid.

Through the analysis of the traditional droop control, an improved droop control with secondary control loop is proposed in chapter 4, and combined with the improved PLL control, it solves the problem of uneven power distribution in real-life microgrids where the line impedances between the parallel inverters are not identical. The improved droop control combined with the SSRF-SPLL pre-synchronization control enables multiple parallel inverters to output according to their own capacity, ensuring the accurate and efficient operation of the microgrid system. At the same time, the improved control method enables the microgrid to operate not only in islanding mode, but also well in grid-connected mode, as well as smooth switching between the two modes. The performance of the proposed improved control method was compared to the traditional control method in simulation. The simulation results show that the improved droop control proposed in this thesis has a faster response to changes in parameters in the microgrid, as well as a smoother and more stable system operation due to less waveform fluctuations.

In chapter 5, a microgrid consisting of three parallel inverters as well as the load and the grid is first presented and simulated for the different operating modes, and the results

obtained are consistent with those in chapter 4. When the line impedance of each parallel inverter is different, by changing the capacity of each inverter and adjusting the operation mode, the simulation results obtained show that the proposed improved droop control combined with SSRF-SPLL pre-synchronization control method enables each inverter to output power according to its own capacity in different cases. For the second part of this chapter, the three-inverter parallel microgrid with the improved control method is connected to the IEEE 14-bus test system and the simulation analysis is performed. The power flow analysis is performed on the IEEE 14-bus test system and the integrated system respectively. The simulation results show that the improved droop control theory proposed in this project can enable each inverter in the microgrid to deliver power according to its own capacity. The problem presented at the beginning of the thesis has been solved.

In summary, the control method proposed in this thesis, which combines improved droop flow control with a pre-synchronous control block, has been shown to be an effective tool for achieving power sharing between parallel distributed generation systems with mismatched line impedances in a microgrid. In contrast to the power sharing control theory proposed by other researchers, this control theory not only enables the proposed parallel microgrid system consisting of multiple distributed generation systems to operate in islanded mode, grid-connected mode, and switch smoothly between islanding and grid-connected, but also ensures that each distributed generation unit outputs power at its own scale and reasonably distributes the power required by the load. This ensures the safe and stable operation of each generation unit. In addition, microgrid systems using this control theory can quickly respond to dispatch commands from the conventional main grid, making the application of microgrid systems more flexible.

6.2 Future research

Potential areas for the further research include:

1. The control method proposed in this thesis are used to solve the power sharing mismatch problems of parallel connected distributed generation system with different line impedance in microgrid, both at island operation mode and grid-connected mode. Further, the control method can be extended to solve the problem of finding the

optimal substation location for each distributed generation system in microgrid, as well as for the sizing of the distributed system.

2. In the current study, only the theoretical feasibility and constraints of the control technology have been considered, but not the cost control and economic benefits of the application of the technology. Therefore, cost control and economic benefits could be a research point in the subsequent research process.
3. An approach to the calculation of circulating current in a microgrid with multiple distributed generation systems connected in parallel is mentioned in Chapter 3, although the effects of circulating current are analysed in four different aspects, all distributed generation systems connected to the same load bus. This approach can be applied to the analysis of parallel distributed generation systems connected to different load busses in a subsequent study.
4. In Chapter 5, the proposed control theory combining improved droop control with pre-synchronous control is applied in such a way that the microgrid can exchange power with the conventional mains grid, making the application of the microgrid system more flexible. The proposed microgrid is connected to an IEEE 14-bus test system and the simulation results are verified. However, in this thesis, due to time constraints, only the theoretical feasibility of integrating the proposed microgrid system into the IEEE 14-bus test system is analysed. There are many more aspects that deserve to be investigated, such as the magnitude of the energy losses incurred during operation when the two systems are connected, and a comparison with the energy losses when using conventional control.
5. Due to the complexity of both the microgrids applied in this thesis and the IEEE 14-bus test system, simulations are used to validate the discussion topics presented in each chapter. The experimental verification is not easy, but it is also possible to use Real-time Network Emulation for this purpose. This could be a follow-up research direction.

Reference

[1] R. H. Lasseter, "Smart distribution: Coupled microgrids," *Proceedings of the IEEE,* vol. 99, no. 6, pp. 1074-1082, 2011.

[2] T. Wu, D.-L. Xu, and J.-B. Yang, "Decentralised energy and its performance assessment models," *Frontiers of Engineering Management,* vol. 8, no. 2, pp. 183-198, 2021.

[3] D. Tan and D. Novosel, "Energy challenge, power electronics & systems (PEAS) technology and grid modernization," *CPSS Transactions on Power Electronics and Applications,* vol. 2, no. 1, pp. 3-11, 2017.

[4] R. H. Lasseter, "Microgrids," in *2002 IEEE Power Engineering Society Winter Meeting. Conference Proceedings (Cat. No. 02CH37309)*, 2002, vol. 1, pp. 305-308: IEEE.

[5] N. Hatziargyriou, H. Asano, R. Iravani, and C. Marnay, "Microgrids," *IEEE power and energy magazine,* vol. 5, no. 4, pp. 78-94, 2007.

[6] Z. Zeng, R. Zhao, H. Yang, and S. Tang, "Policies and demonstrations of micro-grids in China: A review," *Renewable and Sustainable Energy Reviews,* vol. 29, pp. 701-718, 2014.

[7] C.-s. Wang, "Analysis and simulation theory of Microgrid," ed: Science Press: Beijing, China, 2013.

[8] A. Ghazanfari, M. Hamzeh, H. Mokhtari, and H. Karimi, "Active power management of multihybrid fuel cell/supercapacitor power conversion system in a medium voltage microgrid," *IEEE Transactions on Smart Grid,* vol. 3, no. 4, pp. 1903-1910, 2012.

[9] C. Wang, F. Gao, P. Li, B.-b. Huang, C.-d. Ding, and H. Yu, "Control strategy research on low voltage microgrid," *Proceedings of the CSEE,* vol. 32, no. 25, pp. 2-8, 2012.

[10] H. Kakigano, Y. Miura, T. Ise, and R. Uchida, "DC micro-grid for super high quality distribution—System configuration and control of distributed generations and energy storage devices," in *2006 37th IEEE Power Electronics Specialists Conference*, 2006, pp. 1-7: IEEE.

[11] Q. Jiang, M. Xue, and G. Geng, "Energy management of microgrid in grid-connected and stand-alone modes," *IEEE transactions on power systems,* vol. 28, no. 3, pp. 3380-3389, 2013.

[12] X. Liu, P. Wang, and P. C. Loh, "A hybrid AC/DC microgrid and its coordination control," *IEEE Transactions on smart grid,* vol. 2, no. 2, pp. 278-286, 2011.

[13] C. Wu, F. Wen, and Y. Lou, "The existed problems and possible solutions of micro-grid based on distributed generation," in *2008 Third International Conference on Electric Utility Deregulation and Restructuring and Power Technologies*, 2008, pp. 2763-2768: IEEE.

[14] D. Ming, Z. Yingyuan, and M. Meiqin, "Key technologies for microgrids being researched," *Power System Technology,* vol. 33, no. 11, pp. 6-11, 2009.

[15] R. Majumder, F. Shahnia, A. Ghosh, G. Ledwich, M. Wishart, and F. Zare, "Operation and control of a microgrid containing inertial and non-inertial micro sources," in *TENCON 2009-2009 IEEE Region 10 Conference*, 2009, pp. 1-6: IEEE.

[16] M. Savaghebi, A. Jalilian, J. C. Vasquez, and J. M. Guerrero, "Selective compensation of voltage harmonics in an islanded microgrid," in *2011 2nd Power Electronics, Drive Systems and Technologies Conference*, 2011, pp. 279-285: IEEE.

[17] N. Pogaku, M. Prodanovic, and T. C. Green, "Modeling, analysis and testing of autonomous operation of an inverter-based microgrid," *IEEE Transactions on power electronics,* vol. 22, no. 2, pp. 613-625, 2007.

[18] F. Gao *et al.*, "Analysis and design of for paralleled inverter system based on the small signal model using time-varying phasor," in *Zhongguo Dianji Gongcheng Xuebao(Proceedings of the Chinese Society of Electrical Engineering)*, 2011, vol. 31, no. 33, pp. 75-84: Chinese Society for Electrical Engineering.

[19] L. F. Ludwig, "Incremental Deployment of Stand-Alone and Hierarchical Adaptive Cooling and Energy Harvesting Arrangements for Information Technology," ed: Google Patents, 2013.

[20] M. Dewadasa, R. Majumder, A. Ghosh, and G. Ledwich, "Control and protection of a microgrid with converter interfaced micro sources," in *2009 International Conference on Power Systems*, 2009, pp. 1-6: IEEE.

[21] Q. Song, B. Zhao, W. Liu, and R. Zeng, "An overview of research on smart DC distribution power network," *Proceedings of the CSEE,* vol. 33, no. 25, pp. 9-19, 2013.

[22] M. C. Chandorkar, D. M. Divan, and R. Adapa, "Control of parallel connected inverters in standalone AC supply systems," *IEEE Transactions on Industry Applications,* vol. 29, no. 1, pp. 136-143, 1993.

[23] J. M. Guerrero, J. Matas, L. G. D. V. De Vicuna, M. Castilla, and J. Miret, "Wireless-control strategy for parallel operation of distributed-generation inverters," *IEEE Transactions on Industrial Electronics,* vol. 53, no. 5, pp. 1461-1470, 2006.

[24] J. P. Lopes, C. Moreira, and A. Madureira, "Defining control strategies for microgrids islanded operation," *IEEE Transactions on power systems,* vol. 21, no. 2, pp. 916-924, 2006.

[25] E. A. A. Coelho, P. C. Cortizo, and P. F. D. Garcia, "Small-signal stability for parallel-connected inverters in stand-alone AC supply systems," *IEEE Transactions on Industry Applications,* vol. 38, no. 2, pp. 533-542, 2002.

[26] J. M. Guerrero, J. C. Vásquez, J. Matas, J. L. Sosa, and L. G. De Vicuña, "Parallel operation of uninterruptible power supply systems in microgrids," in *2007 European Conference on Power Electronics and Applications*, 2007, pp. 1-9: IEEE.

[27] C. Wang, X. Li, L. Guo, and Y. Li, "A seamless operation mode transition control strategy for a microgrid based on master-slave control," *Science China Technological Sciences,* vol. 55, no. 6, pp. 1644-1654, 2012.

[28] A. Werth *et al.*, "Peer-to-peer control system for DC microgrids," *IEEE Transactions on Smart Grid,* vol. 9, no. 4, pp. 3667-3675, 2016.

[29] D. Tran and A. M. Khambadkone, "Energy management for lifetime extension of energy storage system in micro-grid applications," *IEEE Transactions on Smart Grid,* vol. 4, no. 3, pp. 1289-1296, 2013.

[30] S. Adhikari and F. Li, "Coordinated Vf and PQ control of solar photovoltaic generators with MPPT and battery storage in microgrids," *IEEE Transactions on Smart grid,* vol. 5, no. 3, pp. 1270-1281, 2014.

[31] A. Munoz-Garcia, T. A. Lipo, and D. W. Novotny, "A new induction motor V/f control method capable of high-performance regulation at low speeds," *IEEE transactions on Industry Applications,* vol. 34, no. 4, pp. 813-821, 1998.

[32] K. De Brabandere, B. Bolsens, J. Van den Keybus, A. Woyte, J. Driesen, and R. Belmans, "A voltage and frequency droop control method for parallel inverters," *IEEE Transactions on power electronics,* vol. 22, no. 4, pp. 1107-1115, 2007.

[33] R. Jadeja, N. Bizon, T. Trivedi, A. Ved, and M. Chudasama, "Power quality issues and mitigation techniques in microgrid," in *Microgrid architectures, control and protection methods*: Springer, 2020, pp. 719-748.

[34] P. Karlsson and J. Svensson, "DC bus voltage control for a distributed power system," *IEEE transactions on Power Electronics,* vol. 18, no. 6, pp. 1405-1412, 2003.

[35] R. S. Balog and P. T. Krein, "Bus selection in multibus DC microgrids," *IEEE Transactions on Power Electronics,* vol. 26, no. 3, pp. 860-867, 2010.

[36] T. Dragicevic, J. C. Vasquez, J. M. Guerrero, and D. Skrlec, "Advanced LVDC Electrical Power Architectures and Microgrids: A step toward a new generation of power distribution networks," *IEEE Electrification Magazine,* vol. 2, no. 1, pp. 54-65, 2014.

[37] C. Liu and J.-S. Lai, "Low frequency current ripple reduction technique with active control in a fuel cell power system with inverter load," *IEEE Transactions on Power Electronics,* vol. 22, no. 4, pp. 1429-1436, 2007.

[38] C.-X. Dou and B. Liu, "Multi-agent based hierarchical hybrid control for smart microgrid," *IEEE transactions on smart grid,* vol. 4, no. 2, pp. 771-778, 2013.

[39] J. Zheng, Y. Wang, X. Li, Z. Wang, X. Wang, and S. Zhu, "Control methods and strategies of microgrid smooth switchover," *Dianli Xitong Zidonghua(Automation of Electric Power Systems),* vol. 35, no. 18, pp. 17-24, 2011.

[40] Y. Karimi, H. Oraee, and J. M. Guerrero, "Decentralized method for load sharing and power management in a hybrid single/three-phase-islanded microgrid consisting of hybrid source

PV/battery units," *IEEE Transactions on Power Electronics,* vol. 32, no. 8, pp. 6135-6144, 2016.

[41] D. I. Brandao, T. Caldognetto, F. P. Marafão, M. G. Simões, J. A. Pomilio, and P. Tenti, "Centralized control of distributed single-phase inverters arbitrarily connected to three-phase four-wire microgrids," *IEEE Transactions on Smart Grid,* vol. 8, no. 1, pp. 437-446, 2016.

[42] Q. Sun, J. Zhou, J. M. Guerrero, and H. Zhang, "Hybrid three-phase/single-phase microgrid architecture with power management capabilities," *IEEE Transactions on Power Electronics,* vol. 30, no. 10, pp. 5964-5977, 2014.

[43] W. Chengshan, W. Zhen, and L. Peng, "Research on key technologies of microgrid," *Transactions of China Electrotechnical Society,* vol. 29, no. 2, pp. 1-12, 2014.

[44] J. M. Carrasco *et al.*, "Power-electronic systems for the grid integration of renewable energy sources: A survey," *IEEE Transactions on industrial electronics,* vol. 53, no. 4, pp. 1002-1016, 2006.

[45] Q. Hongxia, W. Chengshan, L. Shu, and L. Yun, "Discussion on the technology of intelligent micro-grid and flexible distribution system," *Power System Protection and Control,* vol. 44, no. 20, pp. 17-23, 2016.

[46] D. De and V. Ramanarayanan, "Decentralized parallel operation of inverters sharing unbalanced and nonlinear loads," *IEEE Transactions on Power Electronics,* vol. 25, no. 12, pp. 3015-3025, 2010.

[47] M. Su, Z. Liu, Y. Sun, H. Han, and X. Hou, "Stability analysis and stabilization methods of DC microgrid with multiple parallel-connected DC–DC converters loaded by CPLs," *IEEE Transactions on Smart Grid,* vol. 9, no. 1, pp. 132-142, 2016.

[48] M. Hosseinzadeh and F. R. Salmasi, "Robust optimal power management system for a hybrid AC/DC micro-grid," *IEEE Transactions on Sustainable Energy,* vol. 6, no. 3, pp. 675-687, 2015.

[49] R. A. Kaushik and N. M. Pindoriya, "Power flow control of hybrid AC-DC microgrid using master-slave technique," in *2014 IEEE Conference on Energy Conversion (CENCON)*, 2014, pp. 389-394: IEEE.

[50] L. Che, M. Shahidehpour, A. Alabdulwahab, and Y. Al-Turki, "Hierarchical coordination of a community microgrid with AC and DC microgrids," *IEEE Transactions on smart grid,* vol. 6, no. 6, pp. 3042-3051, 2015.

[51] C. Jin, P. C. Loh, P. Wang, Y. Mi, and F. Blaabjerg, "Autonomous operation of hybrid AC-DC microgrids," in *2010 IEEE international conference on sustainable energy technologies (ICSET)*, 2010, pp. 1-7: IEEE.

[52] H. Xiao, A. Luo, Z. Shuai, G. Jin, and Y. Huang, "An improved control method for multiple bidirectional power converters in hybrid AC/DC microgrid," *IEEE Transactions on Smart Grid,* vol. 7, no. 1, pp. 340-347, 2015.

[53] X. Wang, K. Sun, Y. Li, F. Nejabatkhah, and Y. Mei, "Parallel operation of bi-directional interfacing converters in a hybrid AC/DC microgrid under unbalanced grid conditions," in *2015 IEEE Energy Conversion Congress and Exposition (ECCE)*, 2015, pp. 4574-4581: IEEE.

[54] J. Holtz, W. Lotzkat, and K.-H. Werner, "A high-power multitransistor-inverter uninterruptable power supply system," *IEEE Transactions on Power Electronics,* vol. 3, no. 3, pp. 278-285, 1988.

[55] J. H. Enslin and P. J. Heskes, "Harmonic interaction between a large number of distributed power inverters and the distribution network," *IEEE transactions on power electronics,* vol. 19, no. 6, pp. 1586-1593, 2004.

[56] M. Sidrach-de-Cardona and J. Carretero, "Analysis of the current total harmonic distortion for different single-phase inverters for grid-connected pv-systems," *Solar Energy Materials and Solar Cells,* vol. 87, no. 1-4, pp. 529-540, 2005.

[57] J. M. Alonso, M. S. Perdigao, M. A. Dalla Costa, G. Martinez, and R. Osorio, "Analysis and experiments on a single-inductor half-bridge LED driver with magnetic control," *IEEE Transactions on Power Electronics,* vol. 32, no. 12, pp. 9179-9190, 2017.

[58] W. Li, L. Ye, S. Li, H. Yao, H. Ade, and J. Hou, "A high‐efficiency organic solar cell enabled by the strong intramolecular electron push–pull effect of the nonfullerene acceptor," *Advanced Materials,* vol. 30, no. 16, p. 1707170, 2018.

[59] R. Wu, S. B. Dewan, and G. R. Slemon, "Analysis of an ac-to-dc voltage source converter using PWM with phase and amplitude control," *IEEE Transactions on industry Applications,* vol. 27, no. 2, pp. 355-364, 1991.

[60] L. Chen and S. Mei, "An integrated control and protection system for photovoltaic microgrids," *CSEE journal of power and energy systems,* vol. 1, no. 1, pp. 36-42, 2015.

[61] X. Yu, Z. Jiang, and Y. Zhang, "Control of parallel inverter-interfaced distributed energy resources," in *2008 IEEE Energy 2030 Conference*, 2008, pp. 1-8: IEEE.

[62] L. Su, G. Li, and Z. Jin, "Modeling, control and testing of a voltage-source-inverter-based microgrid," in *2011 4th International Conference on Electric Utility Deregulation and Restructuring and Power Technologies (DRPT)*, 2011, pp. 724-729: IEEE.

[63] E. Serban and H. Serban, "A control strategy for a distributed power generation microgrid application with voltage-and current-controlled source converter," *IEEE Transactions on Power Electronics,* vol. 25, no. 12, pp. 2981-2992, 2010.

[64] M. Savaghebi, A. Jalilian, J. C. Vasquez, J. M. Guerrero, and T.-L. Lee, "Voltage harmonic compensation of a microgrid operating in islanded and grid-connected modes," in *2011 19th Iranian Conference on Electrical Engineering*, 2011, pp. 1-6: IEEE.

[65] T. M. Rowan and R. J. Kerkman, "A new synchronous current regulator and an analysis of current-regulated PWM inverters," *IEEE Transactions on Industry Applications,* no. 4, pp. 678-690, 1986.

[66] K. Dai, P. Liu, Y. Kang, and J. Chen, "Decoupling current control for voltage source converter in synchronous roating frame," in *4th IEEE International Conference on Power Electronics and Drive Systems. IEEE PEDS 2001-Indonesia. Proceedings (Cat. No. 01TH8594)*, 2001, vol. 1, pp. 39-43: IEEE.

[67] K. Dai, P. Liu, J. Xiong, and J. Chen, "Comparative study on current control for three-phase SVPWM voltage-source converter in synchronous rotating frame using complex vector method," in *IEEE 34th Annual Conference on Power Electronics Specialist, 2003. PESC'03.*, 2003, vol. 2, pp. 695-700: IEEE.

[68] D. N. Zmood and D. G. Holmes, "Stationary frame current regulation of PWM inverters with zero steady-state error," *IEEE Transactions on power electronics,* vol. 18, no. 3, pp. 814-822, 2003.

[69] D. Zhang, J. Li, and D. Hui, "Coordinated control for voltage regulation of distribution network voltage regulation by distributed energy storage systems," *Protection and Control of Modern Power Systems,* vol. 3, no. 1, p. 3, 2018.

[70] X.-h. QU, Y. LIAO, J. YAO, and R. LIU, "Design of grid-connected converter for a permanent magnet synchronous direct-drive wind power generation system [J]," *Power Electronics,* vol. 3, 2008.

[71] V.-T. Phan and H.-H. Lee, "Proportional—Multiresonant current controller for harmonic elimination in stand-alone DFIG wind power systems," in *International Forum on Strategic Technology 2010*, 2010, pp. 390-395: IEEE.

[72] J. C. Vasquez, J. M. Guerrero, M. Savaghebi, J. Eloy-Garcia, and R. Teodorescu, "Modeling, analysis, and design of stationary-reference-frame droop-controlled parallel three-phase voltage source inverters," *IEEE Transactions on Industrial Electronics,* vol. 60, no. 4, pp. 1271-1280, 2012.

[73] J. He and Y. W. Li, "Analysis, design, and implementation of virtual impedance for power electronics interfaced distributed generation," *IEEE Transactions on Industry Applications,* vol. 47, no. 6, pp. 2525-2538, 2011.

[74] L. Hang, B. Li, L. Huang, W. Yao, and Z. Lu, "A multi-resonant PR current controller for grid-connected inverters in renewable energy systems," in *Zhongguo Dianji Gongcheng Xuebao(Proceedings of the Chinese Society of Electrical Engineering)*, 2012, vol. 32, no. 12, pp. 51-58: Chinese Society for Electrical Engineering.

[75] C. Dou, Z. Zhang, D. Yue, and M. Song, "Improved droop control based on virtual impedance and virtual power source in low-voltage microgrid," *IET Generation, Transmission & Distribution,* vol. 11, no. 4, pp. 1046-1054, 2017.

[76] W. Chengshan, X. Zhaoxia, and W. Shouxiang, "Multi-loop feedback control strategy for distributed power inverter in microgrid [J]," *Journal of Electrical Technology,* vol. 24, no. 2, pp. 100-107, 2009.

[77] Q. Zhang, C. Peng, Y. Chen, G. Jin, and A. Luo, "A control strategy for parallel operation of multi-inverters in microgrid," in *Zhongguo Dianji Gongcheng Xuebao(Proceedings of the*

Chinese Society of Electrical Engineering), 2012, vol. 32, no. 25, pp. 126-132: Chinese Society for Electrical Engineering.

[78] Y. W. Li and C.-N. Kao, "An accurate power control strategy for power-electronics-interfaced distributed generation units operating in a low-voltage multibus microgrid," *IEEE Transactions on Power Electronics,* vol. 24, no. 12, pp. 2977-2988, 2009.

[79] M. Zhang, N. Li, Z. Du, E. Xu, and J. Chen, "Control parameter selection and stability analysis of microgrid based on small-signal model," in *Zhongguo Dianji Gongcheng Xuebao(Proceedings of the Chinese Society of Electrical Engineering)*, 2012, vol. 32, no. 25, pp. 9-19: Chinese Society for Electrical Engineering.

[80] S. Wang, Z. Liu, J. Liu, B. Liu, X. Meng, and R. An, "Modeling and analysis of droop based hybrid control strategy for parallel inverters in islanded microgrids," in *2017 IEEE Applied Power Electronics Conference and Exposition (APEC)*, 2017, pp. 3462-3469: IEEE.

[81] J. Ma, X. Wang, and X. Lan, "Small-signal stability analysis of microgrid based on perturbation theory," in *2012 Asia-Pacific Power and Energy Engineering Conference*, 2012, pp. 1-4: IEEE.

[82] I. S. Board, *IEEE Standard for Interconnecting Distributed Resources with Electric Power Systems: 1547-2003*. IEEE, 2003.

[83] J. He, Y. W. Li, and M. S. Munir, "A flexible harmonic control approach through voltage-controlled DG–grid interfacing converters," *IEEE Transactions on industrial electronics,* vol. 59, no. 1, pp. 444-455, 2011.

[84] M. Savaghebi, J. M. Guerrero, A. Jalilian, and J. C. Vasquez, "Mitigation of voltage and current harmonics in grid-connected microgrids," in *2012 IEEE International Symposium on Industrial Electronics*, 2012, pp. 1610-1615: IEEE.

[85] F. Blaabjerg, R. Teodorescu, M. Liserre, and A. V. Timbus, "Overview of control and grid synchronization for distributed power generation systems," *IEEE Transactions on industrial electronics,* vol. 53, no. 5, pp. 1398-1409, 2006.

[86] L. Liquin and L. Chunxia, "A grid-connected PV power system total considers the MPPT and SSRF-SPLL control technologies," *Przegląd Elektrotechniczny*.

[87] X. Luo *et al.*, "Review of voltage and frequency grid code specifications for electrical energy storage applications," *Energies,* vol. 11, no. 5, p. 1070, 2018.

[88] A. S. Chandran and P. Lenin, "A review on active & reactive power control strategy for a standalone hybrid renewable energy system based on droop control," in *2018 International Conference on Power, Signals, Control and Computation (EPSCICON)*, 2018, pp. 1-10: IEEE.

[89] Q.-C. Zhong, "Robust droop controller for accurate proportional load sharing among inverters operated in parallel," *IEEE Transactions on Industrial Electronics,* vol. 60, no. 4, pp. 1281-1290, 2011.

[90] L. XIE, B. SHI, G. HUA, F. WEN, L. YANG, and Q. DONG, "Parallel operation technology of distributed generations based on improved droop control," *Power System Technology,* vol. 4, 2013.

[91] Z. XIAO, C. WANG, and S. WANG, "Small-signal stability analysis of microgrid containing multiple micro sources [J]," *Automation of Electric Power Systems,* vol. 6, p. 022, 2009.

[92] W. C. X. Z. W. Shouxiang, "Multiple feedback loop control scheme for inverters of the micro source in microgrids [J]," *Transactions of China Electrotechnical Society,* vol. 2, 2009.

[93] Y. Haizhu and X. Jinju, "Research of improved droop control strategy for grid-connected inverters in microgrids [J]," *Electronic Measurement Technology,* vol. 39, no. 5, pp. 36-40, 2016.

[94] Q.-C. Zhong and G. C. Konstantopoulos, "Current-limiting droop control of grid-connected inverters," *IEEE Transactions on Industrial Electronics,* vol. 64, no. 7, pp. 5963-5973, 2016.

[95] J. M. Guerrero, L. G. De Vicuna, J. Matas, M. Castilla, and J. Miret, "A wireless controller to enhance dynamic performance of parallel inverters in distributed generation systems," *IEEE Transactions on power electronics,* vol. 19, no. 5, pp. 1205-1213, 2004.

[96] J. M. Guerrero, J. Matas, L. G. de Vicuna, M. Castilla, and J. Miret, "Decentralized control for parallel operation of distributed generation inverters using resistive output impedance," *IEEE Transactions on industrial electronics,* vol. 54, no. 2, pp. 994-1004, 2007.

[97] P. Zhang, H. Zhao, H. Cai, J. Shi, and X. He, "Power decoupling strategy based on 'virtual negative resistor'for inverters in low-voltage microgrids," *IET Power Electronics,* vol. 9, no. 5, pp. 1037-1044, 2016.

[98] G. Andersson, "Modelling and analysis of electric power systems," *EEH-Power Systems Laboratory, Swiss Federal Institute of Technology (ETH), Zürich, Switzerland,* 2008.

[99] W. Zhongxi and Z. Xiaoxin, "Power system analysis software package (PSASP)-an integrated power system analysis tool," in *POWERCON'98. 1998 International Conference on Power System Technology. Proceedings (Cat. No. 98EX151)*, 1998, vol. 1, pp. 7-11: IEEE.

[100] T. J. Overbye, X. Cheng, and Y. Sun, "A comparison of the AC and DC power flow models for LMP calculations," in *37th Annual Hawaii International Conference on System Sciences, 2004. Proceedings of the*, 2004, p. 9 pp.: IEEE.

[101] F. Li and R. Bo, "DCOPF-based LMP simulation: algorithm, comparison with ACOPF, and sensitivity," *IEEE Transactions on Power Systems,* vol. 22, no. 4, pp. 1475-1485, 2007.

[102] J. Zhao, J. Ye, and Y. Deng, "Comparative analysis on DC power flow and AC power flow," *Power System Technology,* vol. 36, no. 10, pp. 147-152, 2012.

[103] U. Eminoglu, T. Gözel, and M. Hocaoglu, "DSPFAP: Distribution systems power flow analysis package using Matlab graphical user interface (GUI)," *Computer Applications in Engineering Education,* vol. 18, no. 1, pp. 1-13, 2010.

[104] R. Maheshwari, G. Gohil, L. Bede, and S. Munk-Nielsen, "Analysis and modelling of circulating current in two parallel-connected inverters," *IET Power Electronics,* vol. 8, no. 7, pp. 1273-1283, 2015.

[105] T. Kawabata and S. Higashino, "Parallel operation of voltage source inverters," *IEEE Transactions on Industry Applications,* vol. 24, no. 2, pp. 281-287, 1988.

[106] R. Mai, Y. Li, L. Lu, and Z. He, "A power regulation and harmonic current elimination approach for parallel multi-inverter supplying IPT systems," *Power Electron,* vol. 16, pp. 1245-1255, 2016.

[107] Q.-C. Zhong and T. Hornik, *Control of power inverters in renewable energy and smart grid integration*. John Wiley & Sons, 2012.

[108] X. Fang, S. Misra, G. Xue, and D. Yang, "Smart grid—The new and improved power grid: A survey," *IEEE communications surveys & tutorials,* vol. 14, no. 4, pp. 944-980, 2012.

[109] Q.-C. Zhong and Y. Zeng, "Universal droop control of inverters with different types of output impedance," *IEEE Access,* vol. 4, pp. 702-712, 2016.

[110] P. Iyambo and R. Tzoneva, "Transient stability analysis of the IEEE 14-bus electric power system," in *AFRICON 2007*, 2007, pp. 1-9: IEEE.

[111] E. N. Azadani, S. Hosseinian, P. H. Divshali, and B. Vahidi, "Stability constrained optimal power flow in deregulated power systems," *Electric Power Components and Systems,* vol. 39, no. 8, pp. 713-732, 2011.

[112] L. Hancher, A. de Houteclocque, and M. Sadowska, *Capacity mechanisms in the EU energy market: law, policy, and economics*. Oxford University Press, USA, 2015.

[113] G.-H. Du and Z.-F. Wang, "Design and research on power network dispatching integration of smart grid," *Power System Protection and Control,* vol. 38, no. 15, pp. 127-131, 2010.

Appendices

A. AC and DC power flow calculation

AC power flow calculation

The power system is composed of a generator, a transformer, a transmission line, and a load. The generator and the load are non-linear components. However, when performing power flow calculation, it can generally be represented by a current injection quantity connected to the corresponding node. Therefore, the power network used for power flow calculation is composed of static linear elements of transformers, transmission lines, capacitors, and reactor, and is simulated by several series or parallel equivalent branches represented by several parameters. Based on the characteristics of the power system, to analyse such a prior network, the node method is commonly used, and the relationship between the node voltage and the node current:

$$\dot{I} = Y\dot{V} \tag{A.1}$$

Y is admittance, equal to the reciprocal of impedance $(1/Z)$. The expansion of equation (A.1) is

$$\dot{I}_i = \sum_{j=1}^{n} Y_{ij}\dot{V}_j \quad (i = 1,2,3 \cdots n) \tag{A.2}$$

Y_{ij} is mutual admittance between node i and node j (known as branch ij); n is the number of nodes in the system.

In engineering practice, the amount of node injection is often not node current but node power. The relationship between node current and node power must be applied

$$\dot{I}_i = \frac{P_i - jQ_i}{V_i^*} \quad (i = 1,2,3 \cdots n) \tag{A.3}$$

Substitute A.3 into A.2:

$$\frac{P_i - jQ_i}{V_i^*} = \sum_{j=1}^{n} Y_{ij}\dot{V}_j \quad (i = 1,2,3 \cdots n) \tag{A.4}$$

Complex voltage variables in AC power systems can be represented in two polar coordinates:

$$\dot{V}_i = V_i e^{j\theta_i} \tag{A.5}$$

θ_i is the voltage phase angle of node i.

Or

$$\dot{V}_i = e_i + jf_i \tag{A.6}$$

And the complex admittance is

$$Y_{ij} = G_{ij} + jB_{ij} \tag{A.7}$$

G is electrical conductance, equal to the reciprocal of resistance $(1/R)$; B is susceptance, equal to the reciprocal of reactance $(1/X)$. In (A.7), G_{ij} is mutual electrical conductance between node i and node j, B_{ij} is mutual susceptance between node i and node j.

Substitute (A.6) and (A.7) into (A.4) which is based on the admittance matrix, and separate the real part and the imaginary part, the following power flow equations can be obtained.

The Cartesian coordinate form of the power flow equation is

$$\begin{cases} P_i = e_i \sum_{j\in i}(G_{ij}e_j - B_{ij}f_j) + f_i \sum_{j\in i}(G_{ij} - B_{ij}e_j) \\ Q_i = f_i \sum_{j\in i}(G_{ij}e_j - B_{ij}f_j) + e_i \sum_{j\in i}(G_{ij} + B_{ij}e_j) \end{cases} \quad (i = 1,2,3 \cdots n) \tag{A.8}$$

The polar coordinate form of the power flow equation is

$$\begin{cases} P_i = V_i \sum_{j\in i} V_j(G_{ij}\cos\theta_{ij} + B_{ij}\sin\theta_{ij}) \\ Q_i = V_i \sum_{j\in i} V_j(G_{ij}\sin\theta_{ij} - B_{ij}\cos\theta_{ij}) \end{cases} \quad (i = 1,2,3 \cdots n) \tag{A.9}$$

In the above formulas (A.9), $j \in i$ indicates that the node j is directly connected to node i and includes the case of $j = i$. θ_{ij} is the phase difference between the two nodes voltages. These two forms of power flow equations are commonly referred to as nodal power equations,

and the main mathematical models used by real-time Newton-Raphson and other power flow algorithms.

Equation (A.9) is the power flow equation. Since the above power flow equation is a nonlinear equation, it needs to be solved iteratively until the equation converges. After obtaining the amplitude and phase angle of the node voltage, the branch power flow can be calculated according to formula (A.10):

$$\begin{cases} P_{ij} = V_i V_j\left(G_{ij}\cos\theta_{ij} + B_{ij}\sin\theta_{ij}\right) - V_i^2 G_{ij} \\ Q_{ij} = -V_i V_j\left(B_{ij}\cos\theta_{ij} - G_{ij}\sin\theta_{ij}\right) + V_i^2 B_{ij} \end{cases} \quad (i = 1,2,3\cdots n, j \in i) \quad \text{(A.10)}$$

Where P_{ij} and Q_{ij} are the active power flow and reactive power flow of branch ij, respectively.

DC power flow calculation

In some applications, the power flow equation needs to be simplified, and the DC power flow is generated in this way. The simplification process is as follows:

Firstly, the voltage of each node of the power system in normal operation is usually near the rated voltage, which can be approximated as $V_i = V_j = 1$.

Secondly, the voltage phase angle difference between the two ends of the line is very small, $\theta_{ij} \approx 0$, so, $\sin\theta_{ij} = \theta_{ij}$, $\cos\theta_{ij} = 1$.

Lastly, in the ultra-high voltage (UHV) network, the line resistance is much smaller than the reactance, and the resistance can be ignored, $r_{ij} = 0$.

Therefore, equation (A.10) is simplified to:

$$\begin{cases} P_{ij} = -b'_{ij}\left(\theta_i - \theta_j\right) = \left(\theta_i - \theta_j\right)/x_{ij} \\ Q_{ij} = 0 \end{cases} \quad (i = 1,2,3\cdots n, j \in i) \qquad \text{(A.11)}$$

Where: $b'_{ij} = -1/x_{ij}$; x_{ij} is branch reactance. Equation (A.11) is a set of linear equations. For node i, applying Kirchhoff's law can get:

$$P_i^{SP} = \sum_{j\in i, j\neq i} P_{ij} = \sum_{j\in i, j\neq i} \frac{\theta_i - \theta_j}{x_{ij}} \tag{A.12}$$

For an n-node network, written in matrix form as:

$$\boldsymbol{P}^{SP} = \boldsymbol{B}\theta \tag{A.13}$$

Where: $\boldsymbol{P}^{SP}$ is node active power injection power matrix; $\boldsymbol{B}$ is $n \times n$ order matrix, its diagonal and non-diagonal elements are:

$$\begin{cases} B_{ii} = \sum_{j\in i, j\neq i} 1/x_{ij} \\ B_{ij} = -1/x_{ij} \end{cases} \quad (i = 1,2,3 \cdots n, j \in i) \tag{A.14}$$

Equation (A.14) is the DC equation which does not require iterations to be solved. It can be used to calculate the voltage phase angle of each node in only one step. The active power flow of the branch can then be calculated from equation (A.11).

B. Low voltage power cable parameters

Fujikura Federal Cables Sdn. Bhd. Page No.:1/2

LOW VOLTAGE POWER CABLE
Rated Voltage : 600/1000V
Technical Data
A.C. Resistance, Reactance And Impedance

Cable Type: Single core XLPE/PVC cable

Size mm²	AC resistance (ohm/km)		Reactance (ohm/km)		Impedance (ohm/km)	
	50Hz	60Hz	50Hz	60Hz	50Hz	60Hz
1.5	15.4	15.4	0.141	0.169	15.4	15.4
2.5	9.45	9.45	0.130	0.156	9.45	9.45
4	5.88	5.88	0.120	0.144	5.88	5.88
6	3.93	3.93	0.113	0.135	3.93	3.93
10	2.33	2.33	0.107	0.128	2.33	2.33
16	1.47	1.47	0.0993	0.119	1.47	1.47
25	0.927	0.927	0.0955	0.115	0.932	0.934
35	0.668	0.669	0.0911	0.109	0.674	0.678
50	0.494	0.494	0.0883	0.106	0.502	0.505
70	0.342	0.343	0.0858	0.103	0.353	0.358
95	0.247	0.247	0.0833	0.0999	0.261	0.266
120	0.196	0.197	0.0817	0.0980	0.212	0.220
150	0.159	0.160	0.0814	0.0976	0.179	0.187
185	0.128	0.129	0.0807	0.0969	0.151	0.161
240	0.0983	0.0992	0.0792	0.0950	0.126	0.137
300	0.0793	0.0805	0.0782	0.0939	0.111	0.124
400	0.0634	0.0648	0.0776	0.0931	0.100	0.113
500	0.0510	0.0528	0.0770	0.0924	0.0924	0.106
630	0.0417	0.0438	0.0751	0.0901	0.0859	0.100
800	0.0350	0.0373	0.0741	0.0890	0.0820	0.0965
1000	0.0304	0.0328	0.0735	0.0882	0.0795	0.0941

Cable Type: Single core XLPE/PVCAWA/PVC cable

Size mm²	AC resistance (ohm/km)		Reactance (ohm/km)		Impedance (ohm/km)	
	50Hz	60Hz	50Hz	60Hz	50Hz	60Hz
16	1.47	1.47	0.129	0.155	1.48	1.48
25	0.927	0.927	0.121	0.146	0.935	0.938
35	0.668	0.668	0.115	0.138	0.678	0.682
50	0.494	0.494	0.110	0.132	0.506	0.511
70	0.342	0.342	0.106	0.127	0.358	0.365
95	0.247	0.247	0.101	0.122	0.267	0.275
120	0.196	0.196	0.0990	0.119	0.220	0.229
150	0.159	0.160	0.0968	0.116	0.186	0.198
185	0.128	0.128	0.0949	0.114	0.159	0.171
240	0.0978	0.0986	0.0924	0.111	0.135	0.148
300	0.0788	0.0797	0.0899	0.108	0.120	0.134
400	0.0626	0.0638	0.0905	0.109	0.110	0.126
500	0.0502	0.0516	0.0883	0.106	0.102	0.118
630	0.0408	0.0426	0.0842	0.101	0.0936	0.110
800	0.0339	0.0358	0.0839	0.101	0.0905	0.107
1000	0.0291	0.0313	0.0826	0.0991	0.0876	0.104

Disclaimers :
Product specifications, technical data and other information are for reference only.
The manufacturer reserves the right to modify or vary the design features and technical data without prior notice.

Fujikura Federal Cables Sdn. Bhd. Page No.:2/2

LOW VOLTAGE POWER CABLE
Rated Voltage : 600/1000V
Technical Data
A.C. Resistance, Reactance And Impedance

Cable Type: Three core XLPE/PVC and XLPE/PVC/SWA/PVC cable

Size mm²	AC resistance (ohm/km)		Reactance (ohm/km)		Impedance (ohm/km)	
	50Hz	60Hz	50Hz	60Hz	50Hz	60Hz
1.5	15.4	15.4	0.101	0.122	15.4	15.4
2.5	9.45	9.45	0.0942	0.113	9.45	9.45
4	5.88	5.88	0.0883	0.106	5.88	5.88
6	3.93	3.93	0.0839	0.101	3.93	3.93
10	2.33	2.33	0.0804	0.0965	2.33	2.33
16	1.47	1.47	0.0767	0.0920	1.47	1.47
25	0.927	0.927	0.0767	0.0920	0.930	0.932
35	0.669	0.669	0.0745	0.0893	0.673	0.675
50	0.494	0.494	0.0735	0.0882	0.499	0.502
70	0.342	0.343	0.0729	0.0875	0.350	0.354
95	0.247	0.248	0.0710	0.0852	0.257	0.262
120	0.196	0.197	0.0707	0.0848	0.208	0.214
150	0.160	0.160	0.0710	0.0852	0.175	0.181
185	0.128	0.129	0.0716	0.0860	0.147	0.155
240	0.0987	0.0998	0.0707	0.0848	0.121	0.131
300	0.0798	0.0812	0.0701	0.0841	0.106	0.117
400	0.0640	0.0657	0.0697	0.0837	0.0946	0.106

C. Detailed simulation model using proposed control method

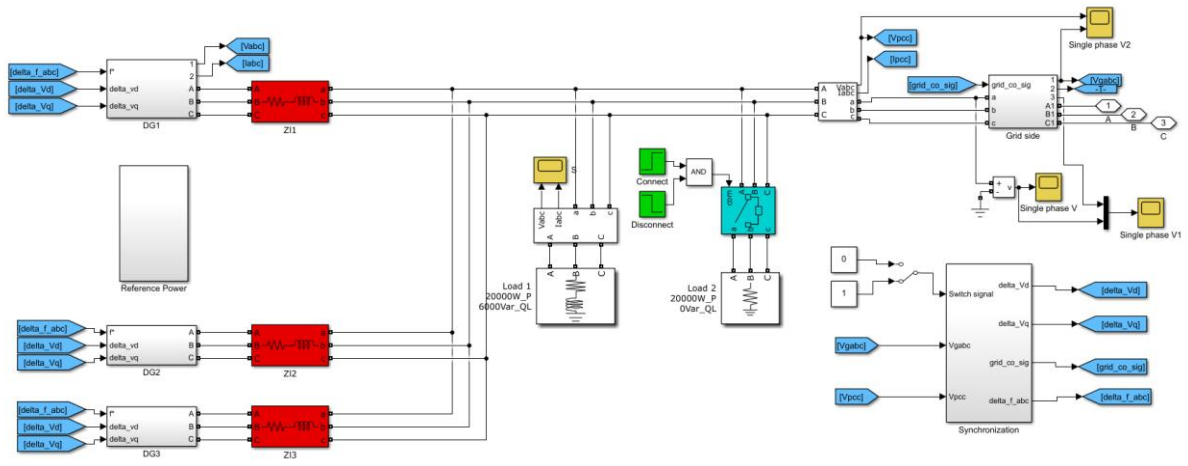

Figure C.1 Overview of the system

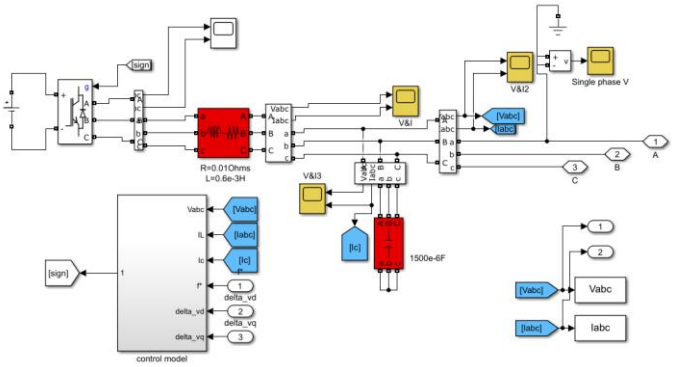

Figure C.2 Connection of each DGs

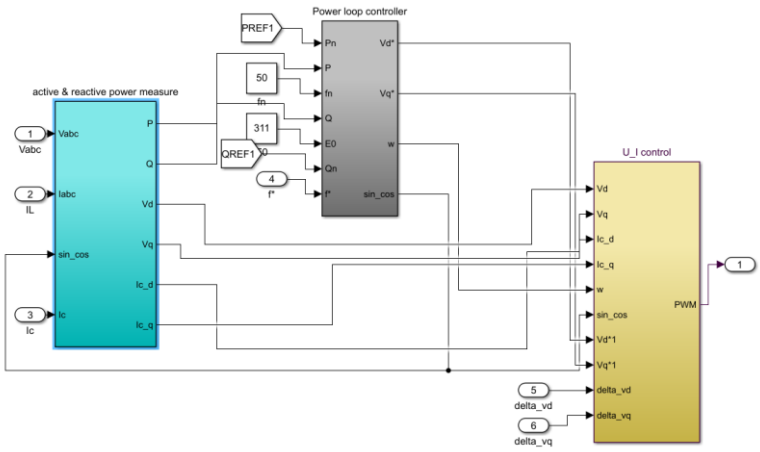

Figure C.3 Control part of each inverter

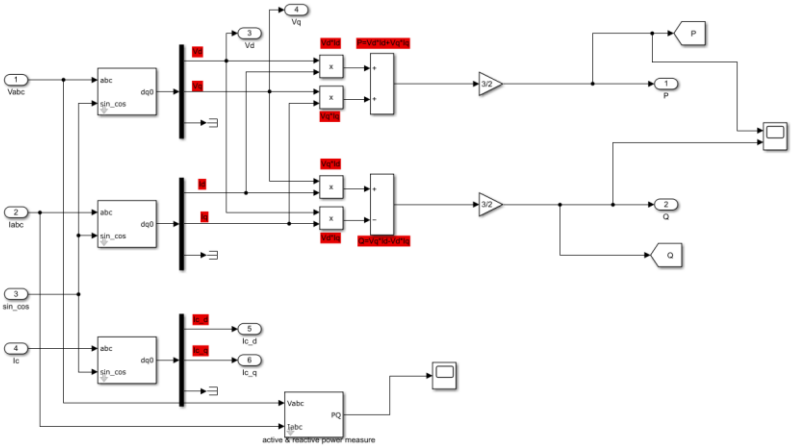

Figure C.4 Active and reactive power measure block

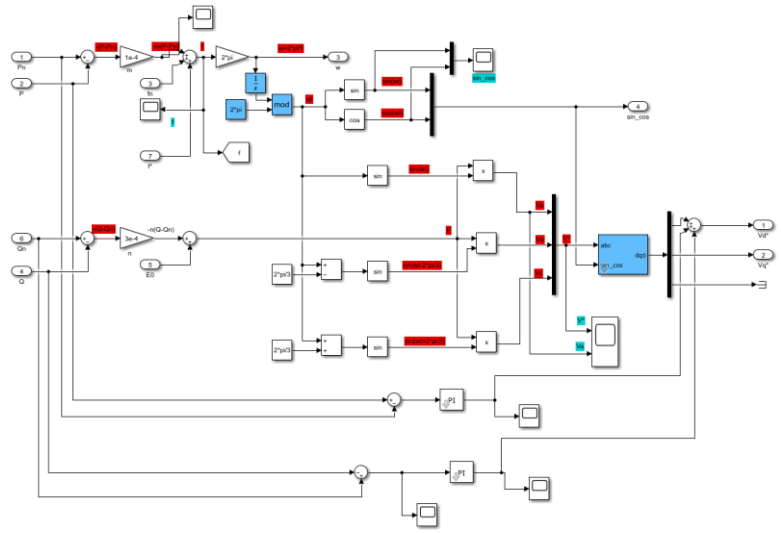

Figure C.5 Power loop controller

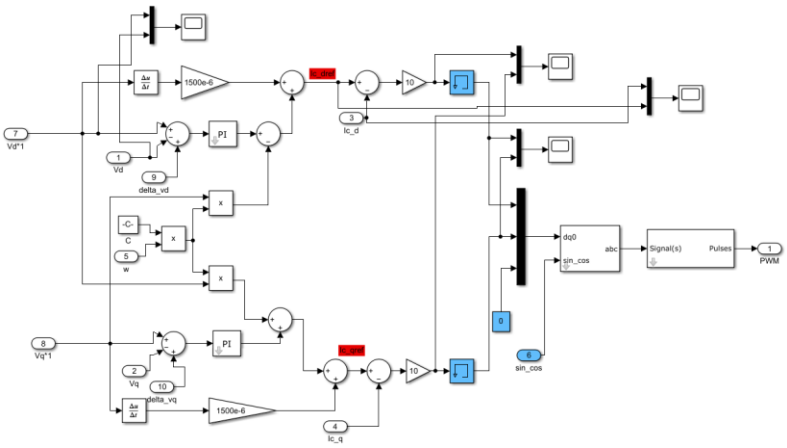

Figure C.6 Voltage and current double loop controller

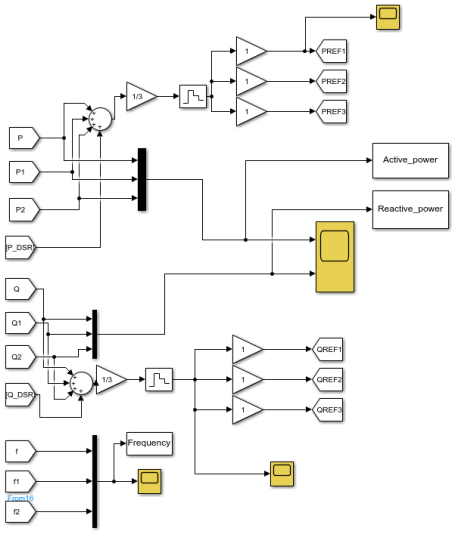

Figure C.7 Power sharing controller

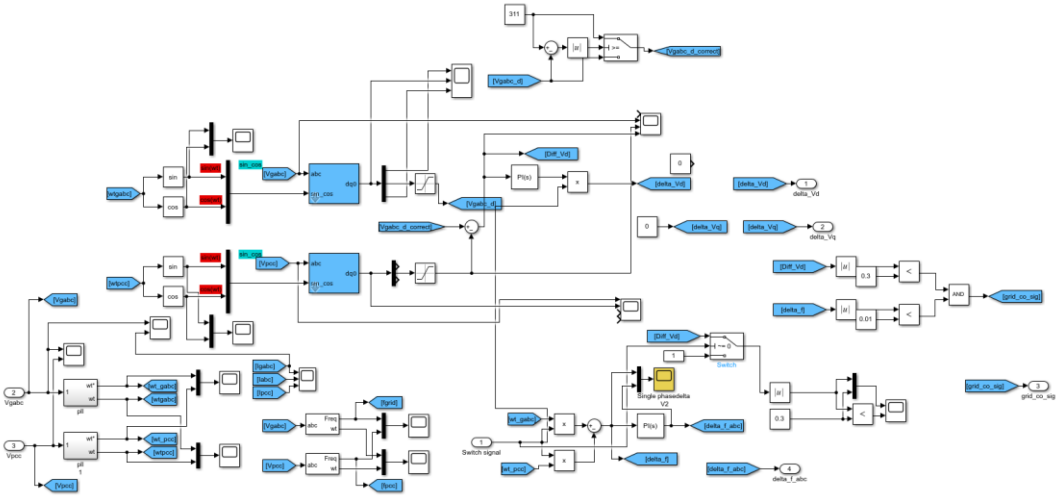

Figure C.8 Pre-synchronization control block

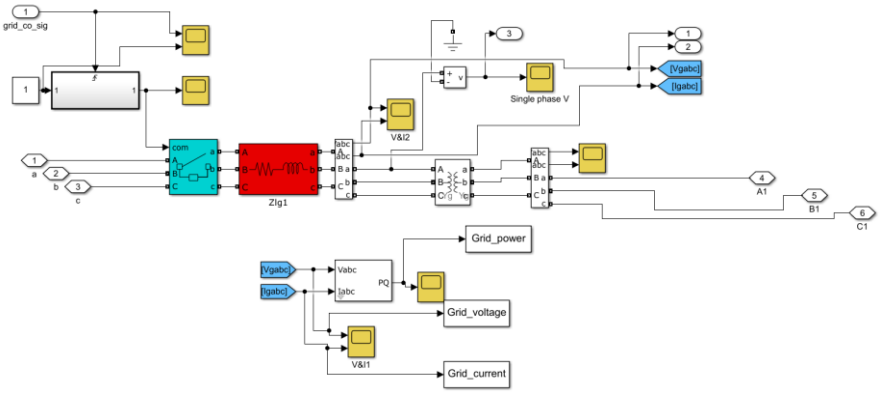

Figure C.9 Grid side block

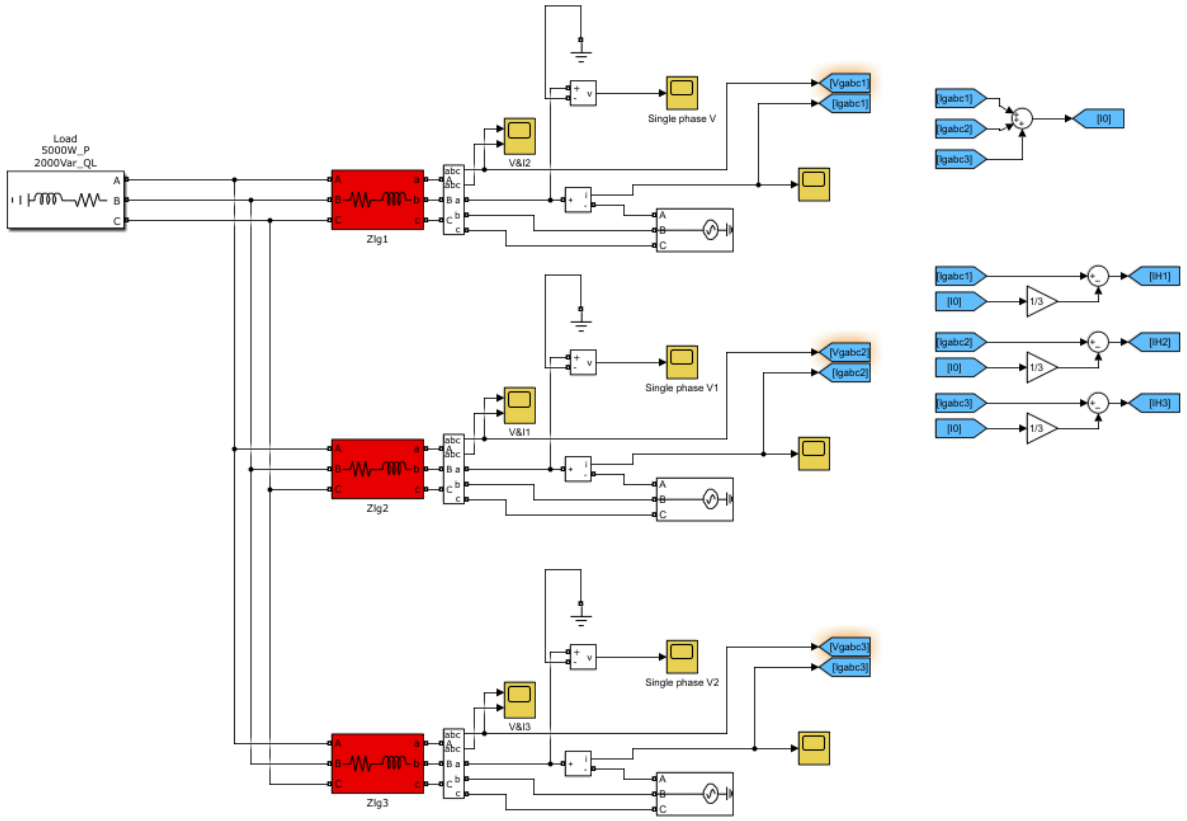

Figure C.10 Circulating current measurement for 3 parallel connected power sources

D. This Technical Note describes the details of the IEEE 14-bus system. The system consists of loads, capacitor banks, transmission lines

Table C-1. Generator features

Bus	V kV]	δ [deg]	P [pu]	Q [pu]
1	146.28	0.0000	2.3239	-0.1655
2	144.21	-4.9826	0.4000	0.4356
3	139.38	-12.7250	0.0000	0.2508
6	147.66	-14.2209	0.0000	0.1273
8	150.42	-13.3596	0.0000	0.1762

Table C-1 summarizes the characteristics of each source, with a base of 100 [MVA] for per unitizing. Transmission lines are modelled using the Bergeron model. Table 2 summarizes the transmission line parameters.

Table C-2. Transmission line features.

Line		R [pu/m]	X [pu/m]	B [pu/m]
From Bus	To Bus			
1	2	1.94E-07	5.92E-07	5.28E-07
1	5	5.40E-07	2.23E-06	4.92E-07
2	3	4.70E-07	1.98E-06	4.38E-07
2	4	5.81E-07	1.76E-06	3.40E-07
2	5	5.70E-07	1.74E-06	3.46E-07
3	4	6.70E-07	1.71E-06	1.28E-07
4	5	1.34E-07	4.21E-07	1.00E-09
6	11	9.50E-07	1.99E-06	1.00E-09
6	12	1.23E-06	2.56E-06	1.00E-09
6	13	6.62E-07	1.30E-06	1.00E-09
7	8	1.00E-09	1.76E-06	1.00E-09
7	9	1.00E-09	1.10E-06	1.00E-09
9	10	3.18E-07	8.45E-07	1.00E-09
9	14	1.27E-06	2.70E-06	1.00E-09
10	11	8.21E-07	1.92E-06	1.00E-09
12	13	2.21E-06	2.00E-06	1.00E-09
13	14	1.71E-06	3.48E-06	1.00E-09

Loads are modelled as a constant PQ load with parameters as shown in Table 3.

Table C-3. Load features.

Bus	P [pu]	Q [pu]
2	0.217	0.127
3	0.942	0.190
4	0.478	-0.039
5	0.076	0.016
6	0.112	0.075
9	0.295	0.166
10	0.090	0.058
11	0.035	0.018
12	0.061	0.016
13	0.135	0.058
14	0.149	0.050

E. Power flow analysis of IEEE 14 buses test system and proposed microgrid integrated with IEEE 14 buses test system

Table D-1: Summary for ieee_14		
	P(MW)	Q(Mvar)
Total generation	260.4745	87.25156
Total PQ load	258.9989	81.39476
Total Z shunt	0.027818	0.023184
Total ASM	0	0
Total losses	1.447759	5.833614
BUS_1: V= 1.000 pu/69kV 0.00 deg ; Swing bus		
	P(MW)	Q(Mvar)
Generation	220.474	-118.814
PQ Load	0	0
Z shunt	-1.1E-08	2.75E-08
BUS_2	158.6939	-113.726
BUS_5	61.78003	-5.08786
BUS_10: V= 0.989 pu/13.8kV -2.43 deg		
	P(MW)	Q(Mvar)
Generation	0	0
PQ Load	9.000063	5.799805
Z shunt	-1.5E-08	4.11E-09
BUS_11	9.873507	-6.39134
BUS_9	-18.8736	0.59153
BUS_11: V= 0.993 pu/13.8kV -3.29 deg		
	P(MW)	Q(Mvar)
Generation	0	0
PQ Load	3.499737	1.799328
Z shunt	-7.6E-09	7.93E-09
BUS_10	-9.81256	6.562535
BUS_6	6.312824	-8.36186
BUS_12: V= 0.991 pu/13.8kV -4.43 deg		
	P(MW)	Q(Mvar)
Generation	0	0
PQ Load	6.099602	1.598861
Z shunt	4.5E-09	1.34E-09
BUS_13	-0.0584	1.730985

BUS_6	-6.0412	-3.32985	
BUS_13: V= 0.988 pu/13.8kV -4.31 deg			
	P(MW)	Q(Mvar)	
Generation	0	0	
PQ Load	13.49922	5.798215	
Z shunt	1.17E-09	-5.6E-09	
BUS_12	0.061945	-1.72713	
BUS_14	-2.93873	5.28043	
BUS_6	-10.6224	-9.35151	
BUS_14: V= 0.980 pu/13.8kV -3.65 deg			
	P(MW)	Q(Mvar)	
Generation	0	0	
PQ Load	14.90009	4.999787	
Z shunt	3.05E-09	-8.2E-09	
BUS_13	2.972279	-5.19847	
BUS_9	-17.8724	0.198683	
BUS_2: V= 1.000 pu/69kV -0.08 deg			
	P(MW)	Q(Mvar)	
Generation	40	106.1715	
PQ Load	21.7	12.6999	
Z shunt	-1.3E-06	2.02E-06	
BUS_1	-158.539	113.9425	
BUS_3	74.91353	-17.3761	
BUS_4	59.18349	-1.62878	
BUS_5	42.74174	-1.46604	
BUS_3: V= 1.000 pu/69kV -0.27 deg			
	P(MW)	Q(Mvar)	
Generation	-9E-07	61.75079	
PQ Load	94.2	18.9999	
Z shunt	-2.9E-07	1.27E-07	
BUS_2	-74.8552	17.62585	
BUS_4	-19.3448	25.12504	
BUS_4: V= 0.999 pu/69kV -0.21 deg			
	P(MW)	Q(Mvar)	
Generation	0	0	
PQ Load	47.80009	3.999807	
Z shunt	0.004284	0.003571	
BUS_2	-59.1407	1.761611	

BUS_3	19.35899	-25.0878	
BUS_5	-74.5675	0.686194	
BUS_7	37.9973	10.64771	
BUS_9	28.54752	7.988901	
BUS_5: V= 1.000 pu/69kV -0.17 deg			
	P(MW)	Q(Mvar)	
Generation	0	0	
PQ Load	7.599925	1.599643	
Z shunt	0.000234	0.002029	
BUS_1	-61.7364	5.270791	
BUS_2	-42.7199	1.535314	
BUS_4	74.58309	-0.63957	
BUS_6	22.27304	-7.76821	
BUS_6: V= 1.000 pu/13.8kV -3.99 deg			
	P(MW)	Q(Mvar)	
Generation	0.00054	38.17236	
PQ Load	11.2	7.4999	
Z shunt	0.007765	0.004634	
BUS_11	-6.25725	8.501519	
BUS_12	6.072498	3.408006	
BUS_13	10.69363	9.519769	
BUS_5	-21.7161	9.238534	
BUS_7: V= 0.995 pu/13.8kV -1.02 deg			
	P(MW)	Q(Mvar)	
Generation	0	0	
PQ Load	6.36E-05	-6.8E-05	
Z shunt	0.011315	0.00943	
BUS_4	-37.9973	-10.0677	
BUS_8	2.58E-06	0.022078	
BUS_9	37.98592	10.03624	
BUS_8: V= 1.000 pu/18kV -1.02 deg			
	P(MW)	Q(Mvar)	
Generation	-6.1E-12	-0.02893	
PQ Load	0	0	
Z shunt	2.64E-14	-4.3E-14	
BUS_7	-6.1E-12	-0.02893	
BUS_9: V= 0.992 pu/13.8kV -1.84 deg			
	P(MW)	Q(Mvar)	

Generation	0	0	
PQ Load	29.50014	16.59968	
Z shunt	0.004222	0.003517	
BUS_10	18.93447	-0.3974	
BUS_14	18.09461	0.368603	
BUS_4	-28.5475	-7.11764	
BUS_7	-37.9859	-9.45677	

Table D-2: Summary for ieee_14_microgrid_connected		
	P(MW)	Q(Mvar)
Total generation	261.7705	87.01451
Total PQ load	259.0389	81.40138
Total Z shunt	0.521196	0.521254
Total ASM	0	0
Total losses	2.210382	5.091876
BUS_1: V= 1.000 pu/69kV 0.00 deg ; Swing bus		
	P(MW)	Q(Mvar)
Generation	221.7159	-449.146
PQ Load	0	0
Z shunt	-1.9E-08	-1.4E-07
BUS_2	143.692	-435.722
BUS_5	78.02389	-13.4234
BUS_10: V= 0.991 pu/13.8kV -2.08 deg		
	P(MW)	Q(Mvar)
Generation	0	0
PQ Load	9.00006	5.799789
Z shunt	3E-08	-1.8E-08
BUS_11	10.05394	-7.06894
BUS_9	-19.054	1.269148
BUS_11: V= 0.994 pu/13.8kV -2.85 deg		
	P(MW)	Q(Mvar)
Generation	0	0
PQ Load	3.499745	1.79943
Z shunt	-7.3E-09	1.26E-08

BUS_10		-9.98765	7.224126
BUS_6		6.487904	-9.02356
BUS_12: V= 0.991 pu/13.8kV -3.84 deg			
		P(MW)	Q(Mvar)
Generation		0	0
PQ Load		6.099626	1.599093
Z shunt		-5E-09	7.09E-09
BUS_13		-0.02818	1.788639
BUS_6		-6.07145	-3.38773
BUS_13: V= 0.990 pu/13.8kV -3.72 deg			
		P(MW)	Q(Mvar)
Generation		0	0
PQ Load		13.49928	5.7986
Z shunt		2.29E-09	-1.2E-08
BUS_12		0.031954	-1.78522
BUS_14		-2.99366	5.69703
BUS_6		-10.5376	-9.71041
BUS_14: V= 0.982 pu/13.8kV -3.10 deg			
		P(MW)	Q(Mvar)
Generation		0	0
PQ Load		14.90007	4.999772
Z shunt		-1.9E-08	-3.5E-09
BUS_13		3.03162	-5.61974
BUS_9		-17.9317	0.619966
BUS_2: V= 1.000 pu/69kV -0.11 deg			
		P(MW)	Q(Mvar)
Generation		40.00004	423.4515
PQ Load		21.7	12.6999
Z shunt		-1.4E-06	-3.5E-06
BUS_1		-142.835	436.0039
BUS_3		73.40276	-22.2686
BUS_4		52.82899	-2.09344
BUS_5		34.90343	-0.89035
BUS_3: V= 1.000 pu/69kV -0.26 deg			
		P(MW)	Q(Mvar)
Generation		-2.5E-07	72.04798
PQ Load		94.2	18.9999
Z shunt		9.54E-07	-2.6E-07

BUS_2		-73.3447	22.45909
BUS_4		-20.8553	30.58899
BUS_4: V= 0.999 pu/69kV -0.20 deg			
		P(MW)	Q(Mvar)
Generation		0	0
PQ Load		47.80007	3.999798
Z shunt		0.004287	0.004285
BUS_2		-52.7949	2.174998
BUS_3		20.8746	-30.5497
BUS_5		-83.1498	6.778606
BUS_7		38.40893	10.05088
BUS_9		28.85679	7.541145
BUS_5: V= 1.000 pu/69kV -0.17 deg			
		P(MW)	Q(Mvar)
Generation		0	0
PQ Load		7.599893	1.599612
Z shunt		5.54E-05	0.002518
BUS_1		-77.9528	13.65229
BUS_2		-34.8889	0.926167
BUS_4		83.16934	-6.73571
BUS_6		22.07233	-9.44488
BUS_6: V= 1.000 pu/13.8kV -3.50 deg			
		P(MW)	Q(Mvar)
Generation		0.000547	40.68115
PQ Load		11.2	7.4999
Z shunt		0.007945	0.005479
BUS_11		-6.42552	9.1542
BUS_12		6.103188	3.45379
BUS_13		10.61041	9.853838
BUS_5		-21.4955	10.71394
BUS_7: V= 0.996 pu/13.8kV -0.89 deg			
		P(MW)	Q(Mvar)
Generation		0	0
PQ Load		4.68E-05	-7.6E-05
Z shunt		0.01134	0.011337
BUS_4		-38.4089	-9.56167
BUS_8		1.78E-06	0.018361
BUS_9		38.39754	9.532049

BUS_8: V= 1.000 pu/18kV -0.88 deg		
	P(MW)	Q(Mvar)
Generation	-2.8E-12	-0.02404
PQ Load	0	0
Z shunt	-1.1E-16	-4.1E-14
BUS_7	-2.8E-12	-0.02404
BUS_9 V= 0.993 pu/13.8kV -1.58 deg		
	P(MW)	Q(Mvar)
Generation	0	0
PQ Load	29.50012	16.59966
Z shunt	0.250941	0.250978
BUS_10	19.11605	-1.10432
BUS_14	18.15459	-0.14583
BUS_4	-28.8568	-6.80628
BUS_7	-38.3975	-9.04329
BUS_microgrid	0.23263	0.249087
BUS_microgrid: V= 0.993 pu/0.38kV -1.58 deg		
	P(MW)	Q(Mvar)
Generation	0.054	0.00365
PQ Load	0.04	0.006
Z shunt	0.246628	0.246662
BUS_9	-0.23263	-0.24901